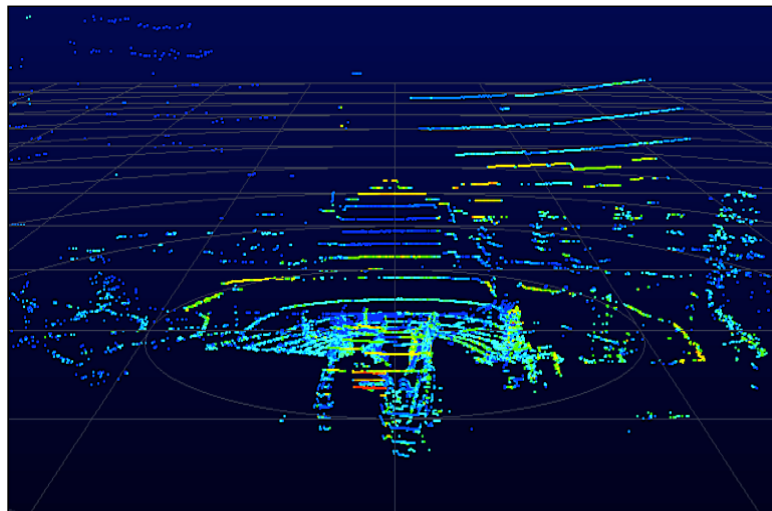


Rainfall estimation using low-cost lidar measurements

Danick Perrin

Under the supervision of Prof. Grégoire Mariéthoz and
PhD student Lionel Benoit
Expert: Dr. Marc-Henri Derron



Title image: screenshot of measurements made during the 9th July 2017 rainfall event, using Velodyne's program, Veloview.

Life is not about waiting for the storm to pass; it is about learning to dance in the rain.

Acknowledgements

This work would not have been what it is today without the help and support of people around me. I would like to give special thanks to the following people:

- ❖ Prof. Grégoire Mariéthoz, my thesis' supervisor, for his help, time and expertise during my research, as well as for reading and commenting on my work.
- ❖ PhD student Lionel Benoit, my thesis' co-supervisor, for all the time he spent helping and advising me; for his enthusiasm and patience. For the time he took to read and comment on my texts. For all he did to help me during this work.
- ❖ Dr. Marc-Henri Derron my expert, for his time and interest.
- ❖ Dr. Joel Jaffrain, for reading this thesis, and for his comments and advice.
- ❖ Jane and Annabel, for reading and correcting the language on my thesis.
- ❖ The people at ECA Vaud DRPE for their welcome and support during the final writing of this thesis. Especially to the EN team: Marc for his agreement; Giuseppe for the idea, his time, advice and discussions; Raphaël and Carmen for their advice, discussions and time.
- ❖ My classmates, Maria, Lara, Anna & the boys, who have been a great class for the past 4 years.
- ❖ Last, but not least, my family, especially my parents, Catherine & Dominique and my grandparents, Pierre, Aimée & Roger; and my friends, particularly Coraline & Maude, for their great support during this work and more during all my studies. Even if they did not understand what I was doing, they were here to listen for hours, and to help and advise me the best they could. They never stopped believing in me and during all these years, they supported me.

Summary

Rainfall has been measured since the 17th century in Europe, and there are several instruments used to do it. From local scale, using rain gauges, to regional or continental scale, with radar or satellites. In addition, rainfall measurement is complex due, in particular to the strong spatio-temporal variability of rainfall. Another point is the resolution (spatial and temporal), which is not always enough. For example radar for which there can be much information in one pixel. As the instruments used allow knowledge in their specific scale, it is to see a missing between meters to kilometers (Adirosi et al., 2016; Gires et al., 2014; Jaffrain & Berne, 2012; Kathiravelu et al., 2016; Krajewski et al., 2009; Mandapaka et al., 2009; Michaelides et al., 2009; Musy & Higy, 2014; Strangeways, 2010). Lidar is an active remote sensing instrument, which sends a laser beam and measures the returning signal. Its range can be from some meters to several kilometers. It used in several field, like to do accurate Digital Elevation Model (DEM), but not only. As there is not only one type of lidar, there are several field using it, such as geological or atmospheric to cite only two possible applications. Over the years we have seen the development of low-cost lidar (Beraldin et al., 2010; Charlton et al., 2009; Derron, 2016; Hudak et al., 2009; Jaboyedoff et al., 2012; Large & Heritage, 2009; Mallet & Bretar, 2007; Mariéthoz, 2016). In general lidar uses several wavelengths from visible to infrared (IR). One of water's properties is to absorb infrared (Manap et al., 2009). There is a strong absorption in the small wavelengths, which correspond to near-infrared (0.7-1.3 μm). Theoretically, it should be possible to estimate rainfall, using a lidar working in IR.

This Master thesis, investigates the possibilities offered by a low-cost terrestrial lidar and how it could be used for rainfall studies. This research has two objectives: 1) having a simple theoretical framework; 2) test theory with measurements.

Results show that it is possible to estimate rainfall using a low-cost lidar. However, the reliability of them depends on the intensity of rainfall. In fact, when the rainfall intensity does not exceed 10 mm/h, the lidar / rainfall relation is less visible; it is explained by a linear function. In addition, it stands out that at low rainfall intensities, lidar signal is more sensitive to noise. Although when the rainfall intensity exceeds 10 mm/h, the presence of extremes brings more information. In this case, the relation is clearer and is similar to the one observed with radars, this is a power-law function, which explains it.

There are some uncertainties and results should be taken cautiously, however they are reliable and promising. There is a relationship between lidar and rainfall rate, which can be found using the methodology developed in this thesis, and it is the first step for new studies.

Key words: rainfall measurements, remote sensing, instrument, lidar

Résumé

Il existe en Europe des mesures de la pluie faite depuis le 17^e siècle. Plusieurs instruments existent pour ces mesures. Que ce soit à échelle locale, avec des pluviomètres, ou à échelle régionale voir continentale, en utilisant des radars ou des satellites. De plus, la mesure de la pluie est complexe à réaliser, notamment de part la variabilité spatio-temporelle des précipitations. Un autre point important est la résolution (spatiale et temporelle) des divers instruments. Par exemple, une image radar contient toute sorte d'informations dans un seul pixel, alors que cela couvre une région complexe. Tous ces instruments permettent d'avoir des connaissances poussées et fiables à leur échelle. Dès lors, il est possible de remarquer un manque dans les échelles, entre les mètres et les kilomètres (Adirosi et *al.*, 2016; Gires et *al.*, 2014; Jaffrain & Berne, 2012; Kathiravelu et al., 2016; Krajewski et al., 2009; Mandapaka et al., 2009; Michaelides et al., 2009; Musy & Higy, 2014; Strangeways, 2010). Le lidar est un instrument de télédétection actif, qui envoie un signal et en mesure le retour. Il a une portée allant de plusieurs mètres jusqu'à plusieurs kilomètres. Il est utilisé dans divers domaines, comme pour faire des modèles numériques de terrain (MNT), mais pas seulement. Comme il n'y a pas qu'un type de lidar, il y a plusieurs domaines d'utilisation, comme en géologie ou étude de l'atmosphère pour n'en citer que deux. Avec les années, les lidar low-cost se sont développés et laissent voir de nouvelles perspectives d'utilisation (Beraldin et *al.*, 2010; Charlton et *al.*, 2009; Derron, 2016; Hudak et al., 2009; Jaboyedoff et al., 2012; Large & Heritage, 2009; Mallet & Bretar, 2007; Mariéthoz, 2016). De manière générale, le lidar travaille dans plusieurs longueurs d'ondes, du visible à l'infrarouge. Et l'une des propriétés de l'eau est qu'elle absorbe les infrarouges (Manap et *al.*, 2009), notamment le proche infrarouge (0.7-1.3 μm). Théoriquement, il devrait être possible de mesurer la pluie en utilisant un lidar émettant dans les infrarouges.

Ce travail de Master s'intéresse aux possibilités offertes par un lidar terrestre low-cost et comment il pourrait être utilisé pour étudier la pluie. Cette recherche a deux objectifs: le premier est de proposer un cadre théorique simple; le second est de tester la théorie avec des mesures.

Les résultats montrent qu'il est possible d'estimer la pluie en utilisant un lidar. Cependant, la fiabilité et la précision de ces résultats dépendent de l'intensité de la pluie. En effet, quand l'intensité de pluie ne dépasse pas les 10 mm/h, la relation lidar/pluie est moins visible; elle est explicable en utilisant une fonction affine. Ce qui ressort également est le fait qu'à faible intensité, le signal lidar est plus sensible aux bruits. Alors que si l'intensité de pluie dépasse les 10 mm/h, la présence d'extrêmes apporte des informations supplémentaires. Dans ce cas, la relation est plus claire et ressemble à celle observée avec les radars: c'est une fonction loi-puissance qui explique la relation.

Même s'il y a des incertitudes et que les résultats doivent être pris avec prudence, ils sont prometteurs. Il y a une relation entre l'intensité de la pluie et le signal lidar, qui peut être trouvé en utilisant la méthodologie développée dans ce mémoire, ce n'est là que la première étape pour de nouvelles études.

Mots clés: mesure de la pluie, télédétection, instrument, lidar

Table of contents

Introduction	11
1. Literature review	13
1.1. Lidar	13
1.2. Rainfall measurements	17
1.2.1. Measurement instruments	17
1.2.2. Measurement errors.....	21
2. Methodology	24
2.1. Measurements location	24
2.2. Instruments	27
2.2.1. Lidar.....	27
2.2.2. Rain gauge.....	30
2.3. Data cleaning	31
2.3.1. Interpolation	31
2.3.2. Scan issues	31
3. Results	35
3.1. Data analysis	35
3.2. Modeling the rainfall / lidar relationship for low intensity rain events (does not exceed 10 mm/h)	41
3.3. Modeling the rainfall / lidar relationship for high intensity rain events (higher than 10 mm/h)	43
3.3.1. Analysis using all measurements.....	43
3.3.2. Analysis using bins	46
3.3.3. Sensitivity of parameters to environmental conditions	51
3.4. Effect of distance	53
4. Discussion	57
Conclusion	58
References	59
Appendixes	
Appendix A - The linear function results	I
A.I. Graphs and results for all the events	I
A.II. Individual events graphic results	IV
Appendix B - The exponential function results	VIII
B.I. Graphs and results for all the events	VIII
B.II. Graphs and results for all the events, using bins.....	XIV
B.III. Individual events graphic results	XX
Appendix C - Scans results	XXVIII
Appendix D - Velodyne LiDAR Puck VLP-16 specifications	XXXVII

Introduction

Rainfall has been measured since the 17th century in Europe, and there are several instruments used to do it. From local scale, using rain gauges, to regional or continental scale, with radar or satellites. In addition, rainfall measurement is complex due to the strong spatio-temporal variability of rainfall. Instruments can measure rainfall, but there are a lot of difficulties. For example with obstacles such as topography or simply the movement of precipitations. Another point is the resolution (spatial and temporal), which is not always enough. For example radar for which there can be much information in one pixel. Further, some of these instruments are expensive. As the instruments used allow knowledge in their specific scale, it is possible to remark a scale gap, a missing between meters to kilometers. Figure 1 shows the resolution of the different instruments used to do measurements (Adirosi *et al.*, 2016; Gires *et al.*, 2014; Jaffrain & Berne, 2012; Kathiravelu *et al.*, 2016; Krajewski *et al.*, 2009; Mandapaka *et al.*, 2009; Michaelides *et al.*, 2009; Musy & Higy, 2014; Strangeways, 2010).

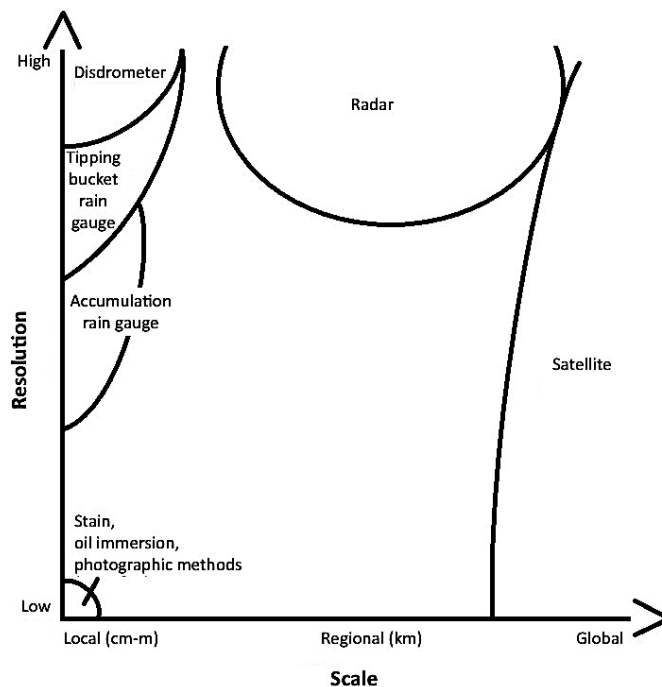


Fig. 1: Interpretation of literature showing a scale gap for rainfall measurements instruments.

Lidar means *Light Detection And Ranging*. It is an active remote sensing instrument, which sends a laser beam and measures the returning signal. Its range can be from some meters to several kilometers. It used in several field, like to do accurate Digital Elevation Model (DEM), but not only. As there is not only one type of lidar, we can make a large spectrum of studies using it, such as geological or atmospheric ones to cite only two possible applications. Over the years we have seen the development of low-cost lidar. They are more affordable, but they have a lower accuracy and resolution. (Beraldin *et al.*, 2010; Charlton *et al.*, 2009; Derron, 2016; Hudak *et al.*, 2009; Jaboyedoff *et al.*, 2012; Large & Heritage, 2009; Mallet & Bretar, 2007; Mariéthoz, 2016).

In general lidar working is based on calculating time between the sending and returning of signal, using several wavelengths from visible to infrared (IR). One of water's properties is to absorb infrared (Manap et al., 2009). Figure 2 shows the absorption spectra of water vapor. There is a strong absorption in the small wavelengths, which correspond to near-infrared (0.7-1.3 μm).

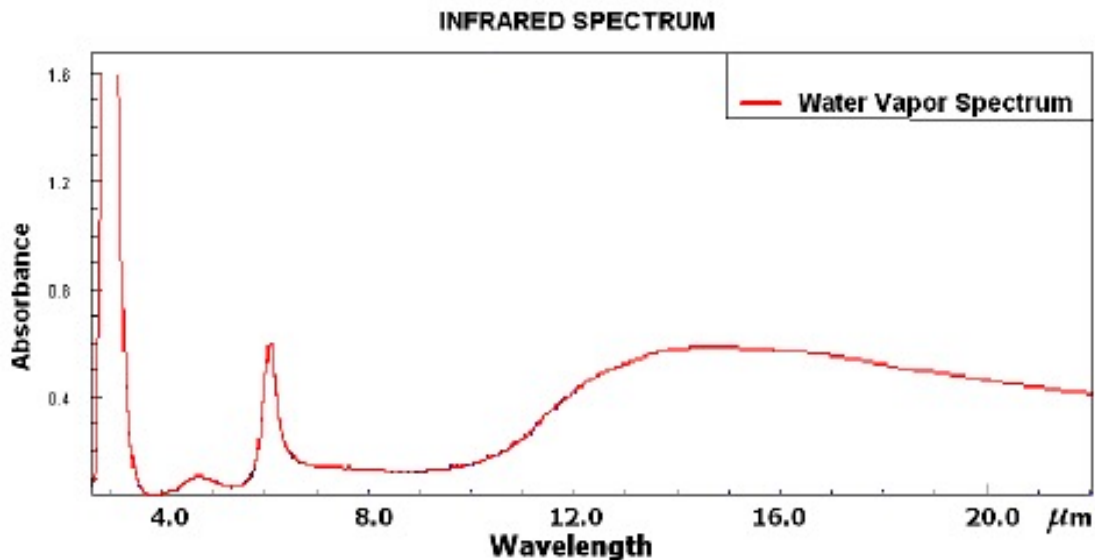


Fig. 2: Water vapor absorption spectra, modified from Manap et al., 2009

Therefore, theoretically we could expect, that a lidar working with infrared used during rainfall, to see its returning signal attenuated by raindrops. Using a terrestrial lidar during rainfall is something that is commonly avoided, but it could allow an unexpected application: another way to measure rainfall. In fact we could use the noise made by rain to estimate its rate. This could be interesting also because it could cover the scale gap implied with rainfall measurement instruments.

For this Master thesis, it has been decided to investigate the possibilities offered using a lidar and how it could be used for rainfall studies. The aim of this Master thesis is to investigate if a low-cost terrestrial lidar emitting pulses at an IR wavelength can be used to estimate rainfall rate. Doing this research has two objectives, which will guide through the work. The first one is to develop a simple theoretical framework, to assess if it is possible to estimate rainfall intensity with a low-cost lidar. The second one is to test theory with measurements. The goal with this research is to answer the following question: is it possible to estimate rainfall with a low-cost topographic lidar? The working hypothesis is that it is possible.

The study start with section 1 which is a literature review and allows having a simple theoretical framework and a view about what has already been done. Section 2 is about the methodology, the methods that are used and about in-situ measurements with a lidar. Later, section 3, presents results that are analyzed from lidar's data, and compared with rain gauge ones. Section 4, discusses issues that came from data. Section 5 is the conclusion in which the research question is answered.

1. Literature review

1.1. Lidar

LiDAR stands for *Light Detection And Ranging* and is a remote sensing instrument (Mariéthoz, 2016b; NOAA, 2015). Lidars were developed in the 1970s, a short time after lasers, which were made in 1950-1960 (Beraldin et al., 2010; Campbell & Whyne, 2011; Large & Heritage, 2009; Lillesand et al., 2008). Both of them evolved at the same time during the next decades. They had their accuracy and reliability improved with time. Since 1980-1990, they have been used in environmental sciences. Airborne lidars have been used since to make DEM (Jaboyedoff et al., 2012). Today, lasers are commonly used in several domains such as engineering or construction. Lidars have also become common in the environmental field, for which they have mainly been developed (Jaboyedoff et al., 2012; Large & Heritage, 2009; Lillesand et al., 2008; Mallet & Bretar, 2007). Lidar is a measurement instrument, which is widely used. Moreover, as it evolves with technique, it will become even more accurate (Jaboyedoff et al., 2012).

It is an active instrument, which means it sends a laser beam and measures the returning signal (Beraldin et al., 2010; Campbell & Whyne, 2011; Derron, 2016; Large & Heritage, 2009; Lillesand et al., 2008; Mallet & Bretar, 2007; Mandapaka et al., 2009; Mariéthoz, 2016b). It has different ranges possible, from 100m to 1km or even 10 km and more (Beraldin et al., 2010; Charlton et al., 2009). Calculating the range between captor and reflecting object is done with the following formula (Large & Heritage, 2009):

$$Range = \frac{Speed\ of\ light * Time}{2} \quad (1)$$

Lidar is a measurement instrument that sends waves, which are characterized by specific wavelengths. The later ones are from several divisions of the electromagnetic spectrum as visible light, infrared or ultraviolet (Derron, 2016; Mariéthoz, 2016a). Table 1 presents the wavelengths that are mainly used with lidars.

Table 1: Values of the electromagnetic spectrum, Mariéthoz, 2016a

Division of electromagnetic spectrum	Values limits
Ultraviolet (UV)	0.3 - 0.38µm
Visible light	0.38 - 0.72µm
Near infrared (NIR)	0.72 - 1.3µm
Middle infrared (MIR)	1.3 - 3µm
Far infrared (FIR)	7µm - 1mm

There are several types of lidars depending on their use, with different characteristics:

- Different sensors
 - Terrestrial/topographic lidar: they are used to characterize complex objects such as buildings or rock wall for example (Lillesand et al., 2008). It works mainly with NIR (Portland State University, s.d.).
 - RAMAN lidar: "*Raman lidars have been used for high resolution vertical profiling of water vapor within the troposphere since the 1970s.*" (Dinoev et al., 2013).

They are used to make atmospheric profiles of water vapor (Brocard et al., 2013; Dinoev et al., 2013), temperature, aerosols and other gases. It works as a terrestrial lidar, but with different wavelengths, it goes from IR to UV (Portland State University, s.d.).

- Different vectors
 - Terrestrial lidar: it is a ground-based instrument (Derron, 2016; Jaboyedoff et al., 2012; Large & Heritage, 2009; Lillesand et al., 2008; Mallet & Bretar, 2007; Mariéthoz, 2016b), which has a high resolution (Jaboyedoff et al., 2012). It is the most common vector to measure rainfall, as RAMAN lidar are ground-based (Westbrook and al., 2010).
 - Airborne lidar: it goes on anything, which can fly such as airplane, helicopter or drone (Derron, 2016; Jaboyedoff et al., 2012; Large & Heritage, 2009; Lillesand et al., 2008; Mallet & Bretar, 2007; Mariéthoz, 2016b; NOAA, 2015). They allow accurate DEM to be generated with topographic lidar (Large & Heritage, 2009; Lillesand et al., 2008).
 - Satellite lidar: the first one was with the Apollo 15 mission. (NTRS, 2010). The agency uses some of them on several missions (Mallet & Bretar, 2007).
- Different signal recording
 - Multi-echo or multiple pulse: it records the first and last pulses (Mallet & Bretar, 2007). It is the most common recording (Lillesand et al., 2008; Mallet & Bretar, 2007).
 - Full-waveform: "*Full-waveform lidars digitize the continuous returning signal at a uniform sampling frequency*" (Lillesand et al., 2008, p.722). It allows better characterization of forms. For example, it is possible to do an analysis of the canopy (Lillesand et al., 2008). "*Since 2004, [...] full-waveform lidar have appeared with the ability to record the complete waveform of the backscattered signal echo*"(Mallet & Bretar, 2007). It is mainly used on airborne platform but also on satellites (Mallet & Bretar, 2007).

Lidar is a measurement instrument that has the following advantages. It can collect data fast (Jaboyedoff et al., 2012) and takes more than thousands of measurements per second (Large & Heritage, 2009; Mallet & Bretar, 2007; Mariéthoz, 2016b). The information obtained is set on a 3D point cloud (Beraldin et al., 2010; Hudak et al., 2009; Jaboyedoff et al., 2012; Mallet & Bretar, 2007). It has a high resolution, from metric to decametric for airborne lidar and from centimetric to millimetric for terrestrial ones (Jaboyedoff et al., 2012) and accuracy (Dinoev et al., 2013; Hudak et al., 2009; Jaboyedoff et al., 2012; Mallet & Bretar, 2007). Airborne lidar are used to do precise DEM on wide surfaces sometimes with difficult access or dangerous areas (Large & Heritage, 2009; Lillesand et al., 2008).

However, there are characteristics that could be either an advantage or disadvantage. That is the case of the georeferencing of images and point clouds (Jaboyedoff et al., 2012; Lillesand et al., 2008). This ability can be useful, but is not used every time, and should be made further by aligning point clouds, with other ones, DEM or images (Derron, 2016; Jaboyedoff et al., 2012).

In fact, if we work with something precise like the monitoring of a landslide, we will use the registration to see exactly how the ground moved between scans. In other cases, like this thesis, it is not useful. Another characteristic, which is both an advantage and a disadvantage, is the high amount of data collected (Jaboyedoff et al., 2012).

It is a drawback because it needs powerful computer to treat data, as it can have millions of points (Jaboyedoff et al., 2012). Nevertheless, it could be seen as an advantage because that characteristic provides high accuracy.

Its main disadvantage is its expensive price, which does not make possible a public utilization (Charlton et al., 2009; Derron, 2016; Large & Heritage, 2009; Mariéthoz, 2016b). It is an instrument mainly used by those who can afford it, such as governments like the USA or Switzerland, which use airborne lidars to do accurate DEM of their country (Derron, 2016; Lillesand et al., 2008).

Lidars allow us to better know and understand our environment. For this, they are used in different fields. Some of them are given as examples in table 2. We can see that measuring rainfall is one of the uses. As said before, RAMAN lidar is used to do rainfall measurements. In fact, RAMAN lidar works the same as a terrestrial one, but with different wavelengths. That allows focusing on different scattering and to take into account what could be a disturbance for a terrestrial lidar.

RAMAN lidar is already used for research with rain. Westbrook and al. (2010) used two lidars with different wavelengths and tried to show scattering profiles, to prove differences in absorption depending the size of the raindrop. Later, Lolli and al. (2013) took Westbrook methodology and repeated the experiment, but with a concentration on Mie scattering, and using different lidar and wavelengths. In the case of the article of Dinoev et al. (2013) and Brocard et al. (2013), the study is to see if data obtained with a lidar is similar to the ones obtained with rain gauges. Their goal is to have continuous data that allows real time following of the atmospheric humidity.

Table 2: Different uses possible of lidar

Field	Application(s)	References
Geomorphology	- Landscape changes	- Campbell & Whyne, 2011; Large & Heritage, 2009
Meteorology	- Water vapor profiles (high temporal resolution of data) - Atmospheric, vertical profiles - Rain studies	- Brocard <i>et al.</i> , 2013; Dinoev <i>et al.</i> , 2013 - Campbell & Whyne, 2011; NASA, 2016 - Lolli <i>et al.</i> , 2013; Mandapaka <i>et al.</i> , 2009; Westbrook <i>et al.</i> , 2010
Geology	- Landslide/Rockfall/Debris-flow detection and characterization, mapping, modeling and monitoring - Fault monitoring	- Jaboyedoff <i>et al.</i> , 2012 - Hudak <i>et al.</i> , 2009
Forestry	- <i>Modeling the shapes of individual tree crowns in lidar point clouds</i> - Vegetation cover - Canopy analysis - Forestry ecology and wildlife	- Lillesand <i>et al.</i> , 2008; - Campbell & Whyne, 2011; Large & Heritage, 2009; Mallet & Bretar, 2007 - Hudak <i>et al.</i> , 2009 - Hudak <i>et al.</i> , 2009
Altimetry	- DEM - Determination of terrain elevation - High resolution DEM - Topography	- Campbell & Whyne, 2011; Jaboyedoff <i>et al.</i> , 2012; Large & Heritage, 2009; Lillesand <i>et al.</i> , 2008; - Lillesand <i>et al.</i> , 2008 - Jaboyedoff <i>et al.</i> , 2012 - Campbell & Whyne, 2011
Bathymetry	- Measuring depth in water	- Lillesand <i>et al.</i> , 2008; Mallet & Bretar, 2007
Archeology	- Survey	- Large & Heritage, 2009
Astronomy	- Atmospheric studies from space (LITE)	- NASA, 1994
Transport	- Autonomous vehicles	- Rasshofer <i>et al.</i> , 2011; Velodyne LiDAR, 2016a;
Urbanism	- Knowing building densities and footprint, as well as urban structures. - Highway, pipeline and wireless communication planning	- Campbell & Whyne, 2011 - Campbell & Whyne, 2011
Risk management	- Flood modeling - Floodplain mapping - Landslide modeling and monitoring	- Large & Heritage, 2009 - Campbell & Whyne, 2011 - Jaboyedoff <i>et al.</i> , 2012

1.2. Rainfall measurements

Rain had been measured since the 4th century BC in India or during 13th century in China (Musy & Higy, 2014; Strangeways, 2010). In Europe, measurements have been made since the 17th century (Strangeways, 2010). Benedetto Castelli did the first measurements on the continent in 1639. Later, Christopher Wren developed the ancestor of the tipping bucket rain gauge. Then Richard Towneley made the "*first continuous record of rainfall*" (Strangeways, 2010) for 33 years. After, Thomas Barker conducted 59 years of measurements and had put in evidence the "*need to measure for a long time to get an accurate mean*" (Strangeways, 2010). In Switzerland, the first measurements are from 1863 (Musy & Higy, 2014). Now there are almost 500 measurement stations in the country (260 automatic measurement stations, 233 manual measurement stations; MeteoSwiss, 2014b).

Rainfall measurement is complex, as it has to deal with obstacles such as topography or simply the movement of precipitations (Musy & Higy, 2014). Furthermore, there is the spatiotemporal variability of precipitations (Gires et al., 2014; Jaffrain & Berne, 2010; Lewandowski et al., 2009; Mandapaka et al., 2009; Michaelides et al., 2009), which complicates rainfall estimation. Rainfall can be very short or on the opposite very long (Mandapaka et al., 2009). Rainfall changes from the different climatic regions but also at the different scales (Jaffrain & Berne, 2010; Mandapaka et al., 2009). In fact, if we take a radar image, one pixel can have an area with rain and another without any, which makes interpretation difficult (Krajewski et al., 2003).

There are several ways to measure rainfall. One of them is with intensity, which can be calculated with the following formula (Musy & Higy, 2014):

$$Rainfall\ rate = \frac{Rainfall\ [mm]}{Time\ [h]} \quad (2)$$

1.2.1. Measurement instruments

There are several instruments used to measure rain. There are different rain gauges that "*measure an incremental mass of accumulated rainfall as a function of time*" (Michaelides et al., 2009). Or disdrometers for which "*rainfall rate and rain accumulation are computed from the summation of drops counted and sized over the sensing area per unit time*" (Michaelides et al., 2009). The latter does not only measure rainfall rate, it gives also information about raindrop size and velocity (Adirosi et al., 2016; Michaelides et al., 2009). These two are the most common devices for active and direct measurements (Gires et al., 2014). There are others, such as weather radar or satellites, which are remote sensing and indirect measurements (Adirosi et al., 2016; Gires et al., 2014; Jaffrain & Berne, 2012). All of these instruments are explained in the following sections.

1.2.1.1. Rain gauges

1.2.1.1.1. Accumulation rain gauge

It is the simplest instrument to use. It can be any graduated cylinder, which allows knowing the height of rainfall between readings (Strangeways, 2010). An important point is the choice of the emplacement of the instrument. In fact, it should be representative of an area and with no direct obstacle (Musy & Higy, 2014). In addition, the rain gauge should be placed at a height of 1.5m (Musy & Higy, 2014).

Rain gauges are widely used in the world, so there had been a standardization of methods. Every country has its own rules about its dimensions and installation of the instrument.

This is used to minimize differences between measurements and allows comparison between rain gauges from different places. In Switzerland, it should be an instrument type Hellmann (fig 3) and on a surface of 200cm² (Musy & Higy, 2014).



Fig. 3: Accumulation rain gauge type Hellmann, ©BLET-climat, 2017.

The measurement is representative of a local scale, few square meters around the instrument (Gires et al., 2014; Michaelides et al., 2009). The main advantage is that it is simple to use (Michaelides et al., 2009). Its resolution is high in time, but it is a point measurement in space (Michaelides et al., 2009).

1.2.1.1.2. Tipping bucket rain gauge



Fig. 4: Tipping bucket rain gauge used by MeteoSwiss, ©MeteoSwiss, 2014c.

It is an instrument composed of a double-sided cylinder, which is filled using a mechanism of a tipping bucket (Strangeways, 2010). Rainfall fills one side, then is dumped in the container as the other side of the tipping bucket is filled. Figure 4 is an example used by MeteoSwiss.

It is used at a local scale and provides data with a high resolution. It is the most common instrument used (Ciach, 2003; Strangeways, 2010).

1.2.1.1.3. Pluvimates

It is an instrument similar to the accumulation rain gauge, but there is a data logger at the end of the container, which records the number of drops. It can be decided which time resolution is used, from days to seconds, which is the higher resolution. This data logger is made by UK society *TinyTag*. This is a specific rain gauge used for precise measurement (Driptych, s.d.a; Driptych, s.d.b).

1.2.1.2. Disdrometer

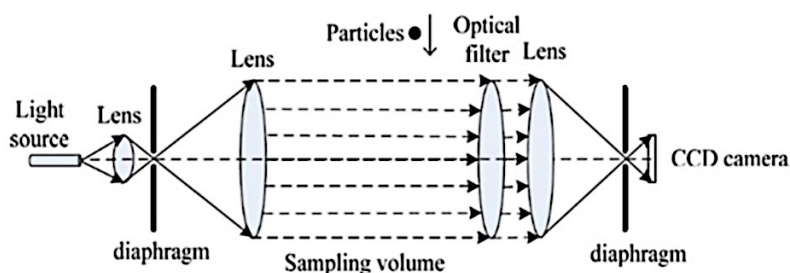
Disdrometer is an instrument accurate that allows precise raindrop counting and size measuring (Kathiravelu, 2016). However, it is still quite marginal. There are several types, using different approaches to measure rainfall.

It is used for a local scale, with high-resolution data and detailed information (Michaelides et al., 2009).



Fig. 5: Impact disdrometer, ©Distromet.

Impact disdrometer (fig 5) uses the impact made by drops when they fall, to calculate size and count drops (Kathiravelu, 2016).



Optical disdrometer (fig 6) uses a beam that is crossed by precipitations, which allows calculations (Jaffrain & Berne, 2012; Kathiravelu, 2016).

Fig. 6: Processing of an optical disdrometer, ©Kathiravelu, 2016.

Disdrometers are widely used to collect information about raindrop size distribution (DSD). An example is the study made by Jaffrain & Berne beginning of 2010, at EPFL. They used a PARSIVEL electromechanical disdrometer to obtain measurements. The latter allows them to collect DSD measurements and quantities derived from them; as much as precipitations types information.

1.2.1.3. Radar



Fig. 7: Radar de la Pointe de la Plaine Morte, ©MeteoSwiss, 2016.

Radar imagery is developed since 1960 (MeteoSwiss, 2012). It gives information about meteorology, especially concerning precipitations, which is complementary with rain gauge data (Benoit & Mariéthoz, 2017). It provides indirect measurements (Adirosi et al., 2016; Jaffrain & Berne, 2012). It "measures quantities related to the electromagnetic properties of falling hydrometeors such as the radar reflectivity factor Z " (Jaffrain & Berne, 2012).

Radar is used to do real time precipitation monitoring (MétéoSwiss, 2012). It is an active remote sensing instrument as it sends laser beam and processes returning signal. It is an important instrument in term of size, as shown with figure 7.

It could tell information for large, regional, scale such as 200-300 km (Adirosi et al., 2016; Jaffrain & Berne, 2012; MeteoSwiss, 2012; Musy & Higy, 2014). However, sometimes it can also go to local scale, such as 5 km or 100m (Benoit & Mariéthoz, 2017; Gires et al., 2014). It has a high resolution (Jaffrain & Berne, 2012; Musy & Higy, 2014). It can localize and monitor precipitations and is used for forecasting and nowcasting (Casieri et al., 2016; Musy & Higy, 2014). All these elements make the radar information precious (Andra et al., 2002; Demir & Krajewski, 2013).

Radar data can be used after processing in different models, climatic or hydrologic (MétéoSwiss, 2012). This involves the need of accuracy from data (Adirosi et al., 2016). However, there are some uncertainties possible during the conversion of data to precipitation amount (Adirosi et al., 2016). The conversion process is generally done using equation (3):

$$Z = a * R^b \quad (3)$$

This is a power-law relation between Z , radar-reflectivity, and R , rain rate (Berne et al., 2012; Jaffrain & Berne, 2012; Uijlenhoet et al., 2003). A and b are parameters, which depend in particular of climatological conditions and DSD (Jaffrain & Berne, 2012).

In addition, there is a scale gap when comparing radar data to point measurements, which is problematic (Gires et al., 2014). However, a geostatistical framework exists to bridge it, but it tends to not take into account or underestimate the rainfall variability and extremes (Gires et al., 2014). Whereas, "*extremes of rainfalls exhibit a power law behavior*" (Gires et al., 2014).

Radar utilization is restricted by its expensive cost. However, it is considered as a common measurement instrument (Gires et al., 2014), as it is mostly used by countries that can afford it (Benoit & Mariéthoz, 2017).

1.2.1.3.1. Raindrop size distribution

Raindrop size distribution (DSD) is defined as "*the number of raindrops in a given volume of rainfall*" (Berne et al., 2012). It is the result of microphysical and dynamical processes, which occur during a rainfall (Adirosi et al., 2016; Berne et al., 2012). "*[DSD] is a convenient statistical way to summarize the variety of drop sizes encountered*" (Berne et al., 2012). This is an important rainfall characteristic, which impacts mainly remote sensing measurements (Adirosi et al., 2016; Berne et al., 2012; Jaffrain & Berne, 2010).

As seen previously, this is an issue with radars (Berne et al., 2012; Jaffrain & Berne, 2012). There is the rainfall spatial variability, in particular the small scale variability, that influence a and b parameters (from power-law, equation (3); Jaffrain & Berne, 2012).

This brings uncertainties as there could be a major difference between ground measurements (rain gauge, disdrometer) and a radar pixel (Jaffrain & Berne, 2012). Whereas there is rainfall variability, there is DSD variability (Jaffrain & Berne, 2010; Jaffrain & Berne, 2012; Macke & Großklaus, 1998).

Another noteworthy point about DSD is the fact within "*rainrates below 10mmh^{-1} [...] since rainfall rates and particles sizes are essentially uncorrelated below this value*" (Macke & Großklaus, 1998). This is interesting, because it puts a limit from which rainfall intensity and DSD are correlated.

1.2.1.4. Satellites

Some missions are used for precipitation monitoring as Tropical Rain Measuring Mission (TRMM) or Global Precipitations Measurement (GPM). These missions use several instruments, including radars and passive microwaves captor, to obtain data. They give information to a global scale (Benoit & Mariéthoz, 2017; Michaelides et al., 2009). Their resolution is medium (Michaelides et al., 2009 says high; Benoit & Mariéthoz, 2017 says low). The advantage is that it gives a global image of precipitations (Michaelides et al., 2009). It can use both active and passive sensors (Michaelides et al., 2009). It is another common way to obtain data (Gires et al., 2014).

1.2.1.5. Telecommunication system

This method to estimate rainfall is unusual and it differs from others, as it is another approach for measurements: it diverts from the initial use as it uses noises caused by rainfall.

In fact these systems are perturbed when it rains, thus it is possible to see precipitations using signal disturbances. It will use the created noise to determine and estimate rainfall. As the telecommunications systems are dense, sometimes it can provide more information than the usual instrument measurements (Musy & Higy, 2014).

It is for a regional scale, with a medium resolution (Musy & Higy, 2014). This method is interesting, as it looks similar to the one developed in this study.

1.2.1.7. Others

Other methods were used before, but can still be used. They are manual and work for small period of time. The following methods are two examples of them.

Stain method: the scale is the size of the paper used, with a low resolution. The principle is to use a chemically treated paper and put it under the rainfall. Raindrops impacts leave a stain, which can be measured and counted (Kathiravelu et al., 2016).

Oil immersion: the scale is small, with a low resolution. The principle is to collect raindrops in a glass filled with viscose liquids, like two oils having different densities. That allows measure drop size and counts them with a camera or microscope (Kathiravelu et al., 2016).

1.2.2. Measurement errors

Some errors can affect data collected. They can be divided into several categories depending on the origin of the element causing errors.

Environmental: they come from the environment itself. All these errors lead to an underestimation of rainfall rate (Musy & Higy, 2014).

- For accumulation and tipping bucket rain gauge: it could be the effect of the wind, which prevents drops from falling in the instrument (Kathiravelu et al., 2016; Michaelides et al., 2009; Musy & Higy, 2014; Strangeways, 2010). There is also evapotranspiration that brings error (Michaelides et al., 2009). On the opposite, when there is a heavy rain, containers can be full and there are splashes possible (Kathiravelu et al., 2016; Michaelides et al., 2009; Musy & Higy, 2014). In the case of the tipping bucket rain gauge, animals and insects can also bring errors (jamming the funnel) (Michaelides et al., 2009).
- For radar: there are some terrain effects, which affect data, such as ground returns or beam overshoot. Additionally, there are disturbances when rain is mixed with some ice (Michaelides et al., 2009).
- For impact disdrometer: heavy rain can create noise that provides errors (Kathiravelu et al., 2016).
- On the one hand, these errors can be systematic and be corrected with algorithms as for the effect of the wind or the evapotranspiration (Balin, 2016; Musy & Higy, 2014). On the other hand, they can be random and cannot be predicted. All of them can either tend to underestimate or overestimate rainfall (Balin, 2016).

Instrumental errors: they come from the instrument itself.

- For tipping bucket rain gauge: for example an asymmetry of the mechanic (Michaelides et al., 2009). Or internal clock disturbance for instruments that have a clock (Michaelides et al., 2009). There could be a time lapse in the process between the dumping and filling again (Michaelides et al., 2009; Musy & Higy, 2014).
- For radar: it needs to transform intensity returns into rainfall, which can lead to errors and an uncertainty of measurements (Musy & Higy, 2014).

- These errors can be systematic and corrected with algorithms, such as the effect of the wind or the evapotranspiration (Balin, 2016; Musy & Higy, 2014).

Otherwise, they are random and cannot be predicted. All of them can either tend to underestimate or overestimate rainfall (Balin, 2016).

With all the information collected in literature, it is possible to see the range of knowledge, concerning lidar and rainfall measurement.

Regarding lidar, what stands out is the fact that this instrument is mainly used in environmental field. Moreover, the different sensors (terrestrial and RAMAN) have their specific use. With the description of characteristics, we can say that the initial use of terrestrial lidar is not to measure rainfall. However, with its properties, it is possible to divert this use to try new methodology.

As seen, for rainfall measurements, a gap is already perceived when comparing remote sensing data to ground level ones (Gires et al., 2014). However, when regarding instruments, we have on the one hand, big scale instrument for a region or even a continent (from kilometer to thousands of kilometers; radars and satellites). On the other hand, instruments, which focus at smaller scale, local (meters). All this is resumed with figure 8 above. We have accurate instruments able to measure at each of these different scales. They provide precise and high-resolution data. Nevertheless, it is possible to see that there is a scale missing. In fact, between them, from meters to kilometers we do not have knowledge available, because we do not have working instruments at this scale (Krajewski et al., 2003). Moreover, this is the reason why lidar can be used: because of the range of lidar that is in this missing scale.

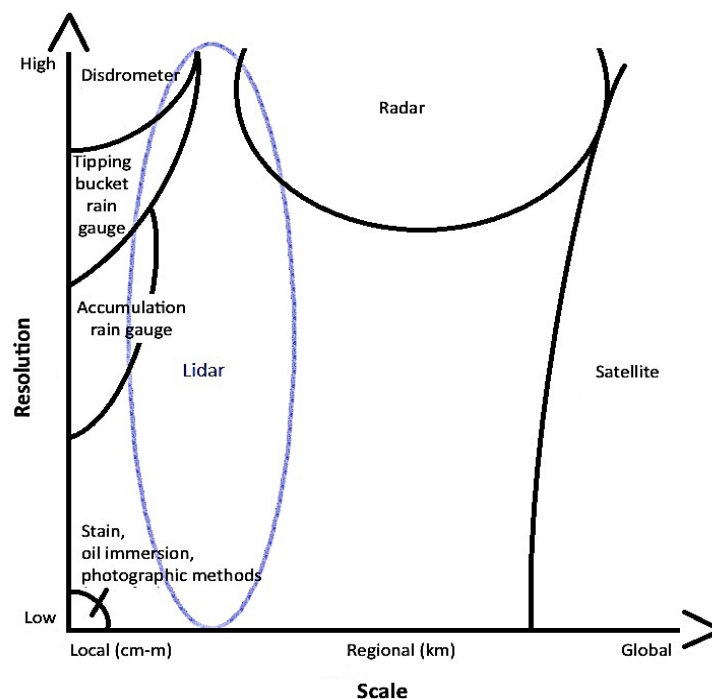


Fig. 8: Interpretation of literature

However, to really bridge the scale gap, we need to perform an expensive experiment with lidars, rain gauges, radars and satellites observing the same rainfall system for a

considerable time period. Such an experiment should be designed so that there is some overlap in the scales observed by different instruments. (Mandapaka et al., 2009).

2. Methodology

This study will estimate rainfall from lidar data. I will use a low-cost terrestrial lidar to reach this goal. In general, people tend to avoid doing measurements with a lidar during a rainfall, because it creates disturbance; rainfall is a noise in these data. I will divert the initial use of this lidar, to work with the noise created by rain.

The principle of measurements is the following: scans are made using a low-cost lidar, working in IR, during several rainfall events. The study location is the same for all events, allowing comparison between scans. There is a focus on a wall, to help concentrating analyses. In addition, there is a rain gauge to compare and validate lidar data.

2.1. Measurements location

The following criteria were set to find an appropriate building. Later analyses will be focused on one wall, so these criteria are important and can be justified as follow:

- No windows in order to avoid unintended reflections and to maximize the strength of the backscattered signal.
- Homogenous wall to help differentiating the target surface from the surrounding environment.
- Presence of eaves to avoid humidity on the wall, which could bring errors.
- No obstacles around or too near, as measurements will be made with a distance of approximately 20 meters between the wall and the lidar.

The location is at Huémoz, near Villars-s-Ollon in canton of Vaud, localized on figure 9 (A). Measurements are made on the north wall of the house, at an approximate 20 meters distance. There is no obstacle between the wall and the lidar.

The wall selected for further testing (fig 9B) fulfills most of the quality criteria detailed above. However, the wall is not entirely homogenous, as there is two distinct materials. Indeed, the upper part which is in the red triangle, is light brown wood. It is expected that this part backscatter more signal as it is a light color and smooth material. On the contrary, the lower part which is in the yellow square, is black expanded polystyrene. Because of the material and color, it is expected that the signal will be more absorbed. As the dark colors tend to absorb signal, less will be returned. The material texture, which is rough, will accentuate the phenomenon of absorption.

Knowing this, the scan has been cut in different parts, allowing focus for analyses of the mean intensity. First, the wall is cut from the scan, figure 9 (E). Then, the wall is split into two distinct parts, because of their distinct interactions with rain: the upper part of the wall (fig 9C) and the lower part of the wall (fig 9D). The upper part of the wall is the smallest part analyzed, as there are fewer points than for the lower part of the wall. However, this part corresponds to the more reflective part of the scan. In addition, the upper part of the wall is the part for which it is sure that there is absolutely no humidity due to rainfall. The focus on the wall is here to help to concentrate on the intensity: it gives results for a smaller part, but it should make it easier to see a difference between scans. Secondly, the scan is analyzed as a whole, without focusing on a particular target (fig 9F). This has been chosen because it is easier to analyze, as there is no cropping. However, the number of points taken into account is much bigger, which means that the mean intensity value calculated can be reasonably the same between scans. This can show less difference between scans.

Figure 9 (G) shows the situation of measurements instruments: the red point is the position of the lidar, the red line the wall scanned and the blue point corresponds to the spot of the rain gauge.

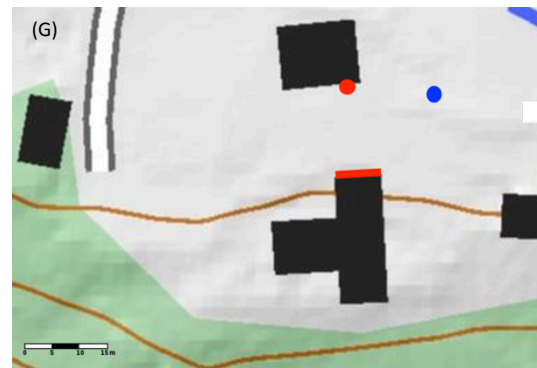
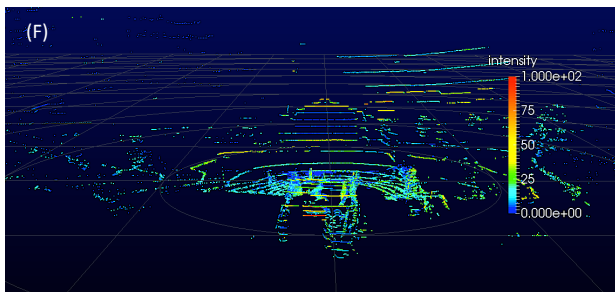
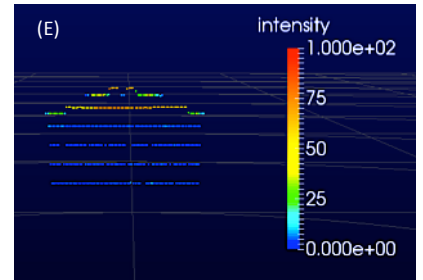
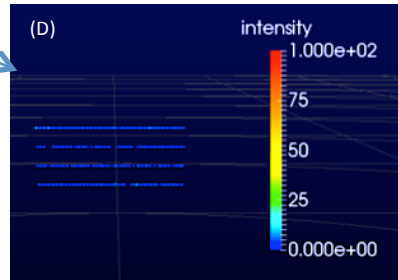
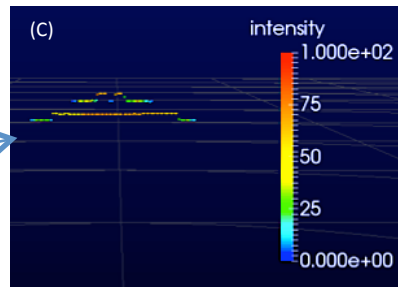
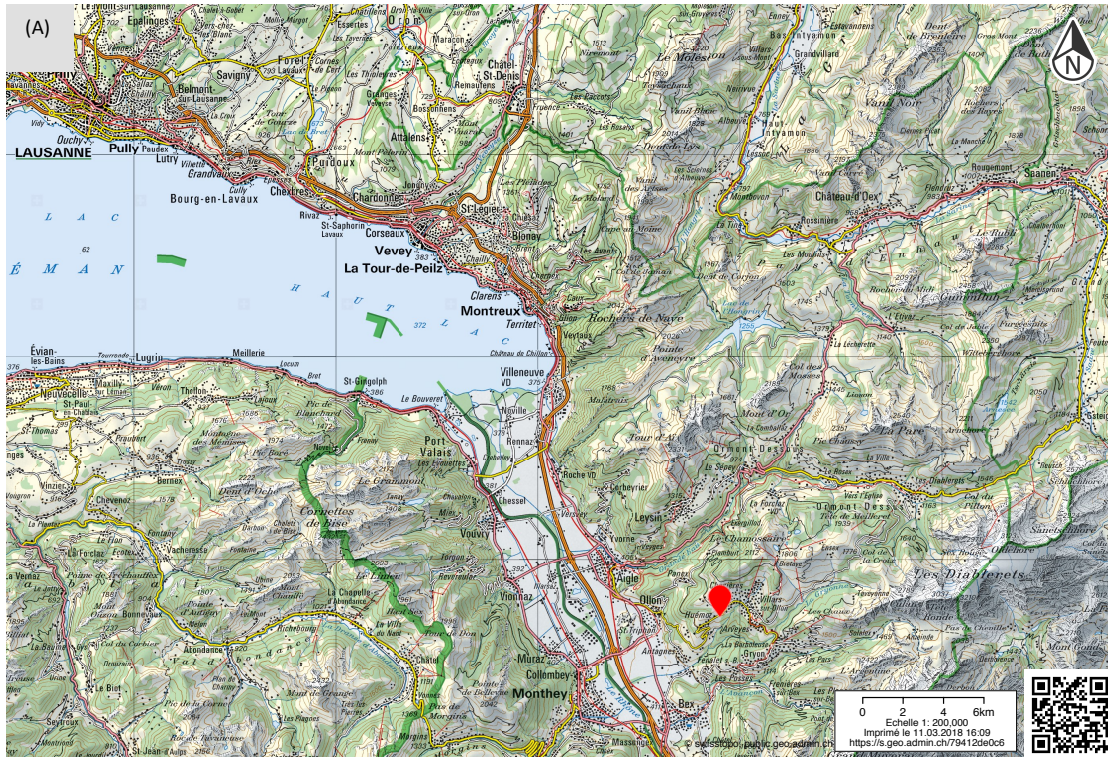


Fig. 9: Measurements localization, ©SwissTopo, scale 1:200 000 (A). Wall used for measurements (B) with corresponding focused cuttings for the scan (screenshots): the up part of the wall (red triangle, C), the bottom part of the wall (yellow square, D) and the entire wall (E). Screenshot of the 9th July 2017, 11:46 pm entire scan (F). Localization of instruments, modified from ©Guichet cartographique Etat de Vaud, scale 1:500 (G).

2.2. Instruments

Several instruments are implied in the present experiment. In order to better understand their operating principle, these instruments are briefly presented hereafter. In addition, I also explain how the raw data are preprocessed prior to being combined to measure rainfall.

2.2.1. Lidar

Figure 10 shows the lidar used for measurements: the Velodyne LiDAR Puck VLP-16. It is a terrestrial low-cost lidar, approximately 20 times cheaper than the usual ones. It is a ground-based instrument, with multiple pulse recording.

Its characteristics are the following (Velodyne, 2016b):

- Laser class 1 (safe)
- Horizontal field of view: 360°
- Vertical field of view: 30°
- Number of lasers: 16
- Number of measurements: ~300'000 points per second
- Rotational speed: 5-20 rotations per second
- Range: about 150 meters
- Wavelength: 903nm (NIR)



Fig. 10: Lidar VLP-16 used for measurements.

Further details about lidar's specifications can be found in appendix D.

The fact that it measures in the IR is an advantage, because it is assumed that this wavelength will interact with raindrops. This will permit to see an attenuation of lidar's signal, as water absorbs IR (Manap, 2009).



Fig. 11: Set-up of lidar, view from in front (A) and view from inside the shelter (B), ©D.Perrin.

Figure 11 shows the set-up of the lidar. It was positioned after the roof of the shelter. The emplacement allows the lidar to be entirely under the rain.

For the measurements, several scans were done at different dates and times. First, when there was good weather to have a reference, to see how it works. In total, there are five dates and 20 reference scans. Second, when there is an event of rainfall. This rainfall event's part represents nineteen events and 355 scans. Then, reference data is also here to compare with rainfall event data. This shows if there is an attenuation of the signal.

Scans last 2 minutes, because during this interval rainfall intensity should not change much. It is also to have a long enough recording to compare with rain gauge data. Measurements were made at different periods, from morning to night. Indeed the goal is to do as many scans as possible when it rains. Moreover, as it is an active measurements instrument, it works during day and night.

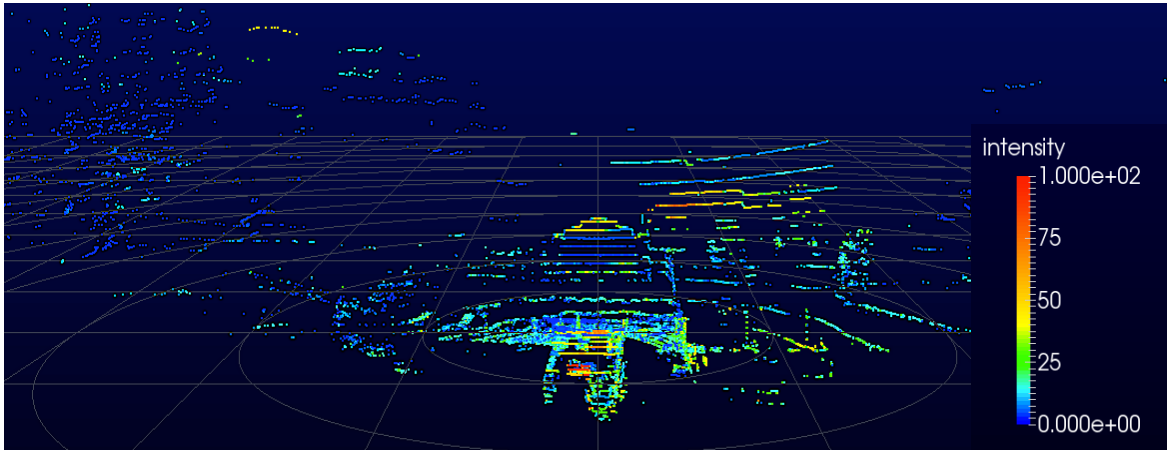


Fig. 12: Screenshot of the 11th August 2017 scan.

Figure 12 is a screenshot of the 11th August scan. This figure shows the interface of Velodyne's program, Veloview, during a scan. It shows the different features explained above: we can see 360° and each line represents one of the lasers.

Information is given within the scan as listed below (Velodyne, 2016b) and shown in figure 13:

- Coordinates: X, Y and Z, centered on the lidar.
- *Intensity*: of the returning signal. The intensity represents the reflectivity of an object. In this study, values are from 1 to 100. The lower values correspond to black, blue on the scan. The higher values correspond to white for reflective diffuse reflector, red on the scan.
- *Laser_id*: tells which laser of the 16 sent the beam.
- *Azimuth*: corresponds to the vertical angle of the beam, from -30° to 30°.
- *Distance_m*: corresponds to the distance between lidar and a coordinate point
- Time: tells about when the beam is sent and the interval between first shot and first firing sequence.

Points_m_XYZ:0	Points_m_XYZ:1	Points_m_XYZ:2	intensity	laser_id	azimuth	distance_m	adjustedtime	timestamp
0.066757821	17.38601112	0.911168993	3	3	22	17.41	1787793766	1787793766
0.069230184	17.24598312	1.508840203	3	5	23	17.312	1787793771	1787793771
0.074645422	17.10736275	2.100539923	4	7	25	17.236	1787793775	1787793775
0.076883748	16.94263077	2.683476925	4	9	26	17.154	1787793780	1787793780
0.127343446	17.37169266	0.910436273	4	3	42	17.396	1787793821	1787793821
0.129489288	17.2536068	1.509537458	3	5	43	17.32	1787793826	1787793826
0.134423167	17.11493874	2.101515055	4	7	45	17.244	1787793831	1787793831
0.139175534	16.96593857	2.687231302	6	9	47	17.178	1787793835	1787793835
0.188175693	17.38911629	0.911378324	3	3	62	17.414	1787793877	1787793877
0.189824358	17.26301003	1.510408998	4	5	63	17.33	1787793881	1787793881

Fig. 13: Information obtained with a scan, from the 7th April 2017

From all this information, the intensity is the main interest for the study. It is this element that is analyzed later with Matlab and that shows the interaction of the lidar with rain. Coordinates are used for the cropping, and distance is used for a later analysis.

2.2.2. Rain gauge

In parallel of lidar use, data is collected from a rain gauge, the Pluvimate high-resolution rainfall logger, figure 14. It is installed near the measurements area (blue point on fig 9G). These data permit comparison and validation of lidar data.

Characterization of the Pluvimate (Driptych, s.d.a):

- Composition: a 50mm high-anodised aluminum funnel of 127mm diameter, with a 110mm diameter and 400mm high plastic tube (fig 14A). A data logger is located centrally on the base of the tube (fig 14B).
- Resolution of the logger: 0.01mm of height
- Rain drop dimension: 0.01mm
- Time stamp of the logger: from 1 second to 11 days. For this study it was 30 seconds.
- Maximum recordable number of drops per interval: 16'348

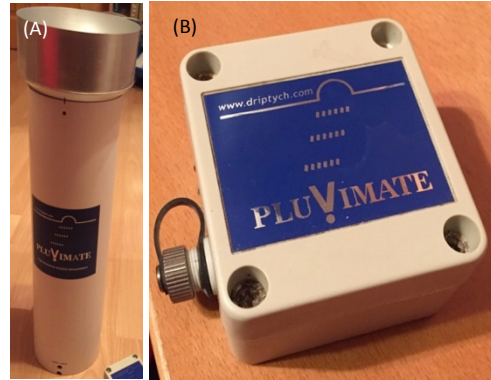


Fig. 14: Pluvimate tube (A) and data logger (B), ©D.Perrin.

The Pluvimate works like a standard rain gauge, as the rainfall accumulates in the tube. Its specification is the data logger, which counts drops falling from the funnel. There are small holes at the bottom of the tube, to evacuate water. This keeps the logger out of water and make possible continuous recording.

It is useful because it permits to have the real rainfall rate during events. In fact, knowing the temporality of measurements and the dimension of drop, it is possible to know the rainfall rate during each scan with the equation (4) following.

$$Rain\ intensity = Nb\ of\ raindrops * \frac{0.01}{Interval\ of\ time\ between\ measurements} * 3'600 \quad (4)$$

With:

Rain intensity, which is the rainfall rate searched.

Nb of raindrops corresponds to the number of raindrops recorded during the time stamp.

Interval of time between measurements, which is the interval between two records. In the case of this study, it corresponds to 30 seconds.



Fig. 15: Entire set-up, ©D.Perrin

Figure 15 shows the set-up in its ensemble. The red line is the wall scanned; the red dot is the localization of lidar. There is approximately 20m between the wall and the lidar. The blue dot is the rain gauge, placed about 20m from the lidar.

2.3. Data cleaning

2.3.1. Interpolation

Lidar scans were made for 2 minutes, the beginning was at second 00 or 30. To correspond to this timing, rain gauge data was interpolated. Equation (5) is used,

$$\text{Rain intensity}_2 = \text{nb of raindrops}_1 * \% \text{ of scan duration}_1 + \text{nb of raindrops}_2 * \% \text{ of scan duration}_2 \quad (5)$$

With:

*Rain intensity*₂, which is the intensity after interpolation.

*Nb of raindrops*₁ corresponds to the recorded number of raindrops during the first time stamp.

*% of scan duration*₁ is the percentage of time of the first time stamp that is part of the scan.

*Nb of raindrops*₂ corresponds to the recorded number of raindrops during the second time stamp.

*% of scan duration*₂ is the percentage of time of the second time stamp that is part of the scan.

The way of doing this could have brought incertitude for interpretation, because it changes the mean value of rain rate. However, it is assumed that the difference found is negligible since on average, the change was small; it was 0.01mm/h per 2 minutes. The biggest difference before and after interpolation is 11.1mm/h for a scan.

2.3.2. Scan issues

During the scans, it has been noticed that some elements seemed to perturb data collecting. First, figure 16 is a scan being done during a summer night, the 9th July with no problem on data.

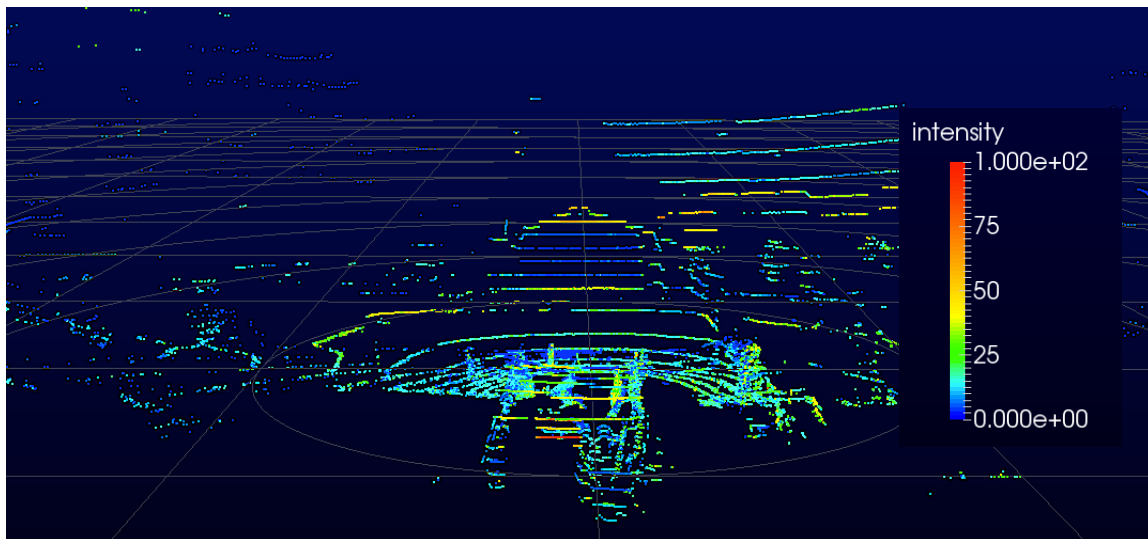


Fig. 16: Screenshot of the 9th July scan, 11:46pm.

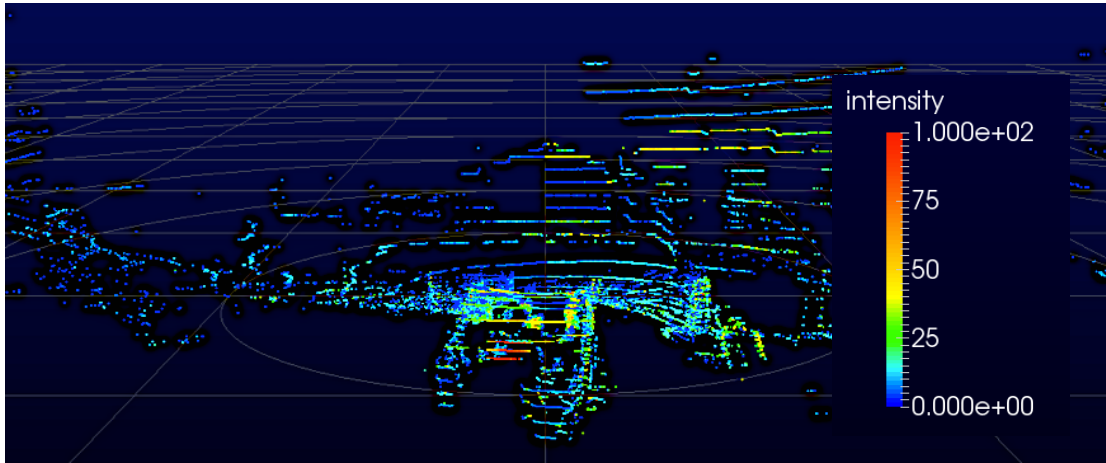


Fig. 17: Screenshot of the 24th August 2017, 2:33 pm.

The first interference was the fact that some heavy rainfall have created a curtain in front of the lidar that degraded data. Even if the lidar was not under the roof, the rainfall was so extreme that it went in front of it. This looked like there was a gap on the scan, as shown on figure 17. As there are few scans with this issue, they have been kept for analyses.

The second and main one was the presence of fog. The different elements of the figure above show the fog and its effect on scans. First of all, presence of fog can be seen with the naked eye, as shown with figure 19 (A), (C), (E). Then, looking at scans, figure 19 (B), (D), (F), it is possible to see directly the effect of fog. Indeed, the more fog there is, the fewer points there are (red circles on screenshots). This can be seen particularly beside and on the wall. Likewise, the intensity is lower with more fog, with a majority of blue on the scan and fewer points.

Not only the fog is visible with the naked eye and on the scan. Indeed, when analyses are made the effect can be clearly seen, as with figure 19 (G) and figure 18. In fact fog absorbs IR sent by the lidar therefore the intensity drops. There is a minimum peak of lidar signal, even if there is no rain, because of fog absorption of IR lidar signal (circled parts of graph).

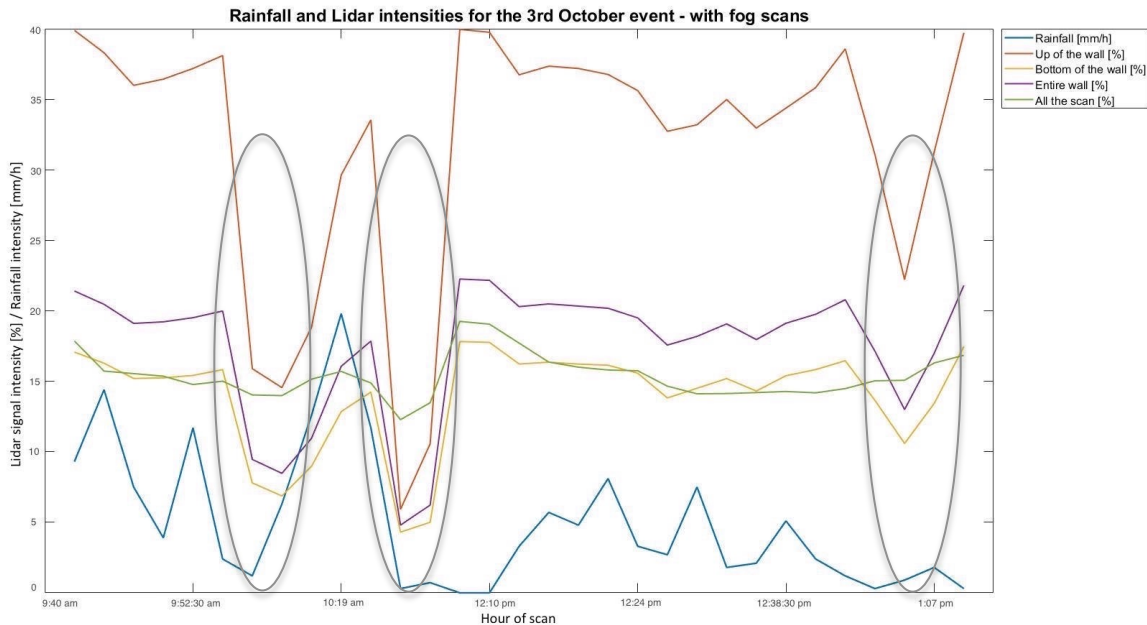


Fig. 18: Relationship between rainfall rate and lidar intensity, for the event of the 3rd October 2017, with fog scans circled.

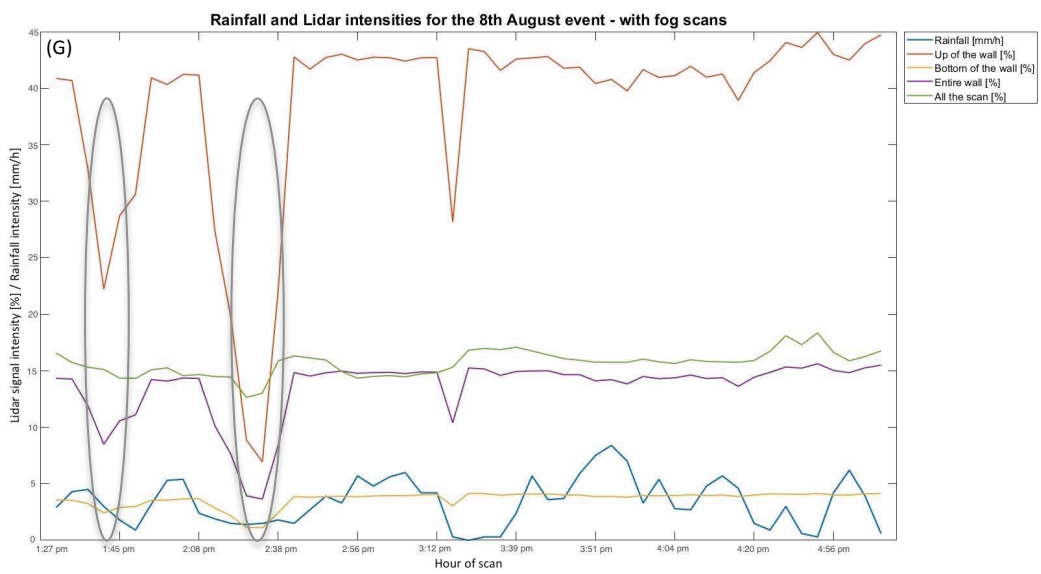
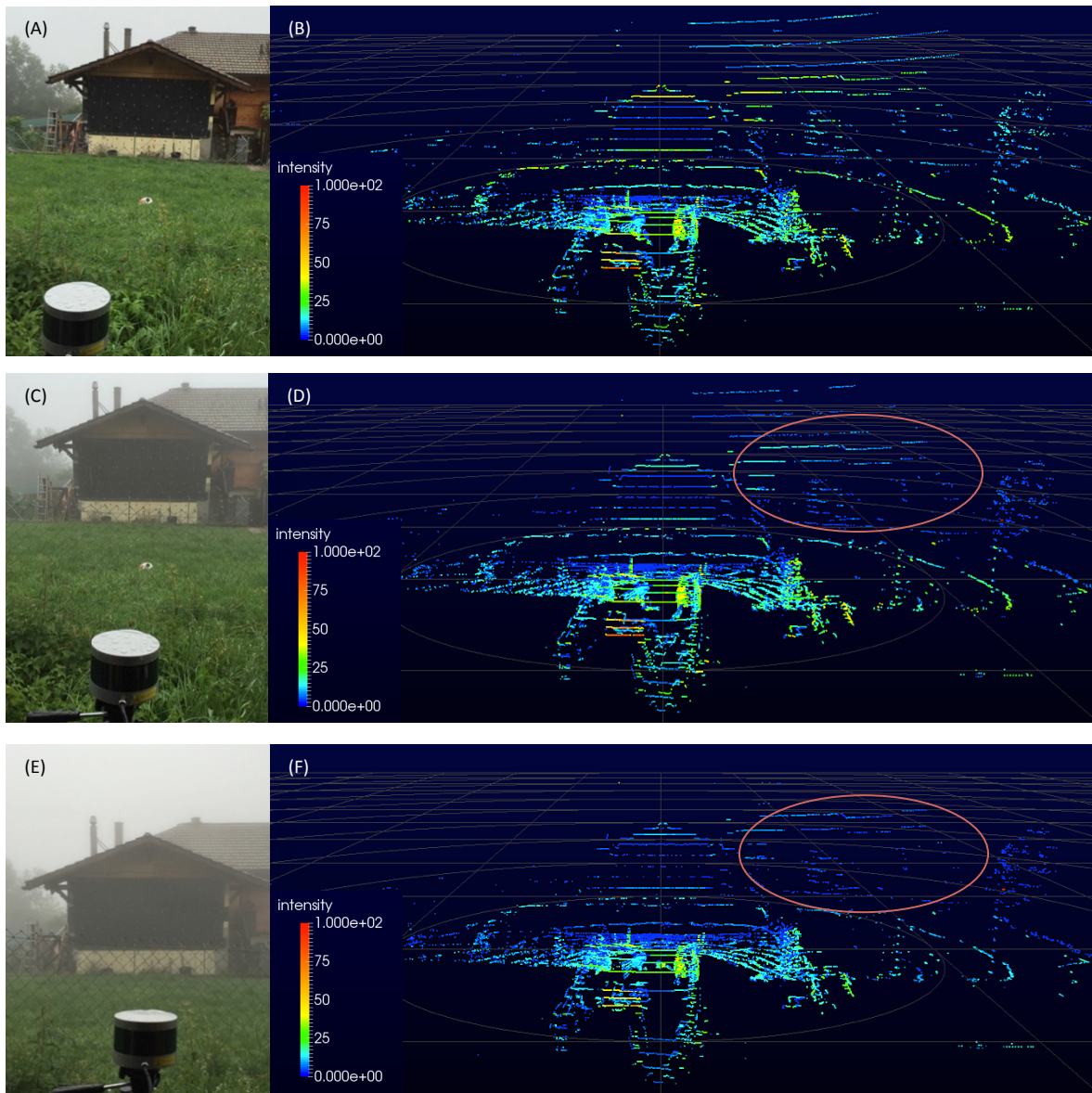


Fig. 19: Effect of fog on the event of the 8th August 2017. Naked eye seeing with photographs and result on scans. Rainfall (A) and scan screenshot (B) at 1:52 pm; rainfall (C) and scan screenshot (D) at 1:43pm; rainfall (E) and scan screenshot (F) at 2:26pm. Corresponding graph (G), with the 1:43pm and 2:26pm scans circled, which shows the impact of fog.

As the fog interferes with the relation between lidar and rainfall, it has been decided that the scans for which the effect of fog was too important were not considered. Hence, the changes make it possible to better see the reaction of the lidar with rain. In addition, it becomes comparable with the other events. On all measurements, 5 dates are concerned with fog issues. A total of 22 scans have not been taken into account for analyses, which leaves 323 scans to analyze. However, it is possible that some fog scans remain in the ones analyzed.

In addition to these elements, I have decided to keep only the events with a minimum of 5 scans. With this minimum, the relation between rainfall and lidar is more visible.

In summary, 372 scans were made between April and November 2017. After cleaning data, sixteen rainfall events have been kept, which represent 323 scans in total. In addition, 20 reference scans were analyzed. This makes a reliable sampling, as there is many data.

3. Results

Regarding scans made during rainfall event, there is an average of 20 scans per event, with a minimum of 5 and a maximum of 48 scans. Table 3 below shows the characteristics of the scans for the sixteen rainfall events, plus the references scans.

Table 3: scans details

Date	Hour of scans	Number of scans	Rainfall intensity [mm/h]	Fog
7 April	17:30 - 17:32	1		
19 May	10:24 - 12:42	11	From 1.6 to 8	X
28 May	16:31 - 16:41	2		
4 June	00:58 - 02:03	6	From 0.8 to 2.8	
6 June AM	09:45 - 12:32	19	From 0 to 6.4	
6 June PM	14:00 - 15:17	7	From 0 to 9.6	
9 July	22:04 - 00:13	40	From 0.3 to 28.8	
17 July	23:01 - 23:31	5		
20 July	21:24 - 21:52	11	From 0 to 84.9	
25 July	20:18 - 20:59	16	From 1.8 to 13.2	
26 July	20:14 - 22:06	12		
30 July	14:29 - 15:06	7	From 0 to 21.9	
8 August	13:28 - 17:16	48	From 0 to 8.4	X
11 August	10:52 - 11:28	7	From 0.3 to 1.2	
18 August (1)	17:51 - 18:32	13	From 0 to 41.4	
18 August (2)	21:37 - 22:39	22	From 0.3 to 93	
24 August	13:37 - 17:16	30	From 0 to 43.7	
31 August	08:01 - 12:22	19	From 0 to 5.2	X
3 October	09:41 - 13:23	24	From 0 to 19.8	X
5 November	07:25 - 11:33	43	From 1.2 to 9.9	X

Further information can be found about the scans in appendix C. It regroups all the results obtained from the scans: the mean values for every cropping of each scan.

3.1. Data analysis

Analysis is done using a step-by-step process and it is achieved using Matlab. As explained before, the calculations are based on the signal intensity. The mean of the value, over a certain area only (upper part of the wall, lower part of the wall, entire wall and all the scan), is kept for each scan. When compared with rainfall intensity measured by the collocated rain gauge, it gives the potential relationship between them.

Therefore, the first step is to see if there is a link between them. Figure 20 shows that this is the case. This graph is the complete event, chronologically. This allows seeing the temporal evolution of the lidar intensity - rain intensity relationship during one event. Axis X is the timeline. Axis Y is the matching lidar intensity. Each cropping of the scan is represented by a different color: orange for the upper part of the wall, yellow for the lower part of the wall, purple for the entire wall and green for all the scan. The blue curve is the rainfall intensity during the event.

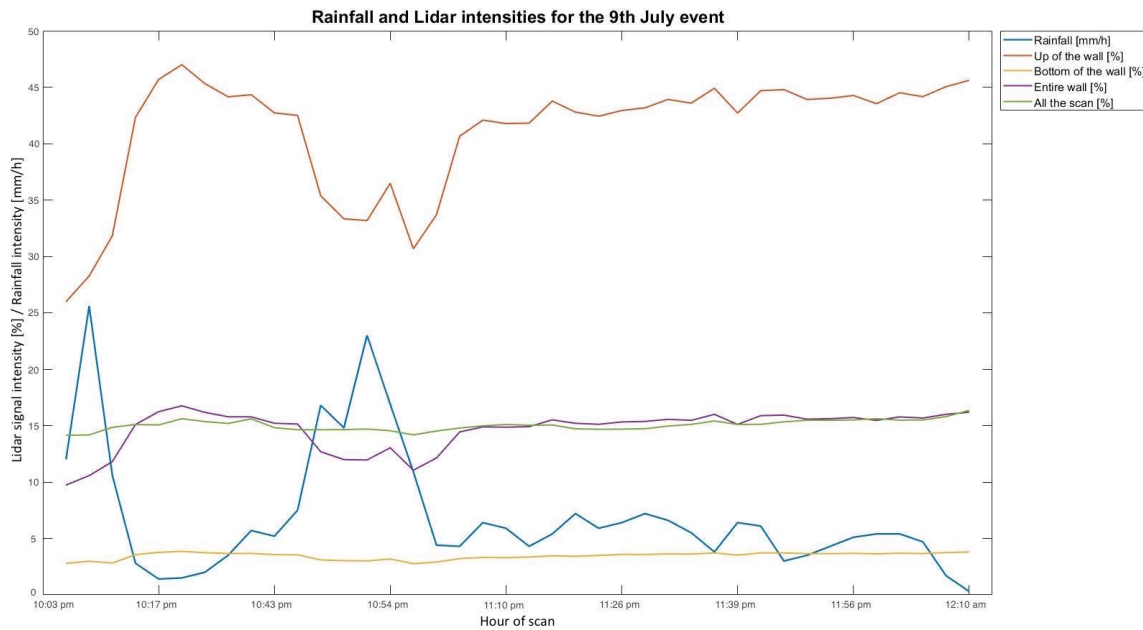


Fig. 20: Relationship between rainfall rate and lidar intensity, for the event of the 9th July.

The graph makes it clear that there is a connection between rainfall and lidar. It is possible to see that if rainfall rate rises, lidar intensity decreases and inversely. This graph also shows that the upper part of the wall is more reflective than the others. Furthermore, it suggests that the higher values of lidar signal are more sensitive to the variations in rainfall intensity.

As parts are taken separately, it is possible to see how reflective they can be. First, regarding the upper part of the wall, the orange curve. It is clear that this part is very reflective. There is an asymmetry between lidar and rainfall intensities. There is a slight interval between rainfall and lidar reaction. In addition, the values of lidar intensity are higher, which corresponds to what has been seen on scan's screenshot (fig 16). On the contrary, the lower part of the wall, the yellow curve, does not practically react. There is one reaction, but it is very small.

Regarding the entire wall (purple curve) the reaction is mixed between both upper and lower parts of the wall. It appears like an average reaction, with quite low values. This can be expected, as the lower part of the wall is imaged by more lidar echoes than the upper one. Another low reaction is the one from the entire scan, the green curve. When all the data is recorded, it seems like there is a smoothing.

For both, lower part of the wall and all the scan, the effect of rain on lidar is especially low. There are few variations and they are small. Those two cropped areas are not very reflective.

With the confirmation that there is a connection between rainfall and lidar intensity, analyses are made to show more details about the reaction of lidar signal. For this, scatter plot is made for the different cropped areas of the scan with multiple events at once. Figure 21 below is the set of graphs for the different cropped parts from the scan. For each plot, axis X is the rainfall intensity in mm/h and axis Y is the intensity of lidar signal given in percent. This percentage represents the amount of lidar that returns to lidar, the part of emission which has not been absorbed.

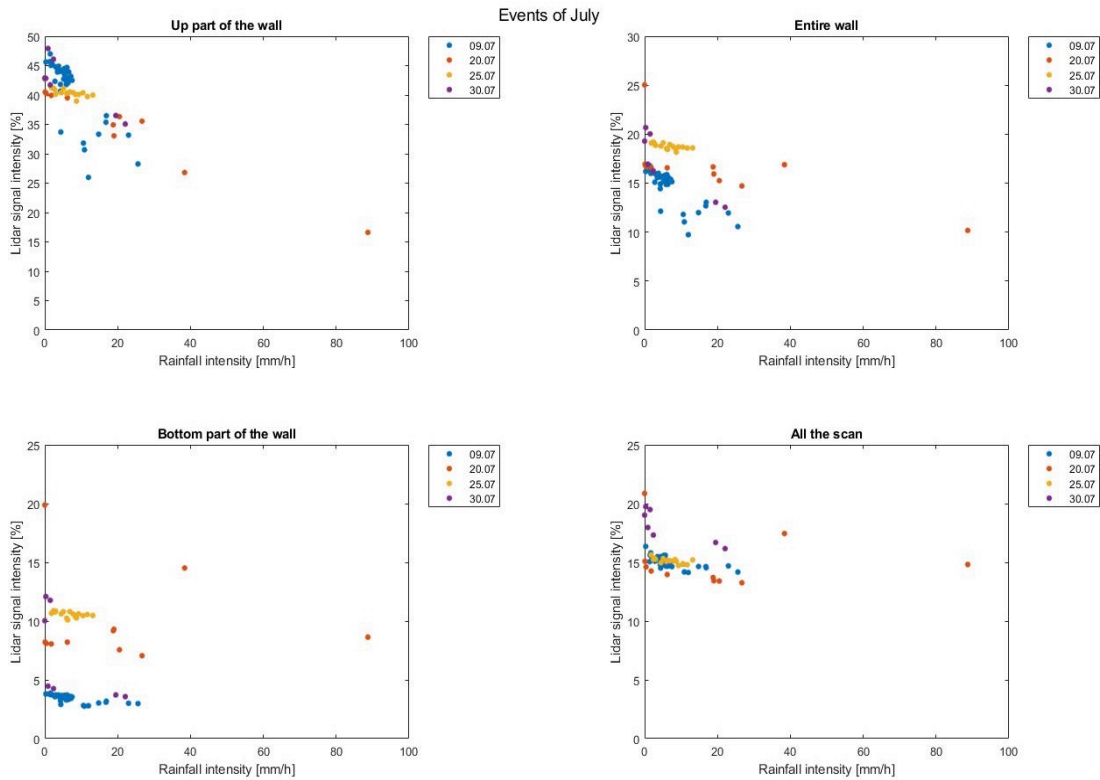


Fig. 21: Events of July for the different cropped area of the scan.

The previous graph shows that the lidar attenuation is dependent on the event. Except for the 30th July event for which purple dots are dispersed, the other events are clustered.

In addition, this graph shows that the relation between rainfall and lidar is a decreasing function. This is especially visible with the upper part of the wall. The 9th July event, blue dots, shows clearly this trend with the latter part of the wall and the entire wall. However, the relationship is less pronounced for the lower part of the wall and the entirety of the scan, for which the reaction tends to weaker. There is an exception for those parts, as the 30th July event shows a decreasing relation. Those results correlate with the ones from figure 20.

These two figures above show that there is a relation between rainfall and lidar signal intensities. They also give the information that the upper part of the wall is the more reflective. Contrary to the lower part of the wall and all the scan, which have a weaker reaction, with few variations.

Figure 22 is the graph with all the measurements made, showing lidar reaction with rainfall on all the scan.

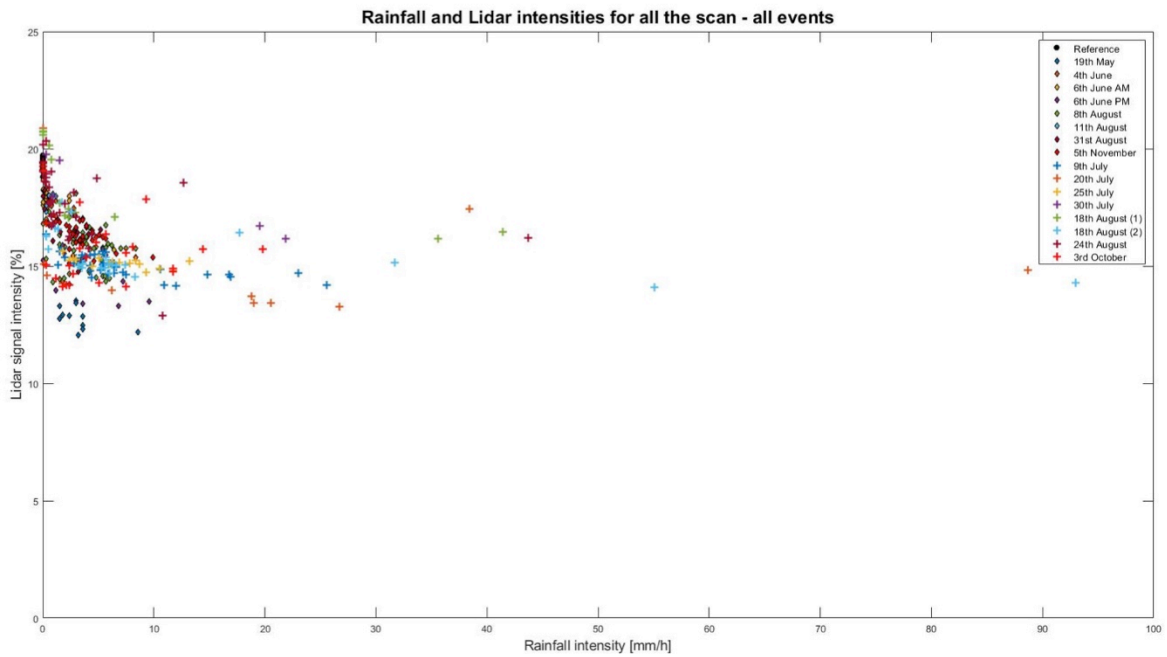


Fig. 22: Scatterplot of all events measurements for all the scan.

This figure shows that the majority of measurements are in the rainfall interval 0 to 10 mm/h. Indeed, among the 323 scans, only 30 of them are measurements made with rainfall intensity higher than 10 mm/h. This means that 9.3% of the data was collected during heavy rainfall (intensity higher than 10 mm/h). Whereas, remaining measurements (90.7%) are clustered between rainfall intensity 0 and 10 mm/h.

This graph (fig 22) also allows seeing a difference of behavior depending on the rainfall intensity. In fact, the high rainfall intensities do not seem to react the same as the lower ones. Here, we can see a decreasing line in the low rainfall intensity, which does not seem to continue with high intensities. For the high intensities, we can tell that the relation is more a curve than a straight line. This suggests a different reaction depending on the rainfall maximum intensity. This is explained more in details in sections 3.2. and 3.3. In particular there are functions and graphs, showing the lidar / rainfall relation, depending the intensity.

We can see that 10 mm/h seems to be the intensity from which the relation is more a curve than a linear relationship; it is a key intensity.

If we focus first on the rainfall intensity between 0 and 10 mm/h, we can understand better how the lidar reacts for this range of rain intensities. Figure 23 is a zoom of the previous graph, limited between rainfall intensity 0 and 10 mm/h. This represents 293 measurements.

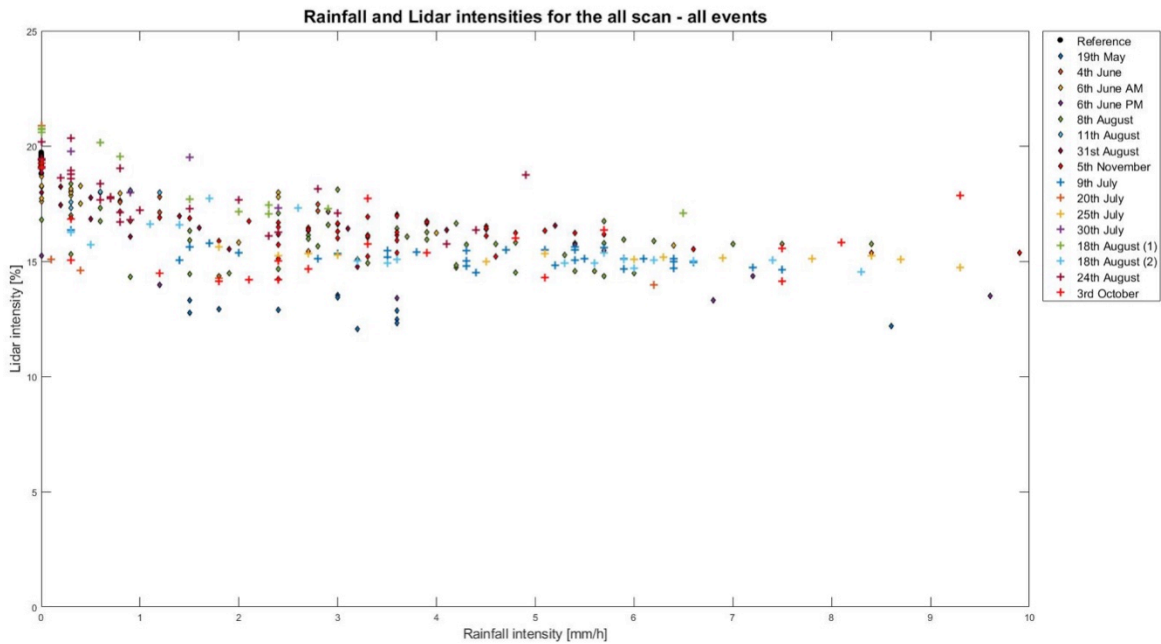


Fig. 23: Scatterplot of all events measurements for all the scan, with a limit of rainfall intensity at 10mm/h.

This figure shows that in this interval the reaction is very similar for all the events. In addition, we can see that measurements are still clustered by events. Moreover, the majority of measurements (226) are grouped between lidar intensity 15% and 20%. We can see that there is a small attenuation of the signal when it rains with low intensity.

Second, we do a focus on rainfall intensities higher than 10 mm/h, to see the reaction. Figure 24 is a zoom of the graph (fig 22), limited between rainfall intensity 10 and 100 mm/h.

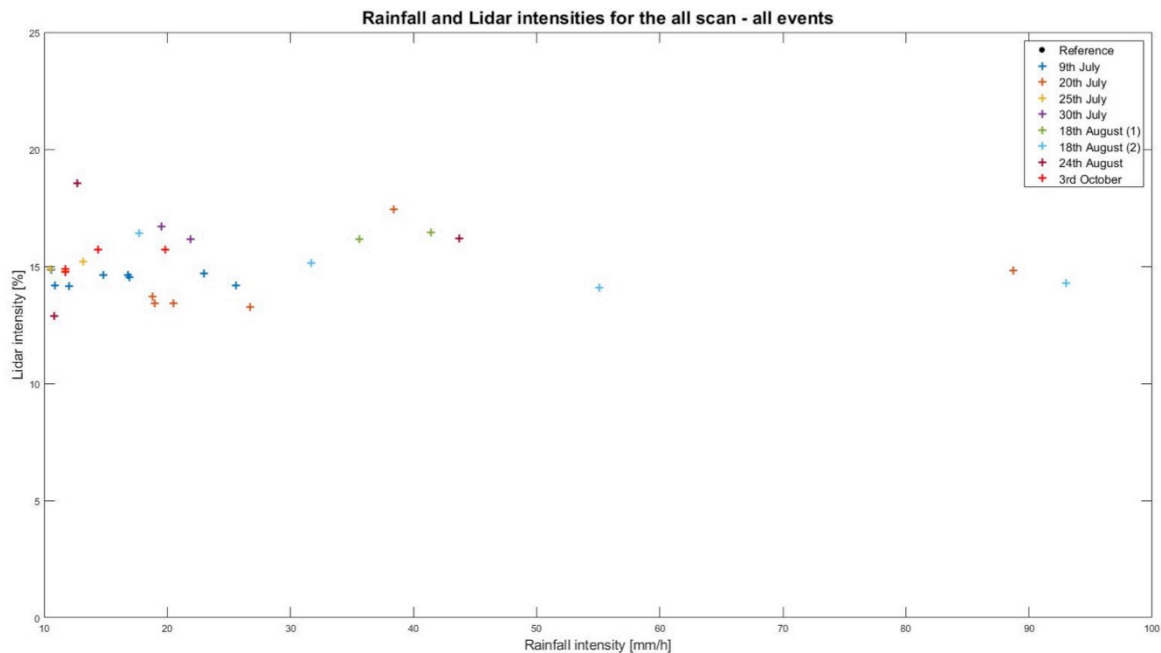


Fig. 24: Scatterplot of all events measurements for all the scan, between a limit of rainfall intensity at 10mm/h and 100mm/h.

This represents 30 measurements. The figure 24 shows that in this interval there are variations between events. However, we can see that the majority of measurements (19) are grouped between lidar intensity 12% and 16%. There is a reaction, but it is less clear than previously. Looking only at this section of rainfall intensity makes it difficult to determine a function, which explains the reaction. However, we can say that these measurements made during rainfall higher than 10 mm/h bring further information about the behavior of the lidar signal.

Knowing this it is possible to split the events depending on the rainfall intensity. It has been decided to put the limit at 10mm/h. The choice of this limit is based on results of the analysis. In fact, 10 mm/h is the point at which the shape of the curve reaction changes. The lower intensities correspond more to a linear reaction. While the higher intensities look more like a curve. The latter one can give more information. This choice is also subjective, as it seems to be a good compromise for the following analyses. However, this can be confirmed with literature, with the article of Macke & Großklaus (1998). In his article, Macke studied DSD and found that below the intensity of 10 mm/h there is no correlation between size and intensity. Therefore, they concentrated the study on higher rainfall intensities. From these elements, results from my measurements are divided in two parts: the ones with a rainfall intensity, which do not exceed 10 mm/h and the ones with an intensity superior to 10 mm/h. Both of them are calculated with different functions. The small intensities are analyzed with a polynomial function, while higher intensities are calculated with an exponential function.

The continuation of the study will give more information about the results separated as explained. As it has already been said, the upper part of the wall is the most reflective. For this reason it has been decided to focus on this cropped area for the study. However, results of the other parts can be found in appendixes.

3.2. Modeling the rainfall / lidar relationship for low intensity rain events (does not exceed 10 mm/h)

The first results are for the events with a maximum rainfall rate of 10 mm/h. This involves eight events: 19th May, 4th June, 6th June AM, 6th June PM, 8th August, 11th August, 31st August and 5th November. This represents 160 scans measurements analyzed.

The measurements of these are more dispersed. For this reason and because of what is seen on graph figure 19, it is thought that a linear function is a good candidate to fit the empirical rainfall / lidar relationship:

$$Z = a_1 * R + a_0 \quad (6)$$

With: Z which is the lidar signal intensity observed; R which is the rainfall measurement; a_1 (= slope of the line) and a_0 (= vertical intercept) that are the parameters to be estimated.

Calculations are made for all events and all parts of the scan separately. The mean intensity from lidar signal and rainfall are taken into account. All the operations are made on Matlab, using the polyfit function with the degree of the polynomial set to 1.

Figure 25 is the outcome graph of the equation for the eight rain events of interest. It is the graph for the upper part of the wall.

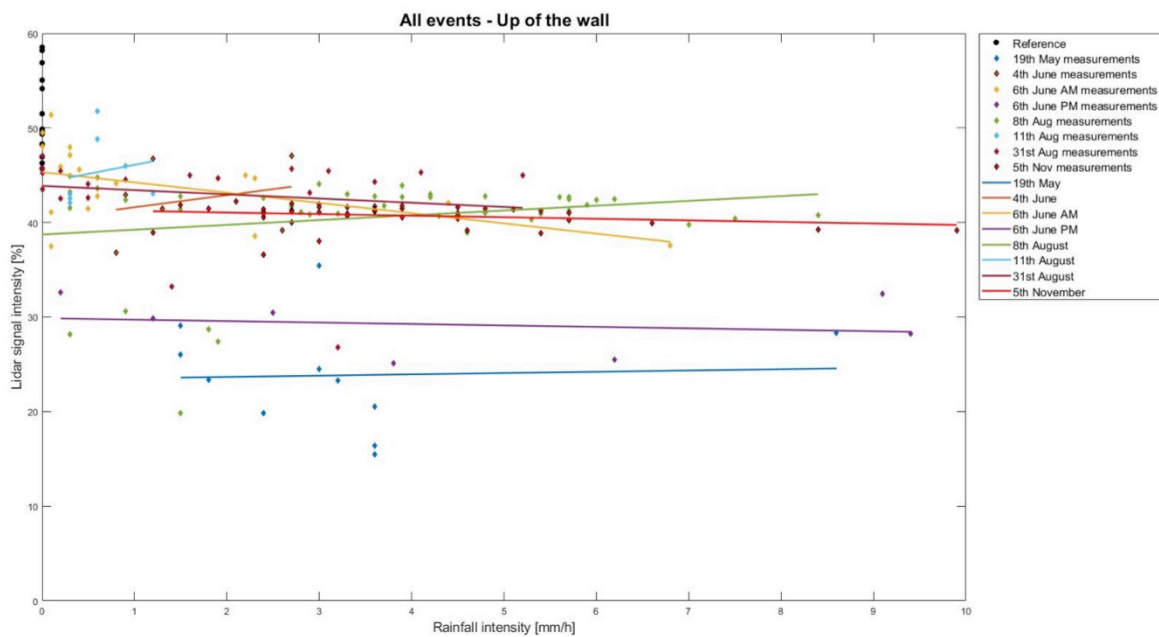


Fig. 25: Results for all events within rainfall intensity which does not exceed 10 mm/h for the upper part of the wall.

There are several things to notice in this figure. First, there are four events for which the slope is positive: 19th May, 4th June, 8th August and 11th August. Secondly, there is a majority of measurements, which are clustered between lidar intensities 40% and 50%. Thirdly, it is the references scans, which are above rainfall event measurements. Finally, in general the slope appears to be low.

Regarding the references scans their values are high. The mean intensity for the upper part of the wall when it is dry is 51.35%. This is above all measurement, made during rainfall events. Concerning the measurements, the majority of them (95) are between intensity 40% and 50% and the mean intensity is 39.94%. This is significant and relevant because it shows that rainfall brings an attenuation of the lidar signal intensity, as reference measurements are higher than rainfall ones.

Considering the slope, predominantly it is low. There are three events, the 4th June, 6th June AM and 11th August, which have a slope more pronounced. This is interesting because it shows that the events that do not exceed 10 mm/h have a minimalistic reaction. It is remarkable how little the lidar's reaction to rainfall is.

For the events of the 19th May, 4th June, 8th August and 11th August that rise, there is a hypothesis that explains this. The first hypothesis is that it could be fog. It is possible that in the scans that were taken, some of them have issues with fog. However, only two events are potentially impacted, the 19th May and 8th August. The second hypothesis, it could be an effect of the night. Perhaps it disrupts the signal, however only the 4th June is a night scan. Still, regarding the data that has been collected and used it is not possible to determine those elements. Nevertheless, the fact that four scans have a reaction that do not have an expected result relating to the hypothesis, make it clear that the environment has an impact on scans.

Table 4: Results of the polynomial function, for the upper part of the wall

Date	a_1	a_0	R^2
19 May	0.1378	23.3766	0.0021
4 June	1.2767	40.3339	0.0699
6 June AM	-1.0824	45.3174	0.2475
6 June PM	-0.1528	29.8671	0.0348
08 August	0.5067	38.7342	0.0047
11 August	1.9006	44.1884	0.0316
31 August	-0.4447	43.8649	0.0221
5 November	-0.1660	41.3857	0.0600

Table 4 above is the numerical results behind the figure 20 graph. It is interesting to have them because it shows the variability between the events. First, parameter a_1 being the slope, it is noticeable that values are low, from -1 to +1. However, there are two exceptions, the 6th June AM and 11th August which have higher values. Another noteworthy point about a_1 is that for the four events that rise, the value is positive whereas it is negative for the others. This explains the orientation of the slope with numbers and this is logical. However, it is a confirmation that for those events the slope will rise. Secondly, parameter a_0 being the vertical intersect, it is possible to see that they are quite clustered, between 38 and 46. Only two events have a lower value.

Finally, what stands out in this analysis is that small rainfall intensities react sparsely. There is few absorption of the lidar's signal, as there are fewer and smaller raindrops. They have no real visible attenuation in the rainfall / lidar relationship: there is too much noise. This noise is probably the reason of the seen variations. The lidar signal does not have a regular reaction: it is more susceptible to noise at those intensities.

Results of the other parts plus individual event's graphs can be found in Appendix A.

3.3. Modeling the rainfall / lidar relationship for high intensity rain events (higher than 10 mm/h)

The second results are for the events with a rainfall rates higher than 10 mm/h. This involves eight events: 9th July, 20th July, 25th July, 30th July, 18th August (1), 18th August (2), 24th August and 3rd October. This represents 163 scans measurements analyzed, with 30 having rainfall intensity higher than 10 mm/h.

The measurements of those ones correspond to rainfall intensity from 0 to 100 mm/h (maximum measured at 93 mm/h). With higher intensity, they become more dispersed. For this reason and because of the curve that can be seen on graph figure 22, it is thought that the relation is similar to the one observed with radars. For this, it is as though it can be explained with power law, an exponential function will have the best fitting (Berne et al., 2012; Jaffrain & Berne, 2012; Uijlenhoet et al., 2003). Equation (7) is an exponential decay that is calculated:

$$Z = a * \exp(-R*b) + c \quad (7)$$

With: Z which is the lidar signal intensity observed; R which is the rainfall measurement; a (= height of curve departure), b (= angle of the curve), c (= vertical, ground level) which are the searching parameters.

3.3.1. Analysis using all measurements

Calculations are made for all events and all parts of the scan separately. The mean intensity from lidar signal and rainfall are taken into account. All the operations are made on Matlab, using the `fminsearch` function. In addition to this formula, the RMSE is calculated to have an evaluation of the fitting.

Figure 26 is the outcome graph of the exponential equation with the eight events. It is the graph for the upper part of the wall.

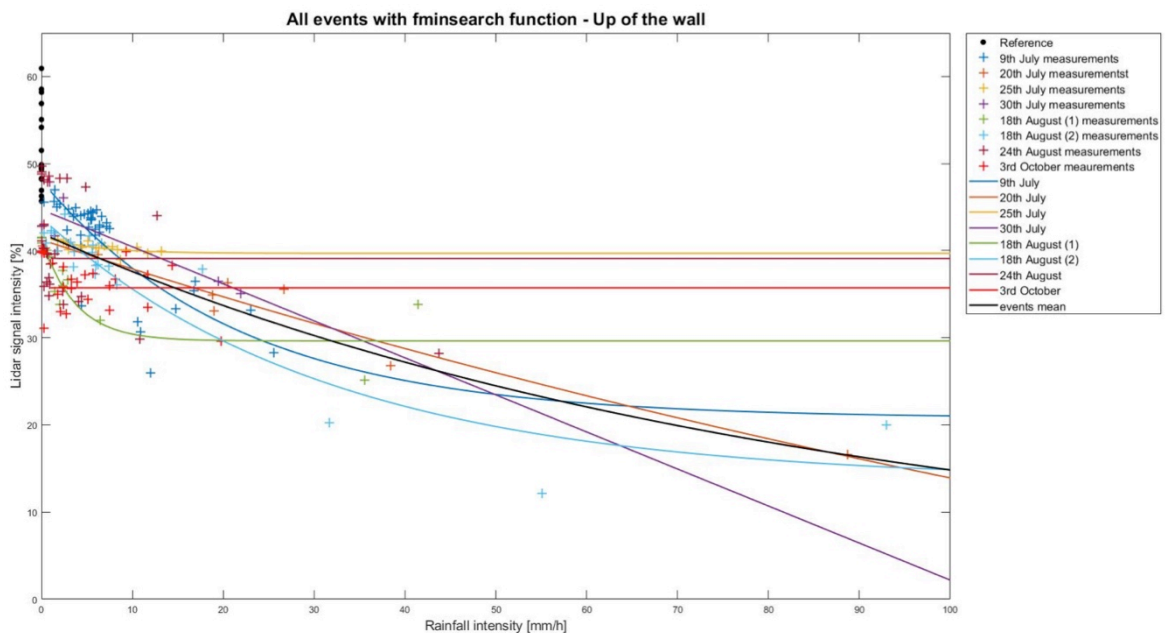


Fig. 26: Results for all events having a rainfall intensity getting higher than 10 mm/h for the upper part of the wall, using the `fminsearch` function on Matlab.

First, we can notice that all the curves do not look similar. Secondly, the reference scans have higher values than the ones during rainfall. Thirdly, the majority of measurements are between values 30% and 50%.

Taking the curves separately, we can see several differences. To start with, for the events of the 24th August and 3rd October, the lidar signal shows no absorption by rainfall. Other events do not have a curving reaction; the 20th July event and 30th July event. It seems that it is the beginning of the exponential curve; that it does not reach its e . However, it is better than 24th August and 3rd October as it goes down, which is what we could expect to see. The functions for the 9th July and 18th August (2) look more like an exponential, with a curve at the beginning that is more marked. In addition, it seems that they are reaching their asymptote. The function of the 25th July has the look of an exponential, it has reached its level, and has a less pronounced curve at the beginning although it is present. The curve of the 18th August (1) is the one that we expected to see. It has a clear curve, with a pronounced angle and it reaches its asymptote.

Looking at the reference scans, we can see that they have higher lidar value than rainy data. The means value when it is dry is at 51.35%, whereas the maximum reached during a rainfall is at 49.7118% (24th August). The majority (152) of measurements have a lidar value that is between 30% and 50%. The mean value during rainfall events is at 38.89%, which is lower than when it is dry. It corresponds to an absorption of the signal by rainfall.

All these observations are interesting because it shows an attenuation of lidar signal during rainfall events. However, the relation is not very clear within the graph. To have another idea of the fitting, table 5 following shows the values of searched a, b and c parameters.

Table 5: Results of the exponential function with fminsearch on Matlab, for the upper part of the wall.

Date	a	b	c	RMSE
9 July	27.2937	0.0461	20.7596	3.1444
20 July	72.9933	0.0047	-31.7518	1.5234
25 July	1.9906	0.1879	39.6892	0.4039
30 July	9.8837E+05	4.3000E-07	-9.8833E+05	2.0841
18 August (1)	11.7262	0.2714	29.6433	2.0694
18 August (2)	30.1897	0.0315	13.5636	2.9181
24 August	14.2274	5.9940	39.0939	5.4763
3 October	1.0179E+05	101.1492	35.7305	2.5179
Events mean	39.0071	0.0119	2.9639	4.1878

Whereas results on graph are acceptable, as they look like what we were expecting, numerical results are surprising. In fact, some of them have extreme (high or low) value, such as the 30th July. Concerning the RMSE, they are low. The 24th August is the event with the lowest quality of fitting. Whereas the 25th July has the best fitting.

To obtain less extreme values in certain cases, it has been decided to change the approach. We settled boundary conditions to restrain the function. This could bring uncertainties as it changes values and affects the function behavior. Doing this, we used the fmincon function with Matlab. The limits for the parameters are the following: a and c parameters are from 0 to 50 and b parameter is from 0 to 10.

Figure 27 below is the resulting graph for the upper part of the wall. It is the exponential function for the eight events, with the constraints decided. Organization is the same as with figure 26.

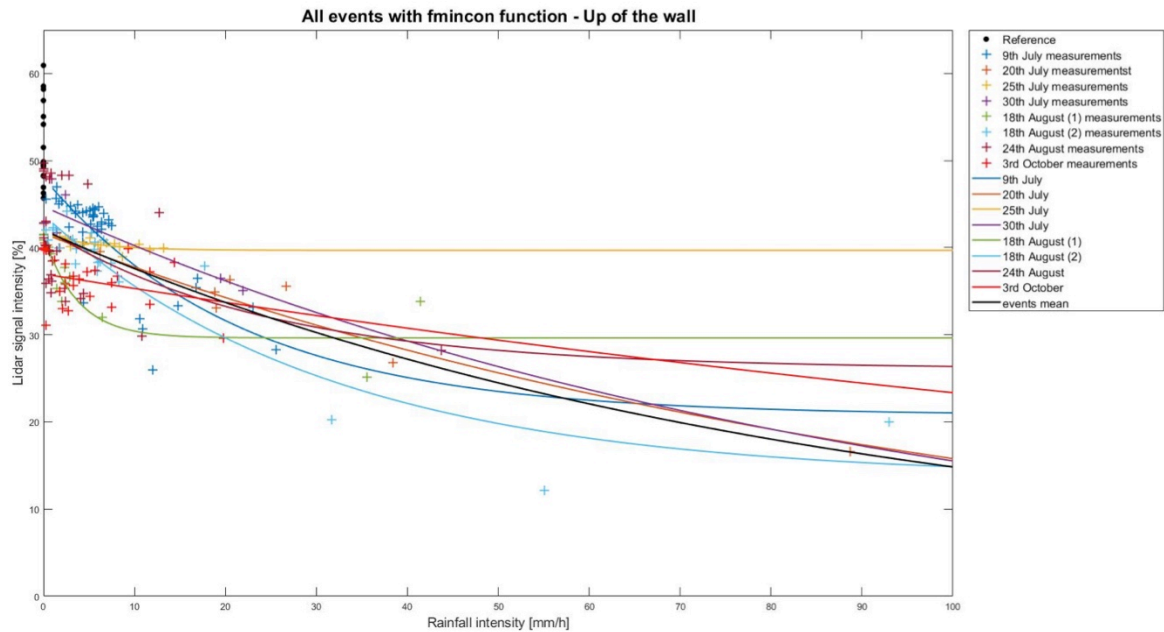


Fig. 27: Results for all events having a rainfall intensity getting higher than 10 mm/h for the upper part of the wall, using the fmincon function on Matlab.

Visually this graph looks more to what we could have expected using exponential decay function. First, there appears to no longer be a straight line, all the events have resulted in a curve. Half of the events see their curve changing; the other half has no visible variation.

Looking in detail to compare with figure 21, the 9th July, 25th July, 18th August (1) and 18th August (2) events are the ones which do not change. There is also the mean events curve, which stays the same. Regarding the one for the 20th July, the curve has a slightly higher lidar value at the end, as the angle is more marked. The 24th August and 3rd October change from a horizontal slope to a curved slope. In addition, they do not stay at the same lidar intensity; they decay, but do not reach their asymptote. Lastly, the 30th July event has a reaction in curve when constrains are enforced. It has a higher lidar value at the end of the curve; it is not a straight line anymore.

The upper part of the wall is the one that sees the more changes between calculations made with or without constrains.

Concerning numerical values for the searched parameters, table 6 gives the results obtained with constrains on boundaries.

Table 6: Results for the exponential function, with fmincon on Matlab, for the upper part of the wall. Red numbers are the major ones, which differ with the fminsearch function (table 5).

Date	a	b	c	RMSE
9 July	27.2939	0.0461	20.7594	3.1444
20 July	41.6018	0.0097	1.4326E-04	1.6137
25 July	1.9906	0.1879	39.6891	0.4039
30 July	44.7039	0.0106	0.0189	2.1003
18 August (1)	11.7262	0.2714	29.6433	2.0694
18 August (2)	30.1896	0.0315	13.5637	2.9181
24 August	16.1717	0.0406	26.0802	5.4665
3 October	36.9658	0.0046	0.0048	2.6401
Events mean	38.9897	0.0119	2.9816	4.1878

Parameters values show the same as the graph, which is that four events have changes in their curve when comparing with fminsearch results (table 5). Taking the 30th July event, which had the strangest values and saw the biggest change, we can see that parameter *a* went from 9.8837E+05 to 44.7039, which is a more usable value. Its *b* parameter went from 4.3000E-07 to 0.0106; and for *c*, it went from -9.8833E+05 to 0.0189. In general, values become smaller when using constrains.

In addition to the big changes noticeable for the previous events, some others events have numerical modification. Indeed, the 18th August (1) is the only event which does not have a single difference. Otherwise, the 9th July, 25th July and 18th August (2) have some slight changes in their values. These differences concern parameters *a* and *c*, with a variation of maximum ± 0.005 . There is no difference concerning parameter *b*. Regarding the events mean, it has a change of ± 0.017 for parameters *a* and *c*.

Changes in parameters also affect RMSE. These ones tend to be less good, as the function is limited. However, it is not the case for the 24th August event that before had a RMSE at 5.4763 and now is at 5.4665, which is an improvement.

In summary, putting constrains on boundaries does not change much the result, except the fact that some slopes are more pronounced.

3.3.2. Analysis using bins

What stands out in the previous analysis is that with higher rainfall intensities, it is possible to determine a power law relation, such as used with radars. There is an attenuation of the lidar signal when rainfall rate increases. There is also less noise than with rainfall intensities below 10 mm/h, the relation is clearer. However, the number of data with rainfall rate higher than 10 mm/h is low (30). This means that they are not taken into account as much as they should. To correct this, the same events are calculated using the same functions. Nevertheless, not all data is taken; bins are made to equilibrate the weight of measurements.

In this part, the same events are analyzed. This time, it is still an exponential that is calculated, but with a changing concerning data. In this case, we do not use all the measurements as before, we make bins. As already mentioned, rainfall intensity between 0 and 10 mm/h counts a majority of data. There are only 30 measurements with higher intensities and they are quite isolated. This method using bins allows giving more weight to these few high intensity data. In this case, bins correspond to the mean intensity in a rainfall intensity interval of 5 mm/h.

This means that every interval counts as one measurement, which changes the results a bit, especially concerning higher intensities.

First, the results using the `fminsearch` function, figure 28.

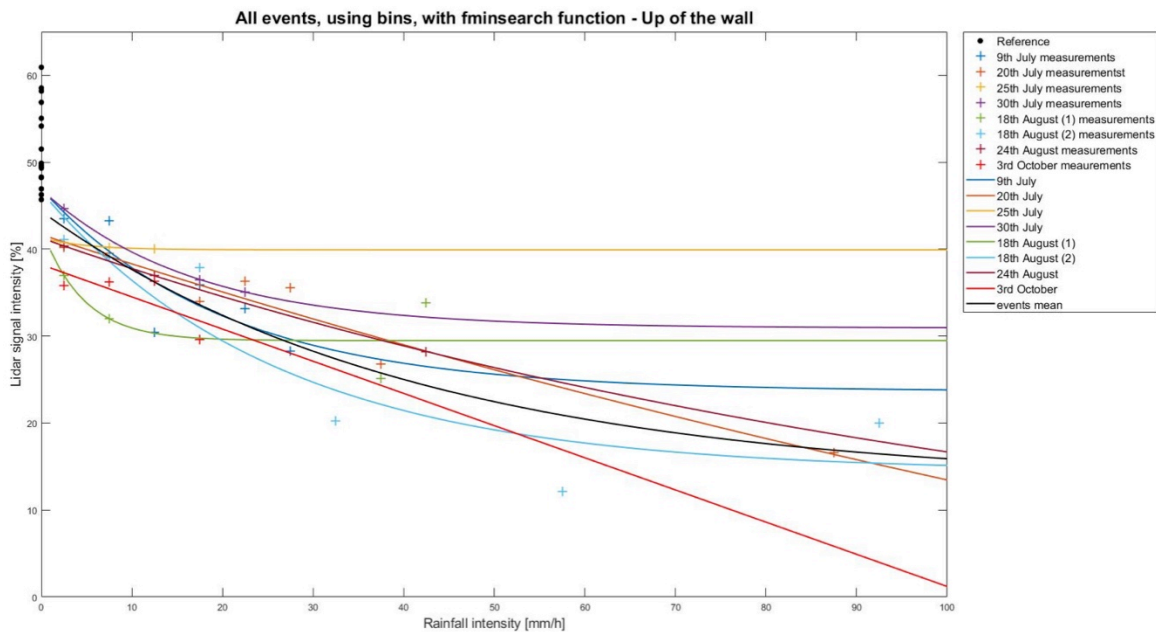


Fig. 28: Results, using bins, for all events having a rainfall intensity getting higher than 10 mm/h for the upper part of the wall, using the `fminsearch` function on Matlab.

On this graph, it is noticeable that the 3rd October event has a decreasing slope. Another interesting date is the 20th July, as it is a curve with a slight increase. The 25th July is nearly only a horizontal slope; the curve at the beginning is small. The 24th August is almost a slope; the curving is slight. Otherwise, the four events left have a curve, some reaching their asymptote (9th July, 30th July, 18th August (1) and 18th August (2)).

Comparing figure 26 with this one, we can remark that all the curves change more or less. For example for minor changes, the 9th July and 25th July which are just a little bit in higher lidar value at the end. The 20th July is less slope, is has a small curve. The 18th August (1) has an angle that is a bit less pronounced. The 18th August (2) begins a bit lower in lidar values, but is slightly higher at the end. Bigger changes are seen with the 3rd October; there is still a slope, but this time it goes down rather than being horizontal. The 30th July changes totally as it is a curve when calculated with bins. Finally, the 24th August, which has a slight curve being almost slope. In addition, it goes down and it has lower lidar values compared with figure 26.

What stands out with this graph is the fact that making bins change the behavior of curves. It really gives more importance to the higher intensities; they are less isolated.

Now it has to be confirmed by numerical values. Table 7 seen below contains the results obtained from the different parameters searched.

Table 7: Results for the exponential function, using bins, with the fminsearch function on Matlab, for the upper part of the wall.

Date	a	b	c	RMSE
9 July	23.2976	0.0494	23.6500	3.0999
20 July	84.3966	0.0041	-42.7185	1.8764
25 July	1.4071	0.2061	39.9255	7.5540E-06
30 July	15.9208	0.0600	30.9332	3.8378E-06
18 August (1)	12.9272	0.2186	29.4828	3.0587
18 August (2)	32.1829	0.0380	14.4166	4.5298
24 August	42.7571	0.0086	-1.4784	5.2614E-07
3 October	2.1498E+06	1.7217E-07	-2.1497E+06	1.9250
Events mean	31.2689	0.0241	13.0820	4.2298

First, looking at RMSE, we can see that results are better using bins, as their results are lower. When compared with results from table 5, three events have a RMSE which downgraded: 20th July (slightly), 18th August (1) and 18th August (2) (significantly). The events mean has also a small change. This can be explained by the fact that we have less data taken into account. However, the repartition in rainfall intensities is different. Higher intensities have more importance, which could also have an impact on results.

Secondly, some extreme values have disappeared, such as for the 30th July. However, some are still there, such as for the 3rd October. Using bins have brought a change in the behavior of curves, which can be seen with numerical values also.

Since there are still some extremes and negative values, calculations are also made with the fmincon function. In this case, constrains are the same as with all the measurements. The limits for the parameters are the following: *a* and *c* parameters are from 0 to 50 and *b* parameter is from 0 to 10. Figure 29 is the outcome graph.

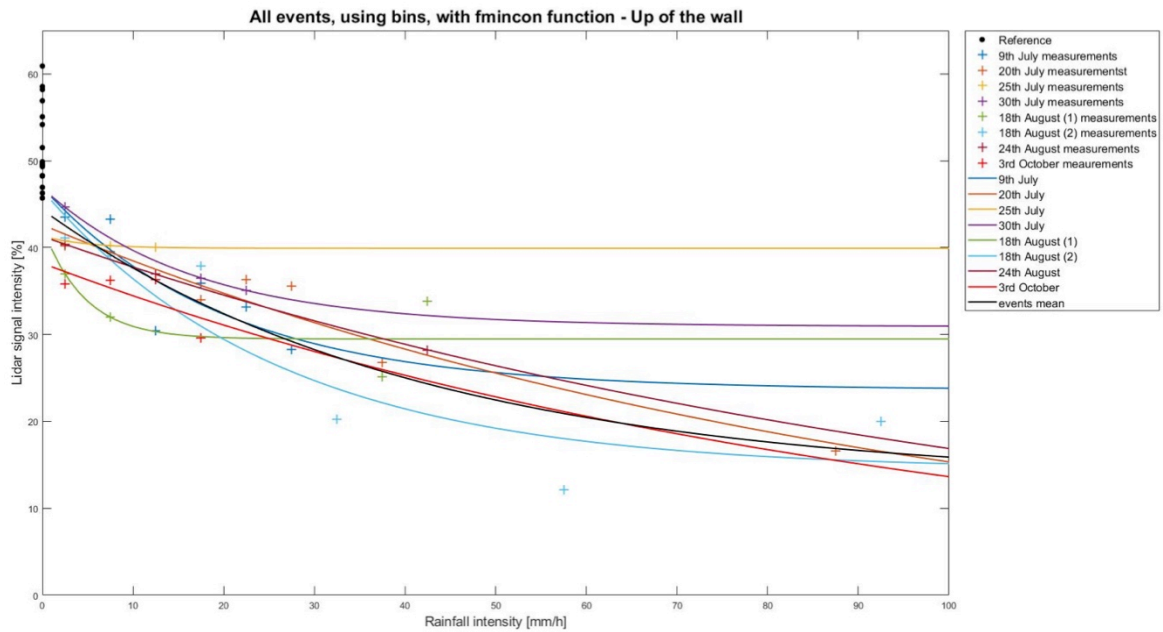


Fig. 29: Results, using bins, for all events having a rainfall intensity getting higher than 10 mm/h for the upper part of the wall, using the fmincon function on Matlab.

As when all measurements were taken into account, the results obtained with constrains is better visually. All events have a curve to describe their reaction. The latter has an angle that is distinct.

Comparing with the figure 28 graph, there are only three events that saw a change: the 20th July, 24th August and 3rd October. These ones switched from a slope relation to a curved one. Their angle is less pronounced than some others, like the one for the 18th August (1). In addition, they do not reach their asymptote.

Comparing with figure 27, we can remark that all the events change more or less. The events with more variations are the 30th July and 3rd October. They see their curve having a more noticeable angle, even if it is only slightly for the 3rd October. Other changes concerning lidar values, is that there are variations at the beginning and end of curves. For example, the 18th August (1) begins with a higher value and finishes with a lower one. The 9th July, 25th July, 30th July and 24th August all have a lidar value that is a bit higher at the end of the curve.

Looking at the numerical results, we can see some differences between these ones and the previous ones (table 7). The following table 8 presents the outcomes.

Table 8: Results for the exponential function, using bins, with the fmincon function on Matlab, for the upper part of the wall. Red numbers are the ones, which differ with the fminsearch function (table 7).

Date	a	b	c	RMSE
9 July	23.2977	0.0494	23.6499	3.0999
20 July	42.6164	0.0102	1.0450E-04	1.9837
25 July	1.4072	0.2061	39.9255	1.4985E-06
30 July	15.9209	0.0600	30.9331	5.1412E-06
18 August (1)	12.9272	0.2186	29.4828	3.0587
18 August (2)	32.1829	0.0380	14.4166	4.5298
24 August	41.2928	0.0089	0.0011	0.0083
3 October	38.1939	0.0103	3.2763E-04	1.9691
Events mean	31.2689	0.0241	13.0821	4.2298

Parameters values show similar results to the graph. Two events mainly change when comparing with the fminsearch results (table 7). The 20th July and 3rd October have their three parameters that change the most. Even if the difference is difficult to see on the graph, it is confirmed by the values.

An interesting point is that on the graph we can see that only three events changed in comparison with fminsearch function (fig 28). However, looking at the values, only two events have absolutely no changing value. The 18th August (1) and 18th August (2) are the events which keep the same values, independently from the function. Regarding the other events, they all have their parameter b that stay the same; it is the parameters a and c that differ. Another noteworthy point is the fact that all values are now positive, even if some are very small.

Regarding the RMSE, only three events' mean values are the same. Otherwise, they have all changed. One improved, the 25th July, the others downgraded. This could be an effect of constrains. As there is less data included for the analysis, they tend to differ more and have a fit that is less accurate.

When comparing with results obtained using all measurements, table 6, we can see that all values have changed. However, the ones with more differences are the 30th July and 24th August. These two have the major modifications. However, these changes are good in some cases, as the RMSE improves. In the comparison between all measurements and bins: four events improved their RMSE (25th July, 30th July, 24th August and 3rd October), while two slightly downgraded it (9th July and 20th July) and two reduced it significantly (18th August (1) and 18th August (2)). The events' mean result worsened a little.

The idea of using bins means there is less data to fit functions. However, the result can be taken as good as it gives more importance to the high intensities. Looking at RMSE, we can say that using bins to fit the exponential can improve results. Nevertheless, it should be taken carefully because it can also have more uncertainties.

What stands out in this analysis is that high rainfall intensities react. There is an absorption of the lidar's signal, as there is a wide range of raindrops. The attenuation in the rainfall / lidar relationship is clearly visible with events having rainfall intensity which exceed 10 mm/h.

Finally, considering all the analyses made, it is not possible to have a generalization of parameters. Indeed, their values have too much variability in order to generalize the observations made and obtain only one value for each parameter. This is the case with all the cropped areas and functions used.

Results of the other parts for the different functions as much as individual events' graphs, all with and without bins, can be found in Appendix B.

3.3.3. Sensitivity of parameters to environmental conditions

The goal is to see if one particular element affects the parameters value. It is an attempt to find if there is an explanation about their dispersion.

It is thought that environmental phenomenon can affect the measurements. This condition can be the measurement surroundings becoming wet at the end of the scanning period. It could be the difference between events. Like with the seasons, for example in this study, measurements were made in Spring, Summer and Autumn. Perhaps the rainfall type, like the seasons changed during the study; there are some thunderstorm events, or Spring and Autumn rainfall. Linked with the rainfall type is the DSD that can affect lidar's reaction. There is also the temperature or humidity that interact with laser beam.

In this analysis, we decided to try with data we could collect. We took measurements made at the meteorological station at Aigle, which is the nearest MeteoSwiss station. It has information among others about temperature, humidity, rainfall, wind and sunshine. The values are collected every hour. We decided to compare temperature with lidar measurements. To do it, some modifications are made to the MeteoSwiss data. First, values are taken from the hour nearest the beginning of the measurement, to the nearest from the end. There are between two and six values kept. Second, the mean value is recorded. The latter value is the one that is compared. However, this gives the mean temperature at Aigle. This station is at 318m; measurements location at Huémoz is approximately at 1080m. Therefore, the third step is to calculate the corresponding temperature from Aigle to Huémoz. We use the coefficient of -0.5°C per 100m to calculate (Fallot, 2014).

We obtain a difference of 3.5°C between the two locations. We deducted the latter value to Aigle's temperature to find the Huémoz one.

Temperatures obtained are approximate, but it is not a problem as the goal is to see if temperature affects lidar signal.

Figure 30 following is the scatterplot showing the relation between temperature and parameter value. This graph is made with parameters values obtained with the exponential decay, using `fminsearch` and `fmincon` functions, with all the measurements. Axis X is the temperature modified from Aigle; axis Y is the parameter value. Diamonds are values from the `fmincon` function, crosses are the ones from the `fminsearch` function.

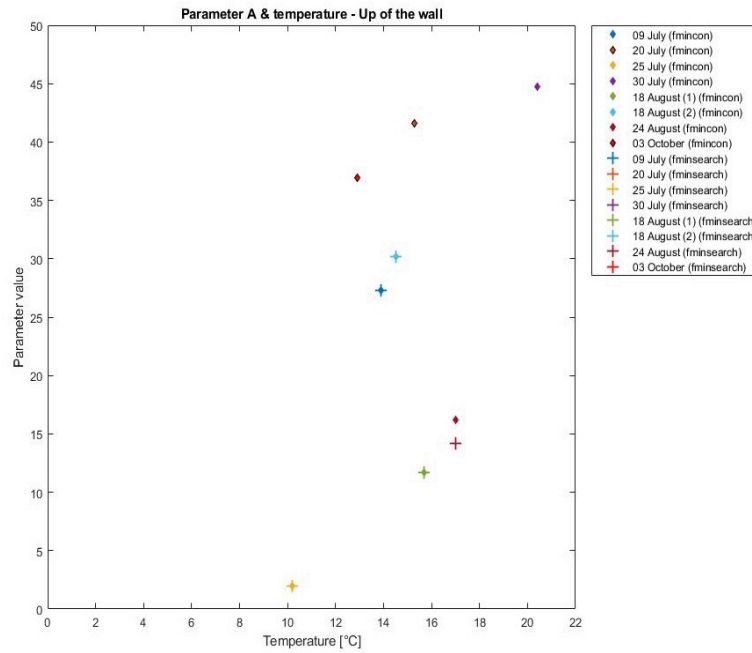


Fig. 30: Scatter plot with parameter a value, from `fminsearch` and `fmincon` functions, and temperature. For the upper part of the wall.

What stands out with this graph is that there is no real relation between temperature and parameter value. Indeed, for a near similar temperature, it is possible to have different values for a . Figure 31 after shows similar results. Parameter c has a similar behavior to a . Parameter b also does not have a clear reaction as there are few variations. Perhaps the latter one could be correlated to temperature, however, it is not obvious.

Therefore, we cannot use temperature to explain some of the changes we had seen previously. This can have an impact on lidar reaction, however we cannot determine it precisely.

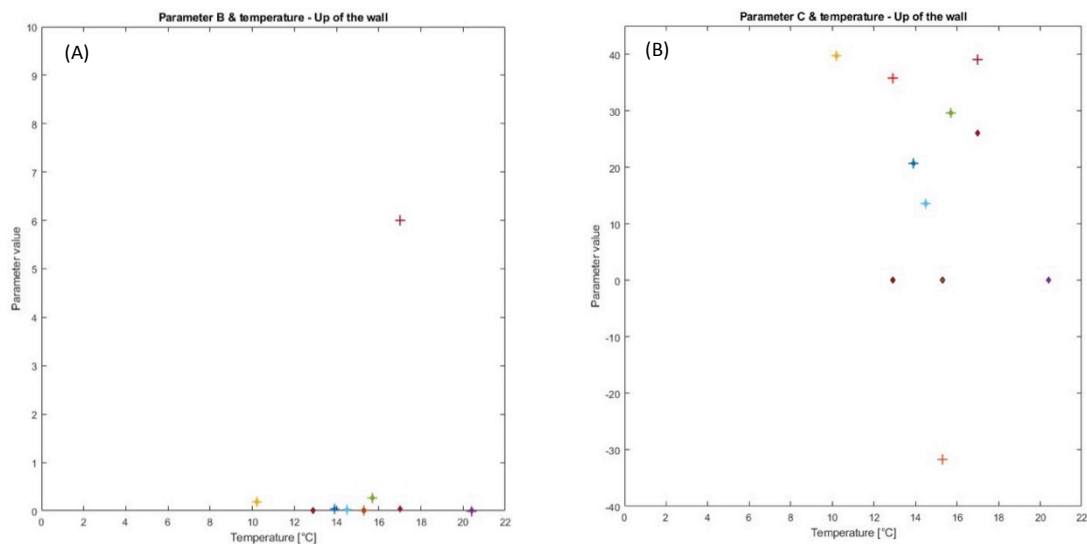


Fig. 31: Scatter plot with parameters values: b (A), c (B) from `fminsearch` and `fmincon` functions and temperature. For the upper part of the wall.

3.4. Effect of distance

The goal is to see if there could be a limit from where intensity changes. If this was the case, it can be find.

Figure 32, is a screenshot of veloview program. This is a first glimpse at the repartition of values with distance. We could think that going far from lidar makes the intensity decrease. This is true but only for a certain distance. Indeed, we can see that from 60m, values stop decreasing and increase. Some obstacles seem to reflect more lidar's beam, even if there are few. Around, there are trees which could reflect and make values increase.

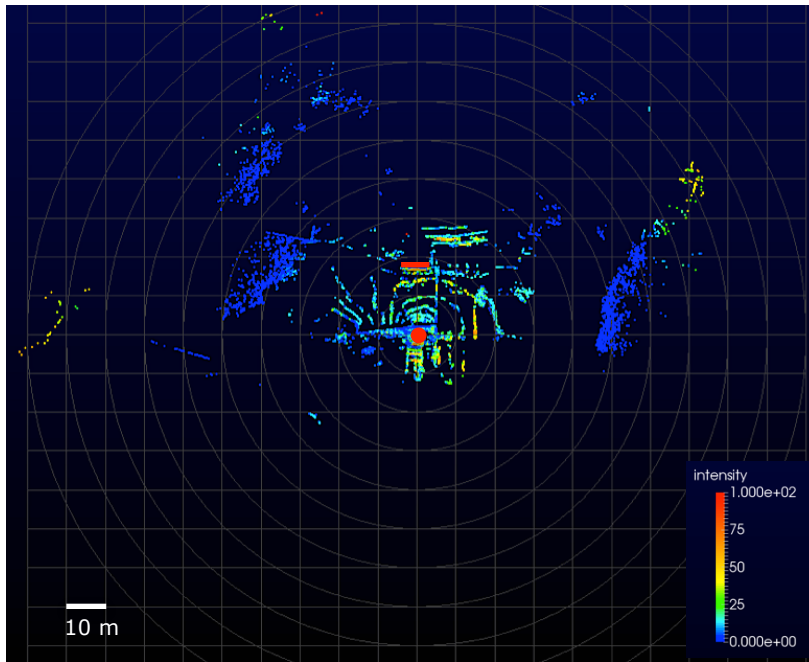


Fig. 32: Screenshot of the 18th August (1) scan. Red dot is the lidar; red line is the scanned wall.

This is a visual representation. Looking at values gives more information. Table 9 below is part of the 18th August (1) event. There are the values corresponding to distances from 5 to 40 meters. It is the mean value of all points being in the distance interval.

Table 9: Mean lidar intensity depending the distance; from 5 to 40 meters.

Hour of scan	Rainfall intensity [mm/h]	Between 5-10m	Between 10-15m	Between 15-20m	Between 20-30m	Between 30-40m
18:06	0.8	24.7333	18.9643	18.1430	19.0313	4.8777
18:08	2.3	21.9384	15.8026	15.7890	16.0597	4.2106
18:10	41.4	21.1015	14.5590	14.6497	14.7291	3.9764
18:12	35.6	20.5096	12.4779	12.3573	12.6510	3.4631
18:14	6.5	21.7659	14.1859	15.2277	15.1968	3.8266
18:16	2	21.7668	14.4956	16.0304	16.1085	3.9668

This is interesting, because it shows that when moved away from lidar, the intensity decreases. In this part, the higher intensity is the closest to lidar. There is a small decrease between 10 and 20 meters. However, at the interval of 20 to 30 meters, there is a slight increase in values.

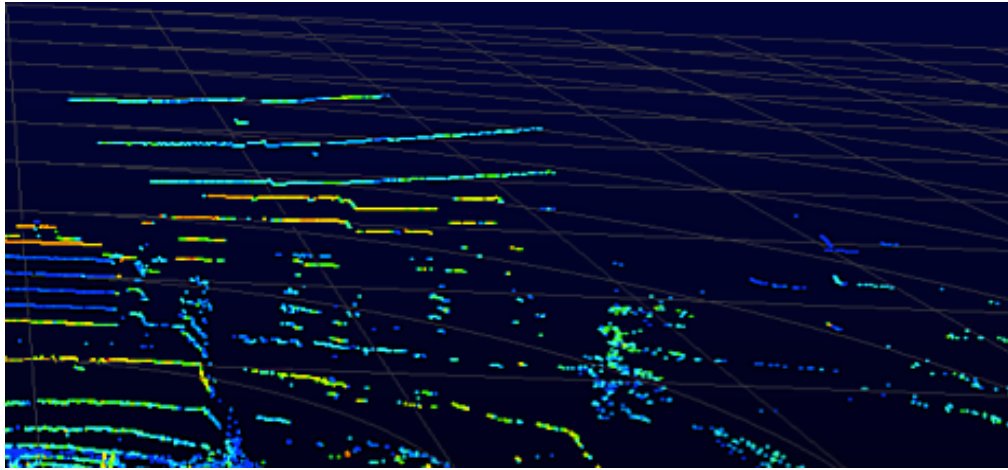


Fig. 33: Screenshot of 18 August (1) scan, with measurements between 20 and 30 meters.

This increase is explained with figure 33. Certainly, between 20 and 30 meters, there is another part of the house, which reflects lidar's beam. All this façade is in wood. It is similar to the upper part of the analyzed wall. In addition, there is a tree on the right of the scan. These elements can explain the increase of intensity between 20 and 30 meters.

Table 10 is the remaining values for part of the 18th August (1) scan. It goes from 40 to 100 meters.

Table 10: Mean lidar intensity depending the distance; from 40 to 100 meters.

Hour of scan	Rainfall intensity [mm/h]	Between 40-50m	Between 50-60m	Between 60-70m	Between 70-80m	Between 80-90m	Between 90-100m
18:06	0.8	0.5625	0.1877	3.6491	19.1251	34.7999	51.6043
18:08	2.3	0.4461	0.1122	3.6151	17.9649	34.8383	51.6632
18:10	41.4	0.3853	0.0900	3.5764	17.2648	33.8417	50.6856
18:12	35.6	0.2976	0.0895	4.0561	16.1634	32.8375	49.6591
18:14	6.5	0.4140	0.1552	4.2484	18.7909	34.8567	46.7118
18:16	2	0.4494	0.1671	4.1317	18.8169	34.7189	49.3518

These values are interesting, as we can see that from 60 meters, values are increasing. This can be explained by the presence of the forest at this distance. In addition, increasing distance reduces the number of measurements. Therefore, it happens that less than ten values represent an interval. Having little data also affects the robustness of the mean that is used in the analyses.

Figure 34 is the graph corresponding to table 9. Axis X is the rainfall intensity in mm/h; axis Y is the lidar signal intensity.

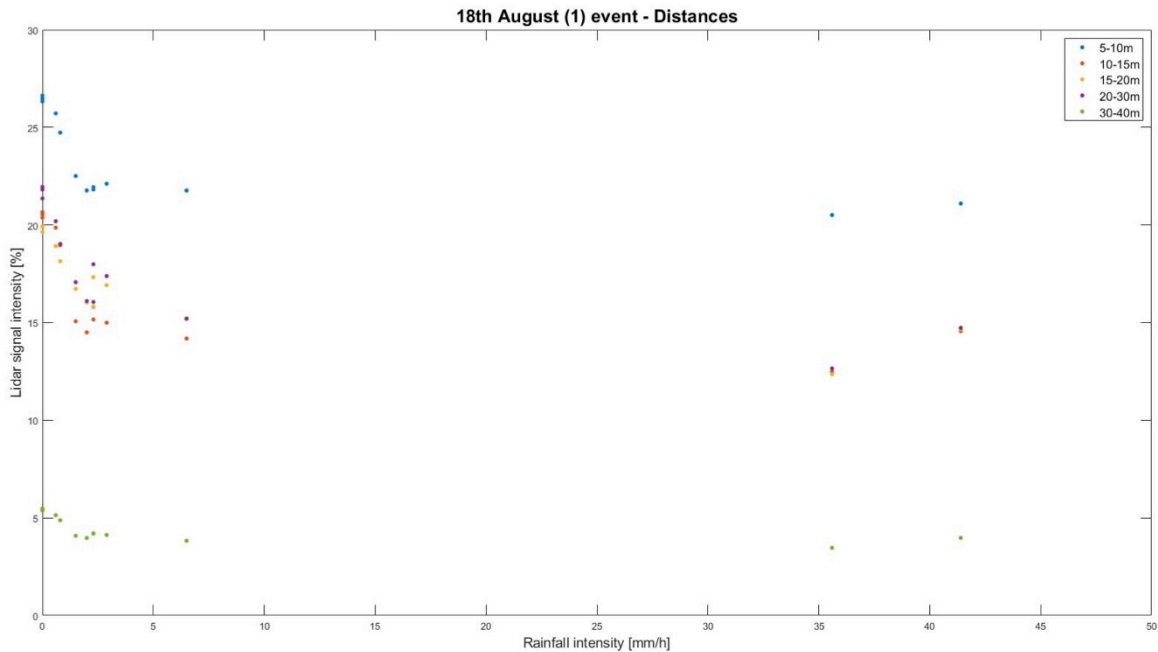


Fig. 34: Scatterplot with results for distances for the 18th August (1) event.

Looking at this figure, we have another confirmation that lidar's signal decreases with higher rainfall intensity. Regarding distances between 5 to 30 meters, they have a similar behavior. These four intervals show the lidar intensity decrease significantly up to rainfall rate 10 mm/h. This is interesting, because we could think that something influences the signal. However, the 18th August (1) event presents nothing particular. In addition, this reaction can be found within the majority of events. Later, lidar reaction continues to reduce. In this graph, it has been decided to not plot the other distances as they increase from 60 meters. This would attenuate the fact that lidar's signal decreases with higher rainfall intensity. The ones between 40 and 60 meters are very low and have a reaction that stays stable; they have few variations.

Another interesting point is that with distances we can see the effect of fog on scan. Figure 35 is an example from the 8th August scan with fog data. Organization is the same as previously. This graph allows fog to be seen, as some scans appear to have it. These ones have lower lidar intensity than the others.

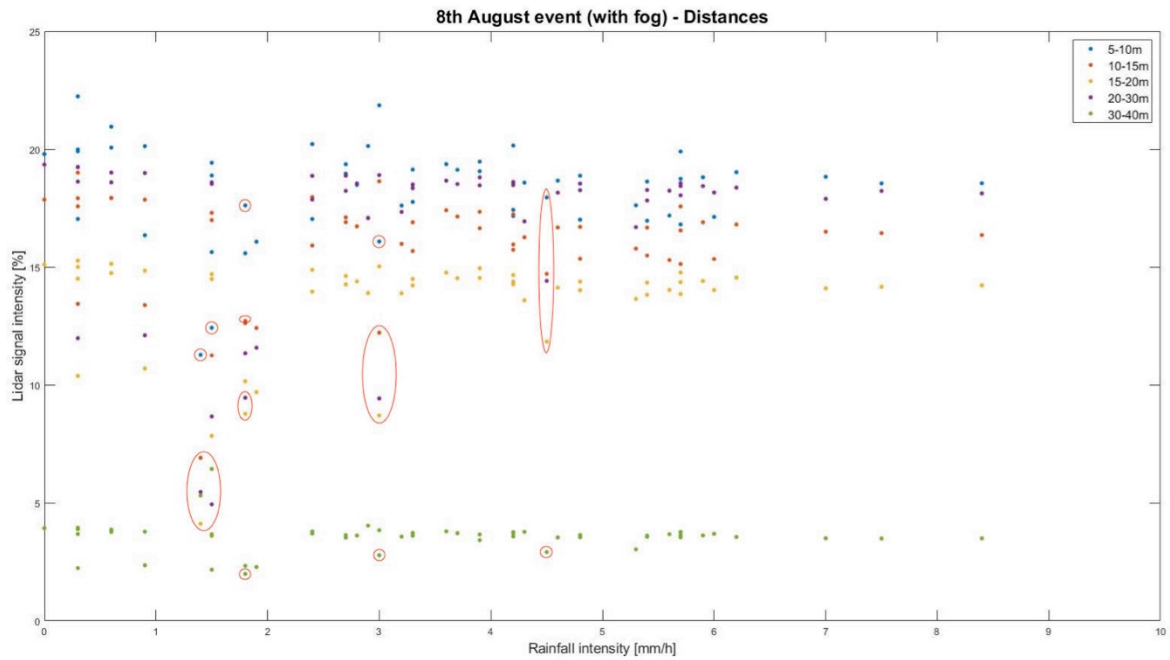


Fig. 35: Scatterplot with results for distances for the 8th August event. Red circles are the scans with fog, that were removed from analysis.

4. Discussion

Several elements stand out with this study. This concerns environmental conditions as well as instrumental ones.

To start with, the environmental conditions intra-event must be examined. During the measurement period, from the beginning to the end of the event, the environment changes. It becomes wetter, particularly when regarding all the scan. For the wall, it is certain that it stays dry. Other parts like trees are wet and this can influence returning lidar signal.

Furthermore, the environmental conditions inter-events must be investigated. Between two measurements periods, the environment changes. The size of raindrops and quantity of them change through events. This is also linked to the season, which also has an impact. A Spring rainfall is not similar to a Summer thunderstorm. This is normal; it is the natural variability of rainfall. However, it has an impact on measurements and the results we obtain. The localization of measurements is also to note, as it is in a mountainous area. This affects the signal, as the rainfall can be another type. All these elements are already known, as it has been shown in the literature review (section 1.2). Gires et al. (2014) talked about rainfall's natural variability, as did Jaffrain & Berne in 2010 and Michaelides et al. in 2009. This variability is well known, but can be underestimated in studies. It is considered that it had an impact on this research.

Linked to the latter condition is the DSD. As Adriosi et al. (2016) and Jaffrain & Berne (2012) stated, it naturally changes as rainfall. It affects radar data and after analysis, we can say that it is almost the same with a lidar. In this study, some varying outcomes can be the result of DSD.

From these last two elements, we can focus on rainfall intensity. It has been seen in section 3.2, that rainfall rate which does not exceed 10 mm/h has a lot of variability. This is reinforced by Macke's statement (1998) who said concerning the intensity of this value, (that) "*rainfall rates and particles sizes are essentially uncorrelated below this value.*" I believe that results for polynomial are less accurate and useful as there is this big variability.

These are mainly environmental issues that have been taken into account. If measurements are made in parallel with the scans, it could be possible to diminish them. Indeed, knowing rainfall type can bring further information, which could improve results. Another complementary measurement that is possible is the temperature or humidity. In this study, this parameter has been considered somewhat, but there are uncertainties. Data that are more reliable could improve results.

Finally, there is an instrumental issue. It would be effective to test this method in a different environment. In fact, wall materials as in this study, wood and expanded polystyrene, are not the best. It would be useful to test using a concrete wall for example. This could reduce some uncertainties, as the reaction should be more homogeneous, it should have less variability. A place to try could be the UNIL campus, on the Amphipôle.

Conclusion

This research had two objectives. The first one was to have a simple theoretical framework. This allowed seeing if it is possible to estimate rainfall rate with a low-cost lidar. The second one was to test the theory with measurements. These two objectives have been completed, through the literature review in section 1; the measurements made between April and November 2017, analyzed and from the results are in section 3.

The goal with this research was to answer the following question: is it possible to estimate rainfall intensity with a low-cost topographic lidar? The working hypothesis was yes. This is also the answer I give to the question. However, results are based on a sampling measured on a limited period. Moreover, observed relations are complex and not everything behind is taken into account in this study. It is a step showing that something can be done in this field.

This work had set up a methodology that can be used further and applied. Using a low-cost terrestrial lidar to estimate rainfall rate is possible. The beginning of the study was to work with a noise, which is the same approach as with radars. From this, we had obtained reliable results, with a great sampling. However, there are uncertainties, coming from different sources: the environment, measurements, mean calculations and interpolations made.

The method used can be improved, by making complementary measurements, such as temperature or humidity. Knowing rainfall type could also give information that would make results more precise. In addition, looking for a homogenous wall would provide accurate data.

In conclusion, even if there are some uncertainties and results should be taken cautiously, they are reliable and promising. There is a relationship between lidar and rainfall rate, which can be found using this method. This simple relation is a result per se, as at the beginning of the research it was unknown.

A further work could use this method, trying to find a generalization. This would be possible by improving the methodology and would make it even more reliable.

References

Articles, books, courses

- Adirosi, E., Volpi, E., Lombardo, F., & Baldini, L. (2016). Raindrop size distribution: Fitting performance of common theoretical models. *Advances in Water Resources*, 96, 290-305. doi: 10.1016/j.advwatres.2016.07.010
- Andra, D. L., Quetone, E. M., & Bunting, W. F. (2002). Warning Decision Making: The Relative Roles of Conceptual Models, Technology, Strategy, and Forecaster Expertise on 3 May 1999. *Weather and Forecasting*, 17(3), 559-566. doi: 10.1175/1520-0434(2002)017<0559:WDMTRR>2.0.CO;2
- Balin, D. (2016). *Hydrologie et cycle de l'eau - cours 3 : Précipitations* (class slides). University of Lausanne, Faculty of Geosciences and environment, Institute of Earth Surface Dynamics (IDYST), Switzerland.
- Benoit, L., & Mariethoz, G. (2017). Generating synthetic rainfall with geostatistical simulations. *Wiley Interdisciplinary Reviews: Water*, 4(2), n/a-n/a. doi: 10.1002/wat2.1199
- Berne, A., Jaffrain, J., & Schleiss, M. (2012). Scaling analysis of the variability of the rain drop size distribution at small scale. *Advances in Water Resources*, 45, 2-12. doi: 10.1016/j.advwatres.2011.12.016
- Beraldin, J.-A., Blais, F., & Lohr, U. (2010). Laser scanning technology. In Vosselman, G., & Maas, H.-G., *Airborne and terrestrial laser scanning* (pp.1-43). Caithness: Whittles Publishing.
- Brocard, E., Philipona, R., Haefele, A., Romanens, G., Mueller, A., Ruffieux, D., ... Calpini, B. (2013). Raman Lidar for Meteorological Observations, RALMO - Part 2: Validation of water vapor measurements. *Atmospheric Measurement Techniques*, 6(5), 1347-1358. doi: 10.5194/amt-6-1347-2013
- Campbell, J., & Whyne, R. (2011). Lidar. In Campbell, J., & Whyne, R.H. *Introduction to Remote Sensing* (pp.243-255). New York: Guilford Press.
- Casari, A., Javelle, P., Ramos, M. H., & Leblois, E. (2016). Generating precipitation ensembles for flood alert and risk management. *Journal of Flood Risk Management*, 9(4), 402-415. doi: 10.1111/jfr3.12203
- Charlton, M.E., Coveney, S. J., & McCarthy, T. (2009). Issues in Laser scanning. In Heritage, G. L., & Large, A. R. G. *Laser scanning for the environmental sciences* (pp.35-48). Chichester: Wiley-Blackwell.
- Ciach, G. J. (2003). Local Random Errors in Tipping-Bucket Rain Gauge Measurements. *Journal of Atmospheric and Oceanic Technology*, 20(5), 752-759. doi: 10.1175/1520-0426(2003)20<752:LREITB>2.0.CO;2
- Demir, I., & Krajewski, W. F. (2013). Towards an integrated Flood Information System: Centralized data access, analysis, and visualization. *Environmental Modelling & Software*, 50(Supplement C), 77-84. doi: 10.1016/j.envsoft.2013.08.009
- Derron, M.-H. (2016). *Remote sensing of the earth - Introduction to Lidar* (class slides). University of Lausanne, Faculty of Geosciences and environment, Institute of Earth Surface Dynamics (IDYST), Switzerland.
- Dinoev, T., Simeonov, V., Arshinov, Y., Bobrovnikov, S., Ristori, P., Calpini, B., ... van den Bergh, H. (2013). Raman Lidar for Meteorological Observations, RALMO - Part 1: Instrument description. *Atmospheric Measurement Techniques*, 6(5), 1329-1346. doi: 10.5194/amt-6-1329-2013
- Driptych (s.d.a). Pluvimate High-resolution rainfall logger.
- Fallot, J.-M. (2014). *Climatologie*. (Polycopié). Université de Lausanne, Faculté des géosciences et de l'environnement, Institut de géographie et durabilité, Suisse.
- Gires, A., Tchiguirinskaia, I., Schertzer, D., Schellart, A., Berne, A., & Lovejoy, S. (2014). Influence of small scale rainfall variability on standard comparison tools between radar and rain gauge data. *Atmospheric Research*, 138, 125-138. doi: 10.1016/j.atmosres.2013.11.008
- Hudak, A. T., Evans, J. S., & Stuart Smith, A. M. (2009). LiDAR Utility for Natural Resource Managers. *Remote Sensing*, 1(4), 934-951. doi: 10.3390/rs1040934
- Jaboyedoff, M., Oppikofer, T., Abellán, A., Derron, M.-H., Loye, A., Metzger, R., & Pedrazzini, A. (2012). Use of LIDAR in landslide investigations: a review. *Natural Hazards*, 61(1), 5-28. doi: 10.1007/s11069-010-9634-2

- Jaffrain, J., & Berne, A. (2010). Experimental Quantification of the Sampling Uncertainty Associated with Measurements from PARSIVEL Disdrometers. *Journal of Hydrometeorology*, 12(3), 352-370. doi: 10.1175/2010JHM1244.1
- Jaffrain, J., & Berne, A. (2012). Influence of the Subgrid Variability of the Raindrop Size Distribution on Radar Rainfall Estimators. *Journal of Applied Meteorology and Climatology*, 51(4), 780-785. doi: 10.1175/JAMC-D-11-0185.1
- Kathiravelu, G., Lucke, T., & Nichols, P. (2016). Rain Drop Measurement Techniques: A Review. *Water*, 8(1), 29. doi: 10.3390/w8010029
- Krajewski, W. F., Anderson, M. C., Eichinger, W. E., Entekhabi, D., Hornbuckle, B. K., Houser, P. R., ... Wood, E. F. (2006). A remote sensing observatory for hydrologic sciences: A genesis for scaling to continental hydrology. *Water Resources Research*, 42(7), W07301. doi: 10.1029/2005WR004435
- Krajewski, W. F., Ciach, G. J., & Habib, E. (2003). An analysis of small-scale rainfall variability in different climatic regimes. *Hydrological Sciences Journal*, 48(2), 151-162. doi: 10.1623/hysj.48.2.151.44694
- Large, A. R. G., & Heritage, G. L. (2009). Laser Scanning - Evolution of the Discipline. In Heritage, G. L., & Large, A. R. G., *Laser scanning for the environmental sciences* (pp. 1-20). Chichester: Wiley-Blackwell.
- Lewandowski, P. A., Eichinger, W. E., Kruger, A., & Krajewski, W. F. (2009). Lidar-Based Estimation of Small-Scale Rainfall: Empirical Evidence. *Journal of Atmospheric and Oceanic Technology*, 26(3), 656-664. doi:10.1175/2008JTECHA1122.1
- Lichti, D., & Skaloud, J. (2010). Registration and calibration. In Vosselman, G., & Maas, H.-G., *Airborne and terrestrial laser scanning* (pp.83-133). Caithness: Whittles Publishing.
- Lillesand, T., Kiefer, R., & Chipman, J. (2008). Microwave and Lidar sensing. In Lillesand, T., Kiefer, R., & Chipman, J. *Remote Sensing and Image Interpretation* (pp. 714-716). Hoboken, N.J.: J. Wiley.
- Lolli, S., Welton, E. J., & Campbell, J. R. (2013). Evaluating Light Rain Drop Size Estimates from Multiwavelength Micropulse Lidar Network Profiling. *Journal of Atmospheric and Oceanic Technology*, 30(12), 2798-2807. doi: 10.1175/JTECH-D-13-00062.1
- Macke, A., & Großklaus, M. (1998). Light scattering by nonspherical raindrops: Implications for lidar remote sensing of rainrates. *Journal of Quantitative Spectroscopy and Radiative Transfer*, 60(3), 355-363. doi: 10.1016/S0022-4073(98)00011-9
- Mallet, C., & Bretar, F. (2009). Full-waveform topographic lidar: State-of-the-art. *ISPRS Journal of Photogrammetry and Remote Sensing*, 64(1), 1-16. doi: 10.1016/j.isprsjprs.2008.09.007
- Manap, H., Dooly, G., O'Keefe, S., & Lewis, E. (2009). Ammonia Detection in the UV Region using an optical fiber sensor. *IEEE Sensors*, pp.140-145. doi: 10.1109/ICSENS.2009.5398215
- Mandapaka, P. V., Lewandowski, P., Eichinger, W. E., & Krajewski, W. F. (2009). Multiscaling analysis of high resolution space-time lidar-rainfall. *Nonlin. Processes Geophys.*, 16(5), 579-586. doi: 10.5194/npg-16-579-2009
- Mariéthoz, G. (2016a). Télédétection - cours 2 : Interactions ondes-atmosphères (class slides). University of Lausanne, Faculty of Geosciences and environment, Institute of Earth Surface Dynamics (IDYST), Switzerland.
- Mariéthoz, G. (2016b). Télédétection - cours 8 : LIDAR (class slides). University of Lausanne, Faculty of Geosciences and environment, Institute of Earth Surface Dynamics (IDYST), Switzerland.
- Marshall, J., & Palmer, W. (1948). The Distribution of Raindrops with Size. *Journal of Meteorology*, 5(4), 165-166. doi: 10.1175/1520-0469(1948)005<0165:TDORWS>2.0.CO;2
- MeteoSwiss (2012). Prévisions météo: mesurer pour anticiper. Office fédéral de météorologie et de climatologie, Zurich.
- MeteoSwiss (s.d.). LIDAR : La vapeur d'eau dans la troisième dimension.
- Michaelides, S., Levizzani, V., Anagnostou, E., Bauer, P., Kasparis, T., & Lane, J. E. (2009). Precipitation: Measurement, remote sensing, climatology and modeling. *Atmospheric Research*, 94(4), 512-533. doi: 10.1016/j.atmosres.2009.08.017
- Musy, A., & Higy, C. (2014). La mesure hydrologique. In Musy, A., Higy, C., & Reynard, E. (éd.), *Hydrologie 1 - Une science de la nature, une gestion sociétale* (pp.223-256). Lausanne : Presses polytechniques et universitaires romande.

- Portland State University (s.d.). *Light Detection and Ranging (LiDAR)* (class slides). Spotted at: <http://web.pdx.edu/~jduh/courses/geog493f12/Week04.pdf>
- Rasshofer, R. H., Spies, M., & Spies, H. (2011). Influences of weather phenomena on automotive laser radar systems. *Adv. Radio Sci.*, 9, 49-60. doi: 10.5194/ars-9-49-2011
- Strangeways, I. (2010). A history of rain gauges. *Weather*, 65(5), 133-138. doi: 10.1002/wea.548
- Uijlenhoet, R. (2001). Raindrop size distributions and radar reflectivity-rain rate relationships for radar hydrology. *Hydrology and Earth System Sciences*, 5(4), 615-627. doi: 10.5194/hess-5-615-2001
- Uijlenhoet, R., Steiner, M., & Smith, J. A. (2003). Variability of raindrop size distributions in a squall line and implications for radar rainfall estimation. *Journal of Hydrometeorology*, 4(1), 43-61. doi: 10.1175/1525-7541(2003)004<0043:VORSDI>2.0.CO;2
- Velodyne (2016b). User's manual and programming guide.
- Westbrook, C. D., Hogan, R. J., O'Connor, E. J., & Illingworth, A. J. (2010). Estimating drizzle drop size and precipitation rate using two-colour lidar measurements. *Atmos. Meas. Tech.*, 3(3), 671-681. doi: 10.5194/amt-3-671-2010

Websites

- BLET-climat (2017). Pluviomètre de type HELLMANN THIES - BLET. *Pluviomètres mécaniques*. Spotted at: <https://www.blet-climat.fr/pluviometres-mecaniques/pluviometre-de-hellmann.html> (consulted the 11th June 2017).
- Disdromet (s.d.). DESCRIPTION OF THE DISDROMETER RD-80. *Product description*. Spotted at: <http://distromet.com/94/product-description/disdrometer-rd-80> (consulted the 11th June 2017)
- Driptych (s.d.b). Pluvimate. *Driptych*. Spotted at: <http://driptych.com> (consulted the 15th June 2017).
- Futura-sciences (2017). Effet Raman. *Sciences, définitions, physique*. Spotted at: <http://www.futura-sciences.com/sciences/definitions/physique-effet-raman-2014/> (consulted the 16th May 2017)
- Lidar (2017, 25 February). *In Wikipédia*. Spotted at: <https://fr.wikipedia.org/wiki/Lidar> (consulted the 4th March 2017)
- Lidar (2017, 25 February). *In Wikipédia*. Spotted at: <https://en.wikipedia.org/wiki/Lidar> (consulted the 4th March 2017)
- MeteoSwiss (2014a, 1st December). LIDAR et ceilomètre. *Système de mesure et de prévision - atmosphère*. Spotted at: <http://www.meteosuisse.admin.ch/home/systemes-de-mesure-et-de-prevision/atmosphere/lidar-et-ceilometre.html> (consulted the 8th May 2017)
- MeteoSwiss (2014b, 1st December). Stations au sol. *Systèmes de mesure et de prévision*. Spotted at: <http://www.meteosuisse.admin.ch/home/systemes-de-mesure-et-de-prevision/stations-au-sol.html> (consulted the 7th March 2017)
- MeteoSwiss (2014c, 1st December). Instruments de mesure. *Systèmes de mesure et de prévision*. Spotted at: <http://www.meteosuisse.admin.ch/home/systemes-de-mesure-et-de-prevision/stations-au-sol/reseau-de-mesures-automatiques/instruments-de-mesure.html> (consulted the 11th June 2017)
- MeteoSwiss (2016, 8 February). Comment fonctionne un radar météorologique?. *Le réseau Suisse de radars météorologique*. Spotted at: <http://www.meteosuisse.admin.ch/home/systemes-de-mesure-et-de-prevision/atmosphere/le-reseau-suisse-de-radars-meteorologiques/comment-fonctionne-un-radar-meteorologique.html> (consulted the 11th June 2017)
- NASA (1994, 1 August). LITE : Measuring the atmosphere with laser precision. *Fact sheet*. Spotted at: <https://www.nasa.gov/centers/langley/news/factsheets/LITE.html> (consulted the 25th April 2017)
- NASA (2016, 29 June). CALIPSO payload. *About CALIPSO*. Spotted at: <https://www-calipso.larc.nasa.gov/about/payload.php#CALIOP> (consulted the 25th April 2017)
- NOAA (2015, 29 May). What is LIDAR?. *Ocean facts*. Spotted at: <http://oceanservice.noaa.gov/facts/lidar.html> (consulted the 4th March 2017)
- NTRS (2010, 1st January). NASA's space Lidar measurements of earth and planetary surfaces. *NASA Technical Reports Server (NTRS)*. Spotted at: <https://ntrs.nasa.gov/search.jsp?R=20100031189> (consulted the 8th May 2017)

Velodyne LiDAR (2016a). Puck VLP-16. *Products*. Spotted at: <http://velodynelidar.com/vlp-16.html>
(consulted the 20th December 2016)

Appendixes

Appendix A - The linear function results

A.I. Graphs and results for all the events

This part regroups graphs from the three parts, which are not explained in the main manuscript.

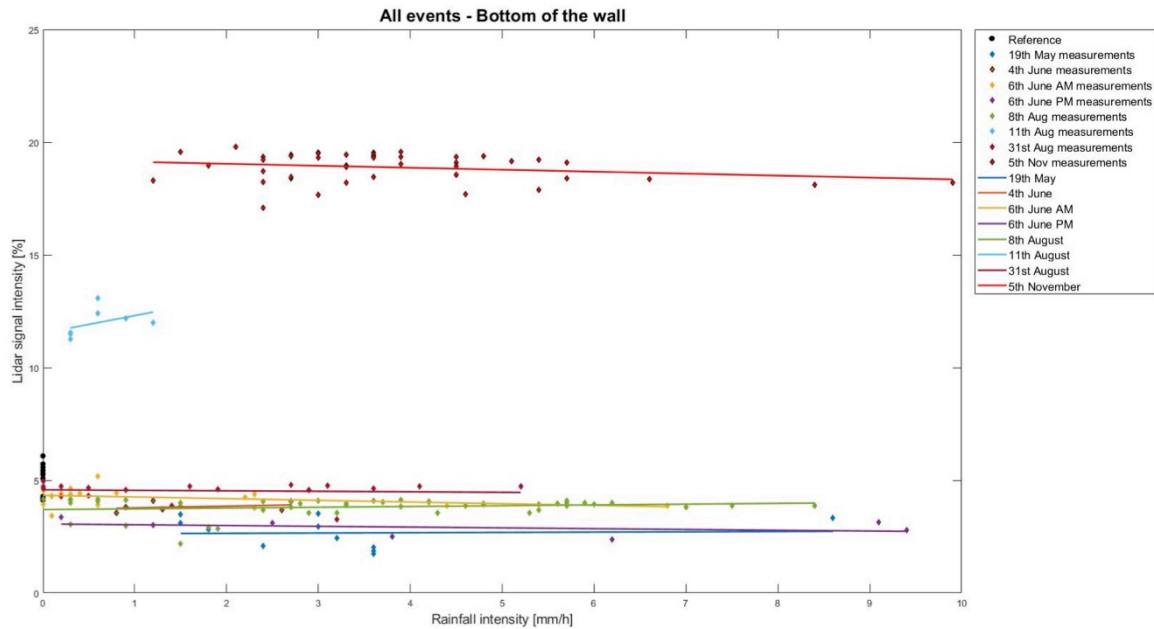


Fig. I: Results for all events within rainfall intensity which does not exceed 10 mm/h for the lower part of the wall.

Table I: Results of the linear function, for the lower part of the wall.

Date	a_1	a_0	R^2
19 May	0.0129	2.6217	0.0014
4 June	0.0776	3.6960	0.0916
6 June AM	-0.0747	4.3333	0.1188
6 June PM	-0.0347	3.0602	0.1307
8 August	0.0344	3.6980	0.0336
11 August	0.7816	11.5231	0.1812
31 August	-0.0219	4.5755	0.0084
05 November	-0.0874	19.2143	0.0554

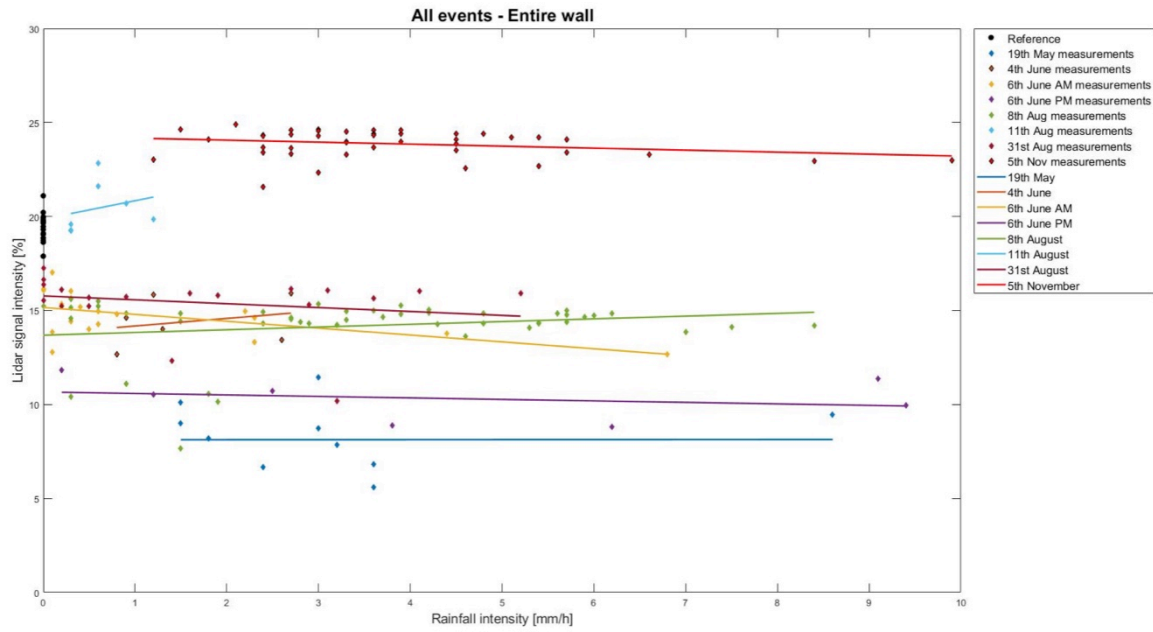


Fig. IV: Results for all events within rainfall intensity which does not exceed 10 mm/h for the entire wall.

Table II: Results of the linear function, for the entire wall.

Date	a_1	a_0	R^2
19 May	0.0016	8.1233	3E-06
4 June	0.4021	13.7744	0.0684
6 June AM	-0.3659	15.1599	0.3088
6 June PM	-0.0790	10.6649	0.0639
8 August	0.1453	13.6849	0.0395
11 August	0.9763	19.8619	0.0622
31 August	-0.2067	15.7758	0.0451
05 November	-0.1065	24.2751	0.0624

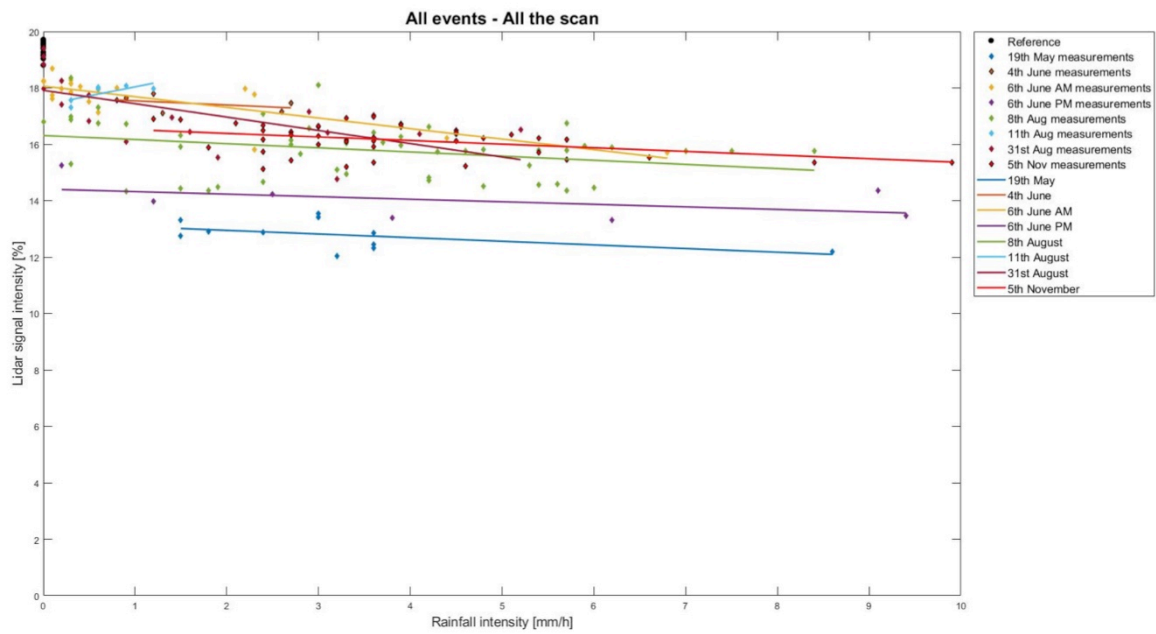


Fig. V: Results for all events within rainfall intensity which does not exceed 10 mm/h for all the scan.

Table III: Results of the linear function, for all the scan.

Date	a_1	a_0	R^2
19 May	-0.1290	13.2052	0.2534
4 June	-0.1471	17.6922	0.2164
6 June AM	-0.3768	18.0663	0.6417
6 June PM	-0.0902	14.4104	0.2328
8 August	-0.1471	16.3127	0.1005
11 August	0.6455	17.3946	0.5875
31 August	-0.4740	17.9170	0.4102
05 November	-0.1294	16.6489	0.1746

A.II. Individual events graphic results

This part is the different graphs for the events individually.

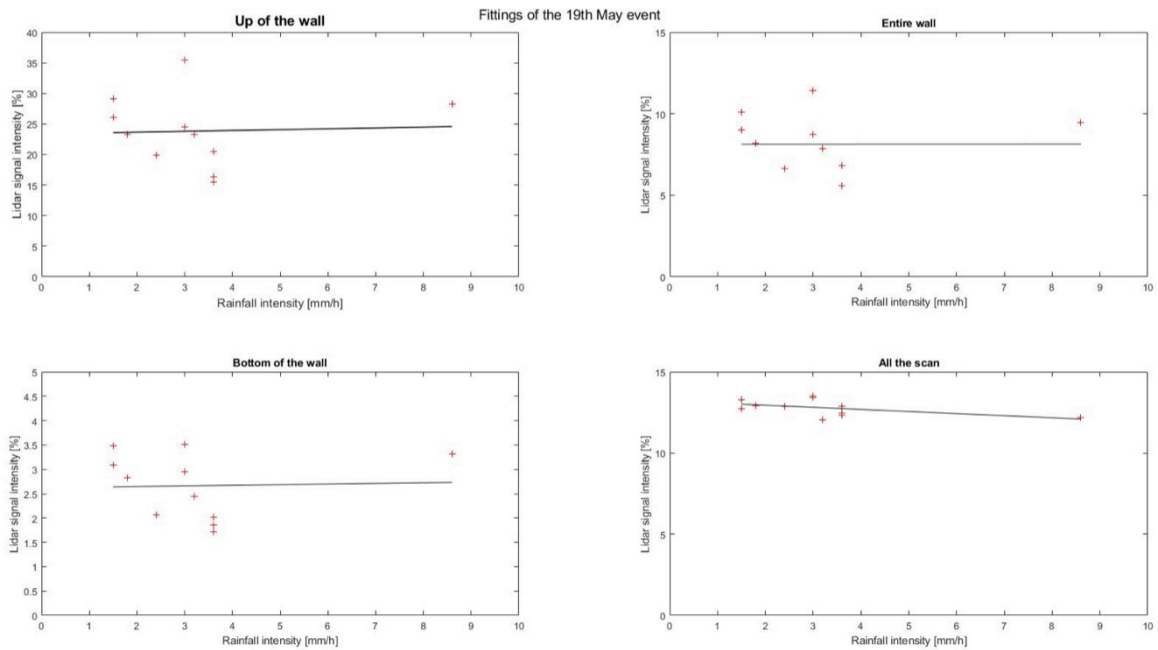


Fig. VI: Graphs for all the parts, for the 19th May event.

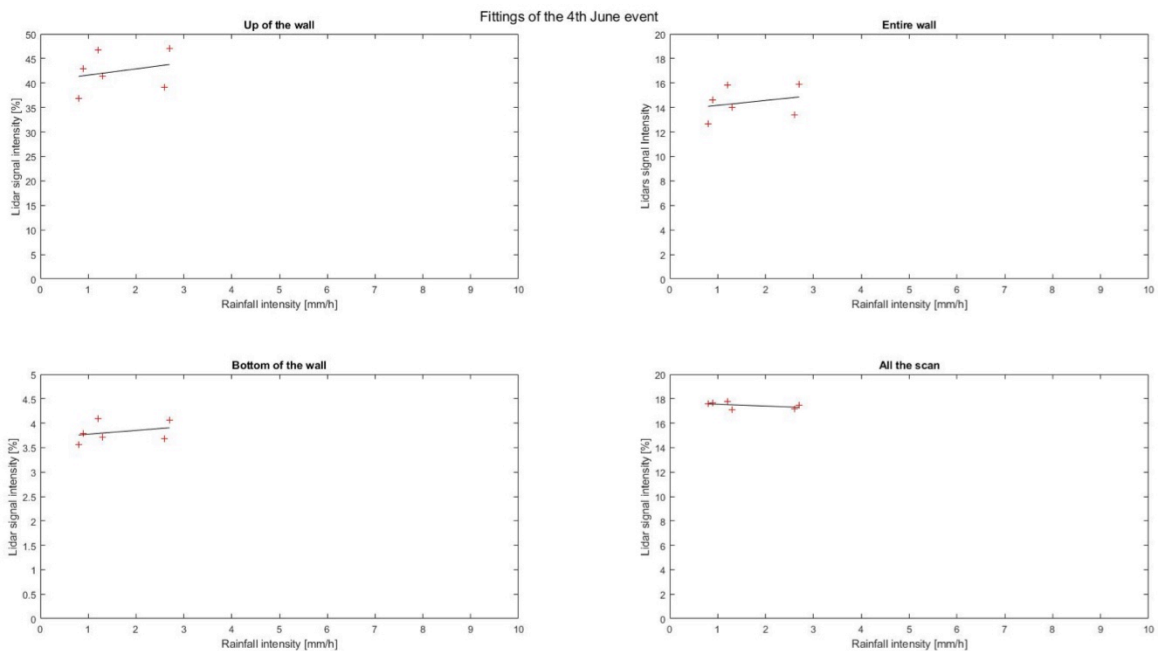


Fig. VII: Graphs for all the parts, for the 4th June event.

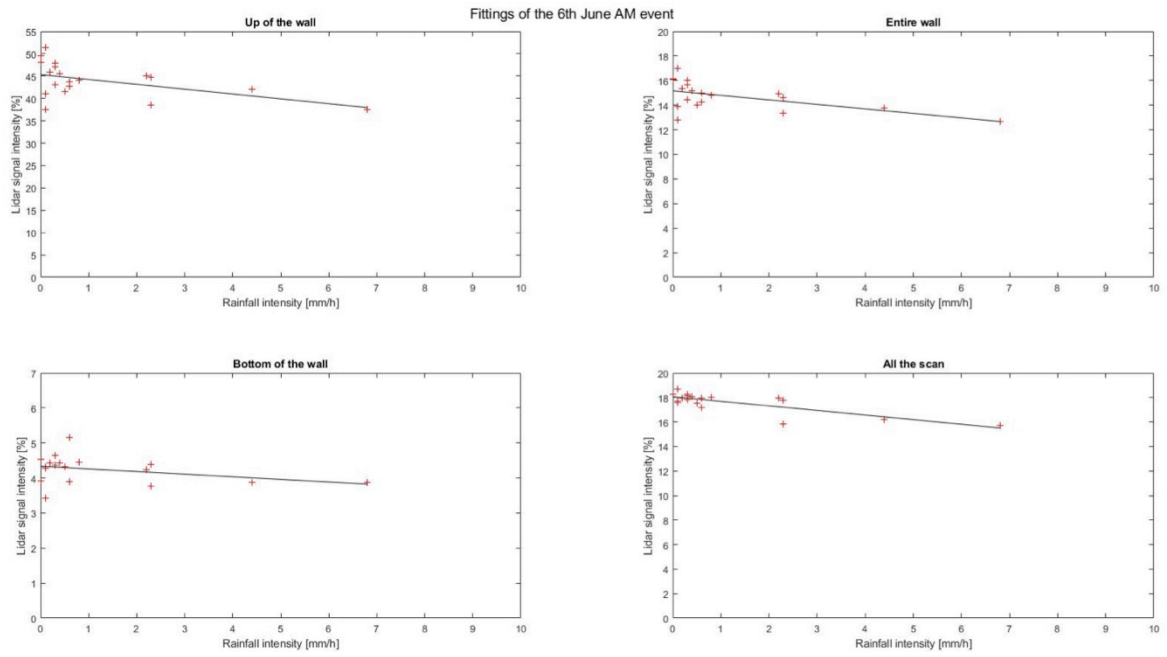


Fig. VIII: Graphs for all the parts, for the 6th June AM event.

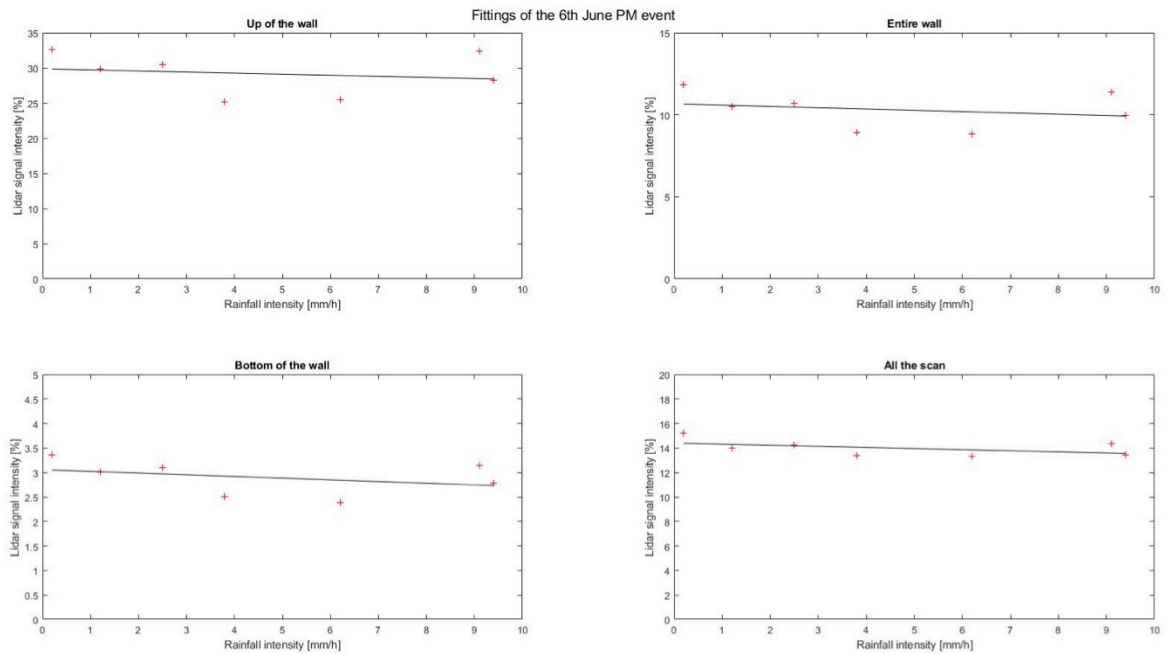


Fig. IX: Graphs for all the parts, for the 6th June PM event.

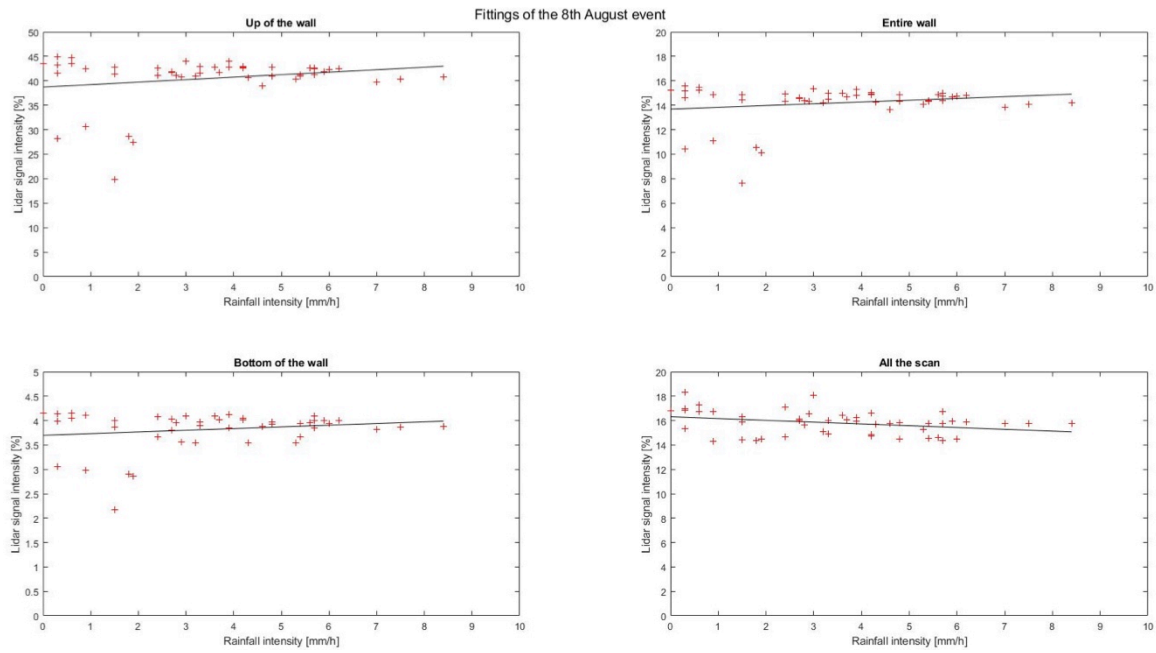


Fig. X: Graphs for all the parts, for the 8th August event.

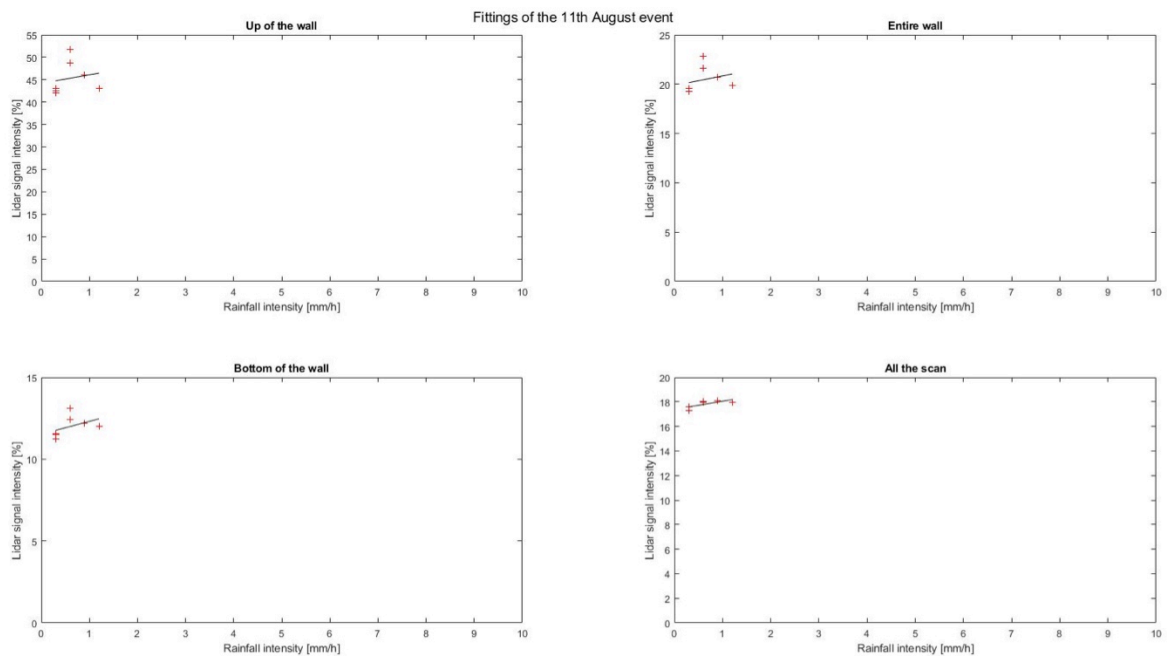


Fig. XI: Graphs for all the parts, for the 11th August event.

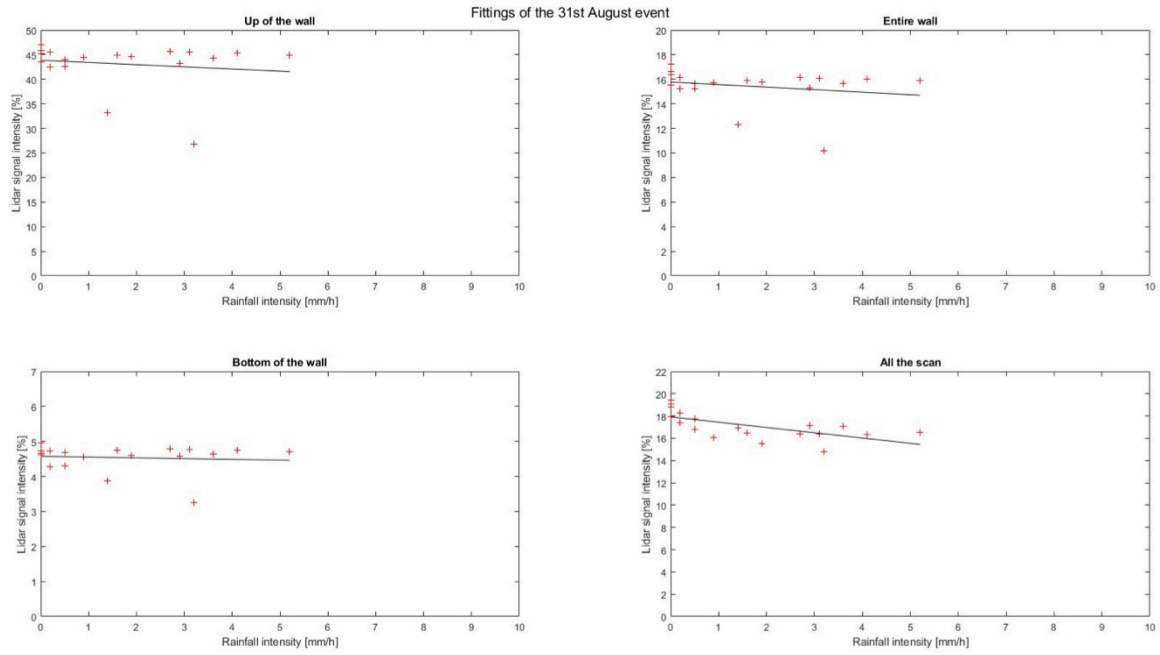


Fig. XII: Graphs for all the parts, for the 31st August event.

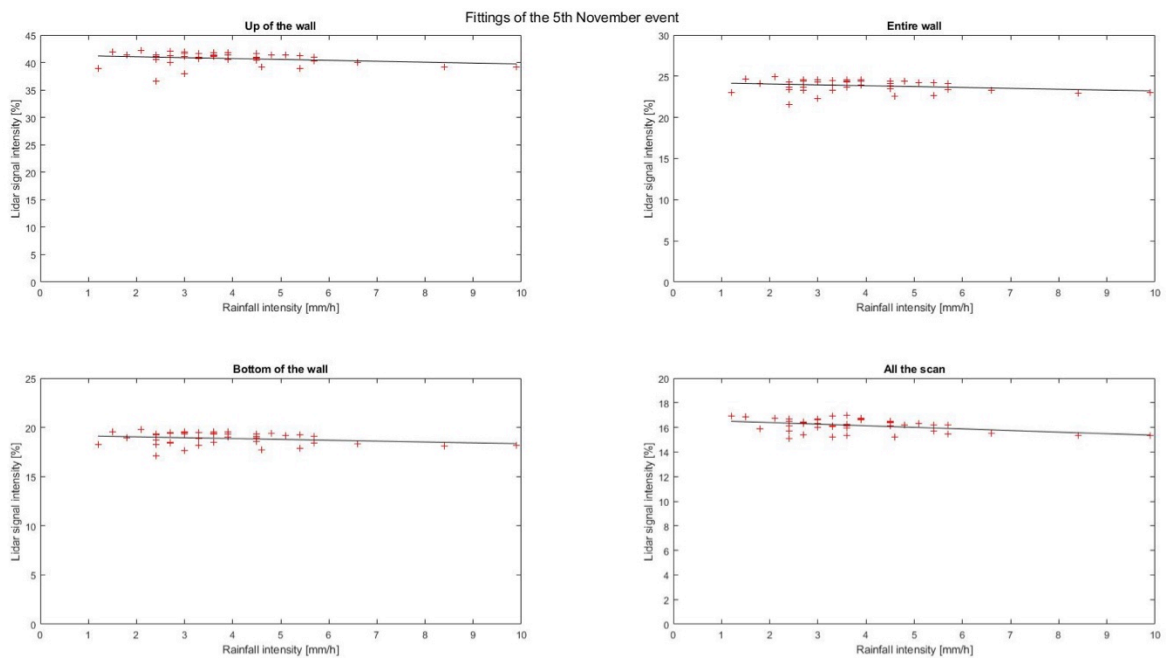


Fig. XIII: Graphs for all the parts, for the 5th November event.

Appendix B - The exponential function results

B.I. Graphs and results for all the events

This part regroups graphs from the three parts, which are not explained in the main manuscript.

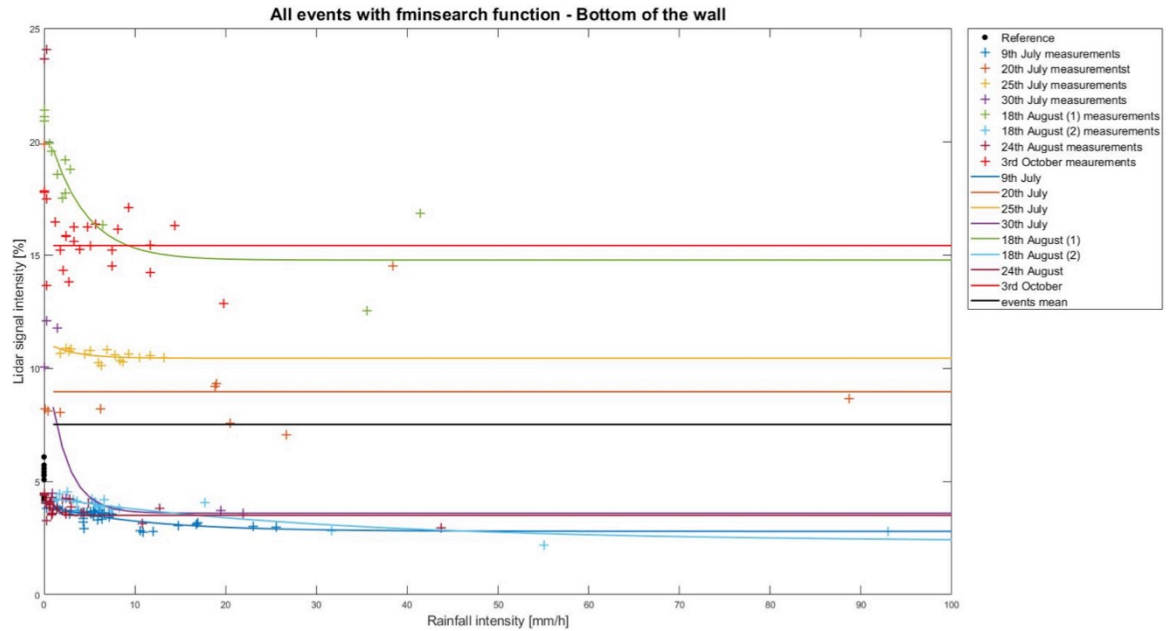


Fig. XIV: Results for all events having a rainfall intensity getting higher than 10 mm/h for the lower part of the wall, using the fminsearch function on Matlab.

Table IV: Results for the exponential function, with fminsearch on Matlab. For the lower part of the wall.

Date	A	B	C	RMSE
9 July	1.1414	0.0926	2.7916	0.2022
20 July	5.8044E+03	70.3947	8.9575	3.1185
25 July	0.7426	0.3377	10.4367	0.1890
30 July	7.5179	0.4713	3.5915	2.5044
18 August (1)	6.2503	0.2467	14.7683	1.0141
18 August (2)	1.9628	0.0309	2.3344	0.2595
24 August	7.7421	2.7622	3.4987	4.5559
3 October	9.4147	13.7493	15.4078	1.0734

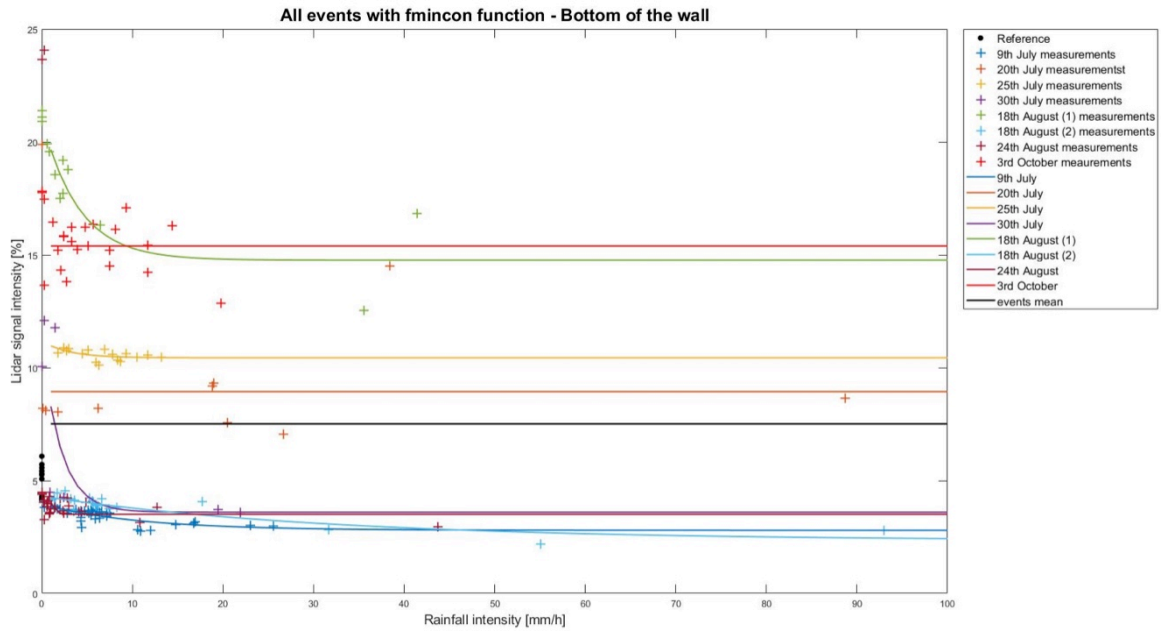


Fig. XV: Results for all events having a rainfall intensity getting higher than 10 mm/h for the lower part of the wall, using the fmincon function on Matlab.

Table V: Results for the exponential function, with fmincon on Matlab. For the lower part of the wall.

Date	A	B	C	RMSE
9 July	1.1415	0.0926	2.7916	0.2022
20 July	13.8174	10.0000	8.9354	3.1257
25 July	0.7426	0.3377	10.4367	0.1890
30 July	7.5179	0.4713	3.5915	2.5044
18 August (1)	6.2503	0.2467	14.7683	1.0141
18 August (2)	1.9628	0.0309	2.3345	0.2595
24 August	7.7421	2.7621	3.4987	4.5559
3 October	6.4505	10.0000	15.3944	1.0744

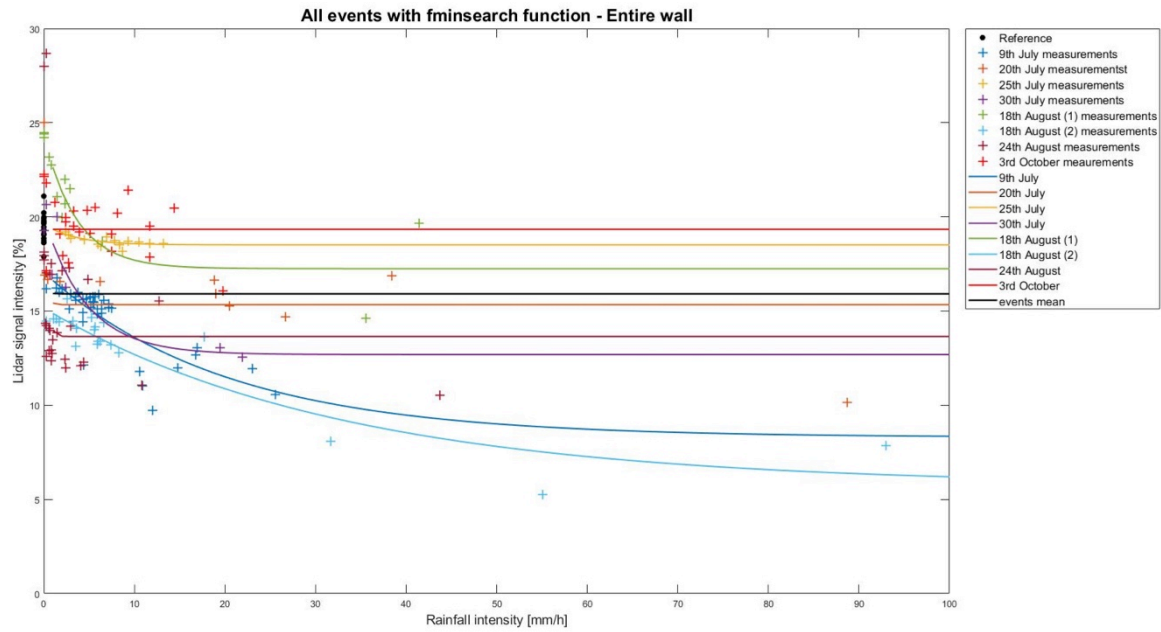


Fig. XVI: Results for all events having a rainfall intensity getting higher than 10 mm/h for the entire wall, using the fminsearch function on Matlab.

Table VI: Results for the exponential function, with fminsearch on Matlab. For the entire wall.

Date	A	B	C	RMSE
9 July	8.7569	0.0501	8.2926	1.0364
20 July	9.0369	4.7333	15.3409	2.4779
25 July	1.1025	0.2874	18.5154	0.1900
30 July	7.3254	0.2150	12.6888	1.1750
18 August (1)	7.0844	0.2755	17.2516	1.1701
18 August (2)	9.4098	0.0303	5.7470	0.9813
24 August	9.2163	3.3862	13.6508	3.4050
3 October	13.5053	15.5101	19.3408	1.3313

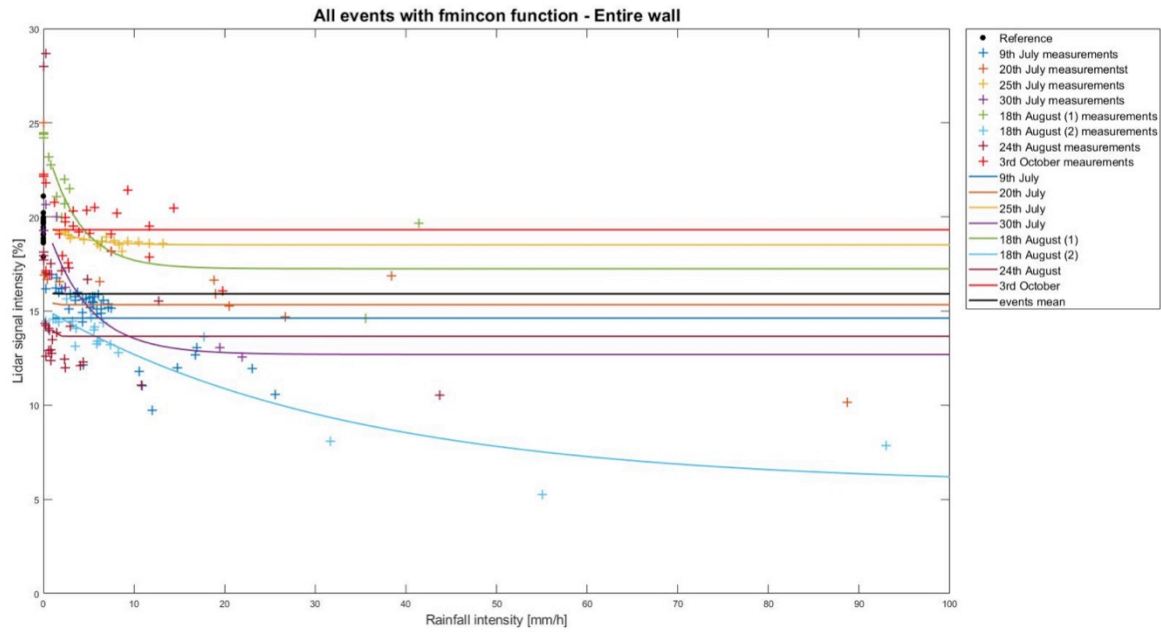


Fig. XVII: Results for all events having a rainfall intensity getting higher than 10 mm/h for the entire wall, using the fmincon function on Matlab.

Table VII: Results for the exponential function, with fmincon on Matlab. For the entire wall.

Date	A	B	C	RMSE
9 July	24.0806	9.1190	14.6265	1.7209
20 July	9.0369	4.7333	15.3409	2.4779
25 July	1.1025	0.2874	18.5154	0.1900
30 July	7.3255	0.2150	12.6888	1.1750
18 August (1)	7.0844	0.2755	17.2516	1.1701
18 August (2)	9.4098	0.0303	5.7469	0.9813
24 August	9.2163	3.3862	13.6508	3.4050
3 October	7.7525	9.9999	19.3203	1.3332

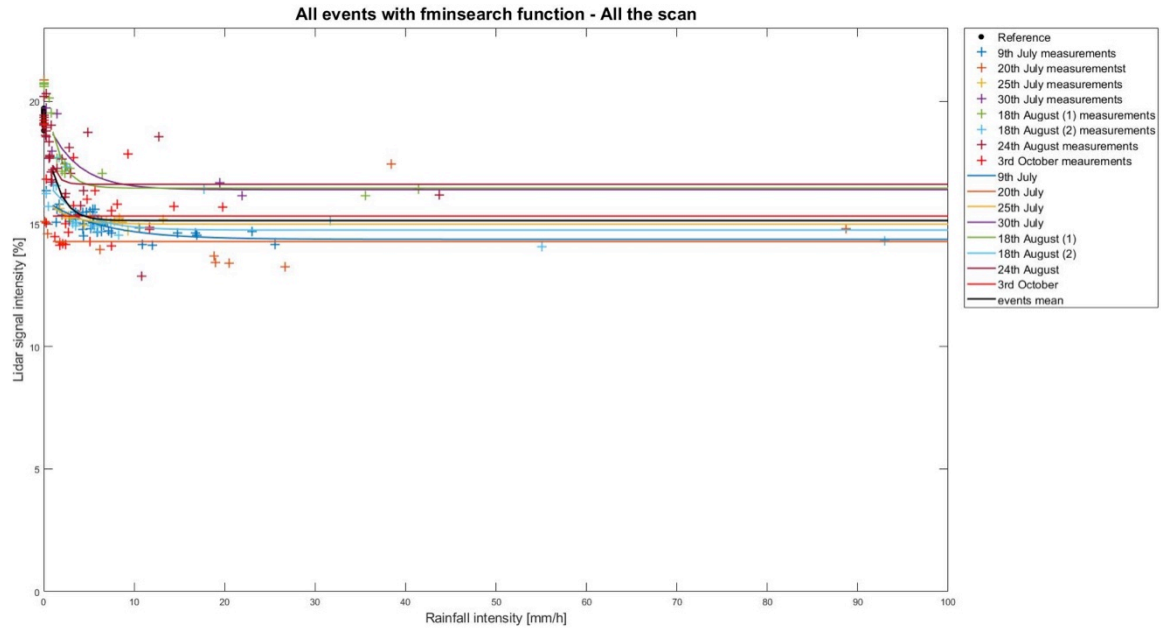


Fig. XVIII: Results for all events having a rainfall intensity getting higher than 10 mm/h for all the scan, using the fminsearch function on Matlab.

Table VIII: Results for the exponential function, with fminsearch on Matlab. For all the scan.

Date	A	B	C	RMSE
9 July	1.6356	0.1651	14.3757	0.3033
20 July	8.2917	8.0969	14.2871	1.6498
25 July	1.0283	0.4004	14.9951	0.1537
30 July	3.0632	0.2999	16.4036	0.6300
18 August (1)	4.6853	0.7156	16.4688	0.3419
18 August (2)	2.1666	0.2820	14.7545	0.7169
24 August	3.4283	1.4878	16.6241	1.0689
3 October	9.5470	9.1498	15.3257	1.0080

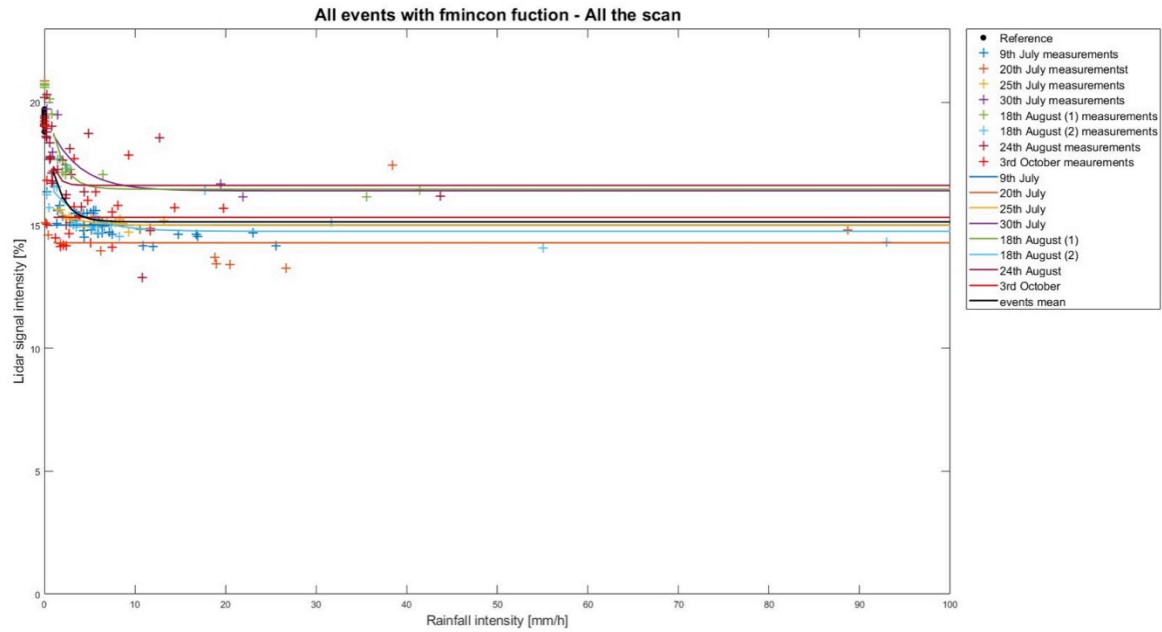


Fig. XIX: Results for all events having a rainfall intensity getting higher than 10 mm/h for all the scan using the fmincon function on Matlab.

Table IX: Results for the exponential function, with fmincon on Matlab. For all the scan.

Date	A	B	C	RMSE
9 July	24.0136	9.5994	15.0090	0.4158
20 July	8.2915	8.0967	14.2871	1.6498
25 July	1.0283	0.4004	14.9951	0.1537
30 July	3.0632	0.2999	16.4037	0.6300
18 August (1)	4.6853	0.7156	16.4688	0.3419
18 August (2)	2.1666	0.2820	14.7545	0.7169
24 August	3.4283	1.4878	16.6241	1.0689
3 October	9.5469	9.1497	15.3257	1.0080

B.II. Graphs and results for all the events, using bins

This part regroups graphs from the three parts, which are not explained in the main manuscript.

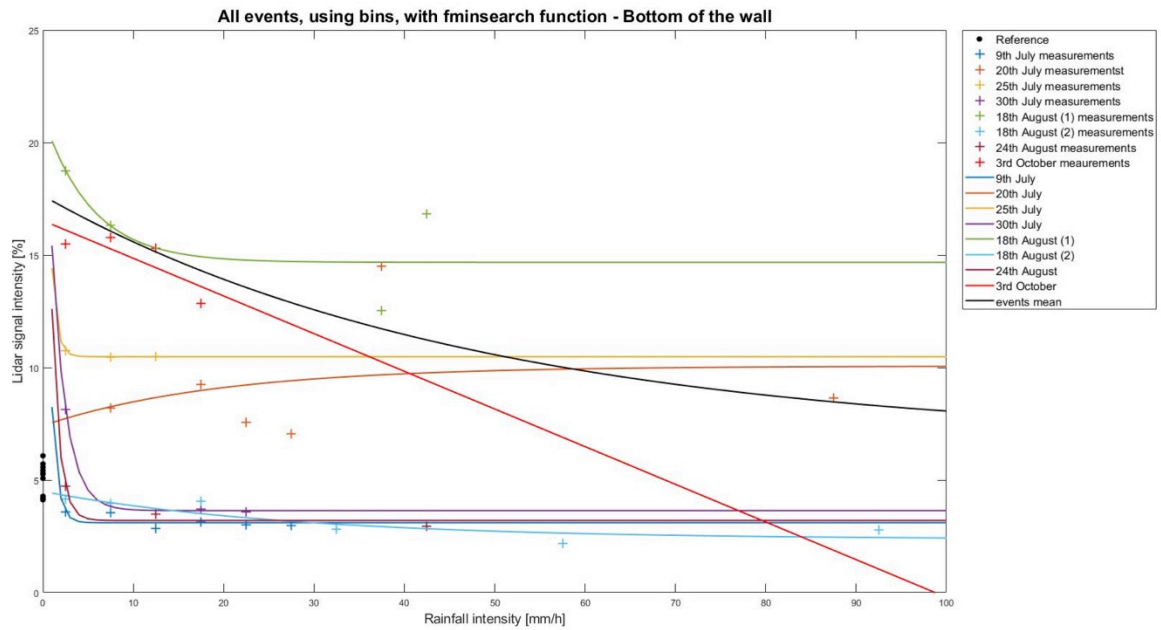


Fig. XX: Results, using bins, for all events having a rainfall intensity getting higher than 10 mm/h for the lower part of the wall, using the fminsearch function on Matlab.

Table X: Results for the exponential function, using bins, with fminsearch, for the lower part of the wall.

Date	A	B	C	RMSE
9 July	24.5502	1.5639	3.1050	0.2206
20 July	-2.6507	0.0509	10.0703	2.2045
25 July	23.5812	1.7916	10.4866	0.0110
30 July	22.3621	0.6413	3.6431	0.0612
18 August (1)	6.4947	0.1853	14.6747	1.5220
18 August (2)	2.1257	0.0354	2.3666	0.3395
24 August	31.6674	1.2144	3.2037	0.2225
3 October	1.1273E+06	1.4852E-07	-1.1273E+06	0.7022

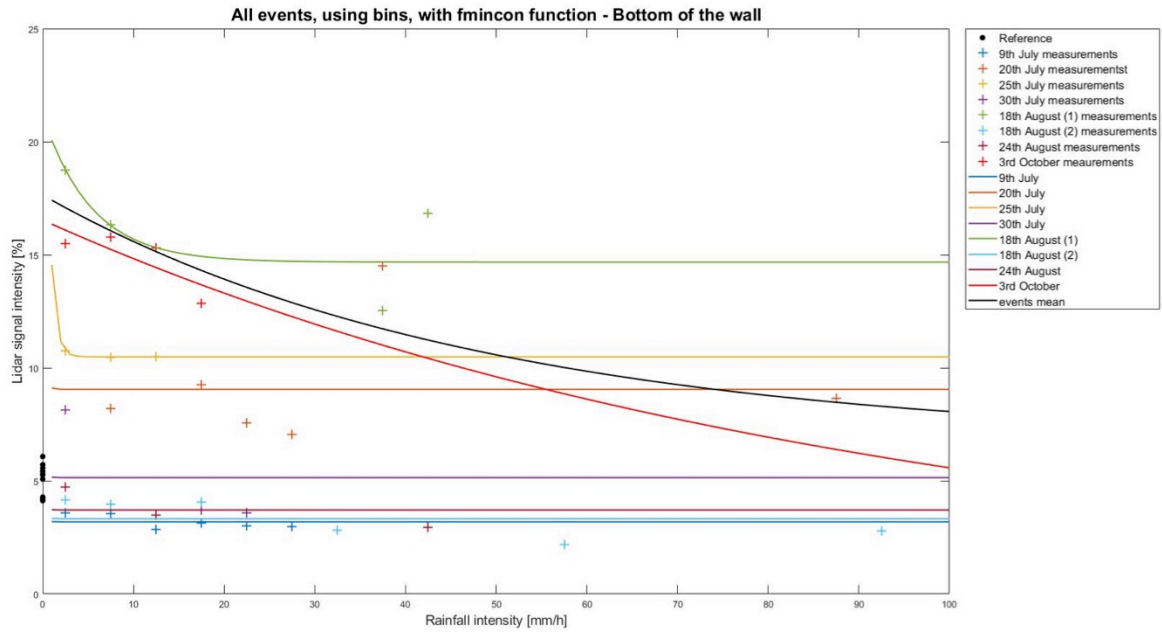


Fig. XXI: Results, using bins, for all events having a rainfall intensity getting higher than 10 mm/h for the lower part of the wall, using the fmincon function on Matlab.

Table XI: Results for the exponential function, using bins, with fmincon, for the lower part of the wall.

Date	A	B	C	RMSE
9 July	24.8861	7.6607	3.1870	0.2868
20 July	24.9132	6.1271	9.0482	2.3272
25 July	24.9842	1.8147	10.4866	0.0110
30 July	24.8871	7.2660	5.1431	2.1219
18 August (1)	6.4947	0.1853	14.6747	1.5220
18 August (2)	24.8879	7.6144	3.3251	0.7602
24 August	24.8771	7.7178	3.7106	0.7506
3 October	16.5316	0.0109	2.7786E-04	0.7245

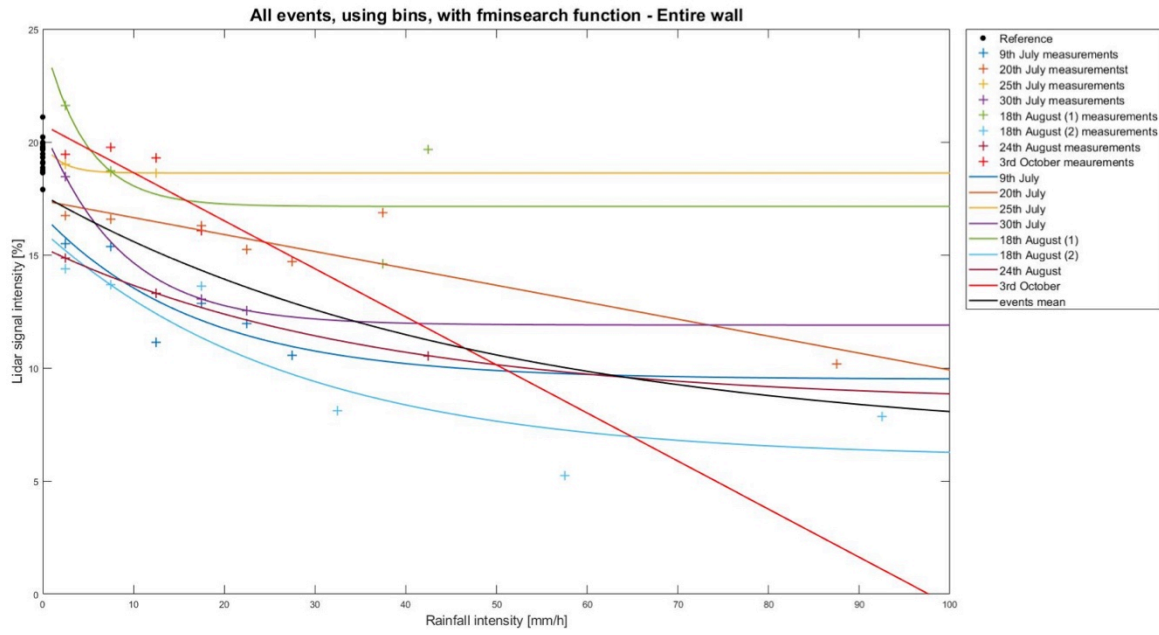


Fig. XXII: Results, using bins, for all events having a rainfall intensity getting higher than 10 mm/h for the entire wall, using the fminsearch function on Matlab.

Table XII: Results for the exponential function, using bins, with fminsearch, for the entire wall.

Date	A	B	C	RMSE
9 July	7.2558	0.0585	9.4924	0.9914
20 July	1.5291E+06	4.9002E-08	-1.5291E+06	0.9753
25 July	1.3180	0.4948	18.6147	4.2510E-07
30 July	8.7929	0.1161	11.8923	1.3897E-05
18 August (1)	7.5937	0.2124	17.1402	1.7831
18 August (2)	10.0615	0.0362	5.9967	1.4803
24 August	6.8968	0.0278	8.4258	4.0113E-06
3 October	1.0858E+06	1.9579E-07	-1.0857E+06	0.9038

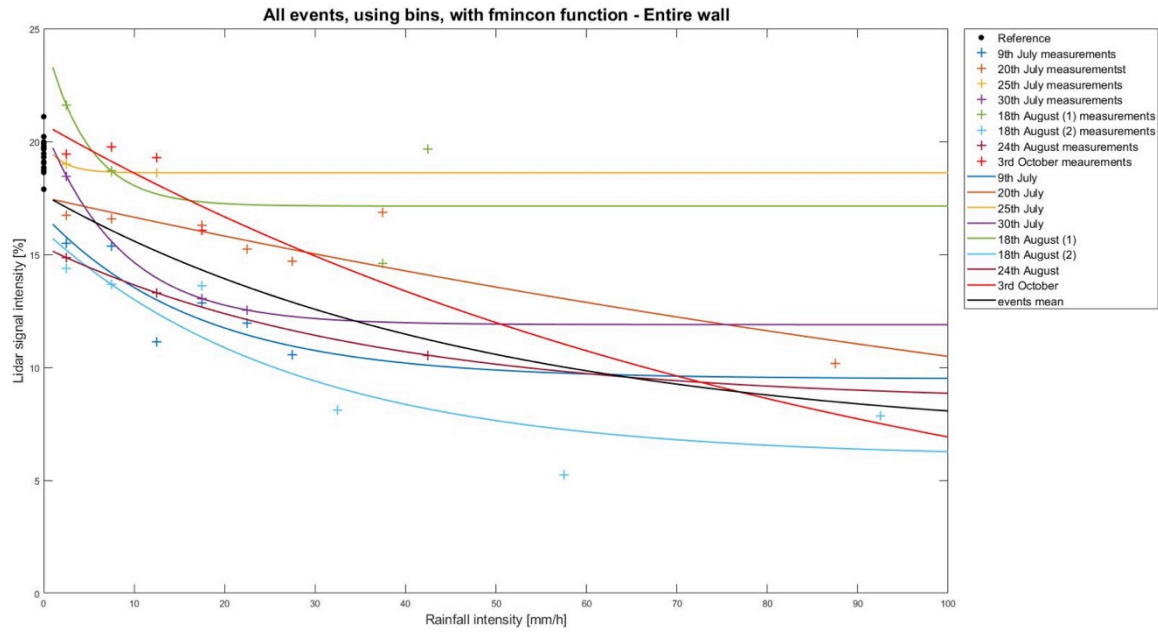


Fig. XXIII: Results, using bins, for all events having a rainfall intensity getting higher than 10 mm/h for the entire wall, using the fmincon function on Matlab.

Table XIII: Results for the exponential function, using bins, with fmincon, for the entire wall.

Date	A	B	C	RMSE
9 July	7.2558	0.0585	9.4924	0.9914
20 July	17.5166	0.0051	0.0069	1.0547
25 July	1.3180	0.4948	18.6147	3.0922E-07
30 July	8.7929	0.1161	11.8923	3.4737E-07
18 August (1)	7.5936	0.2124	17.1402	1.7831
18 August (2)	10.0614	0.0362	5.9968	1.4803
24 August	6.8969	0.0278	8.4257	3.4707E-06
3 October	20.7604	0.0110	2.1963E-04	0.9320

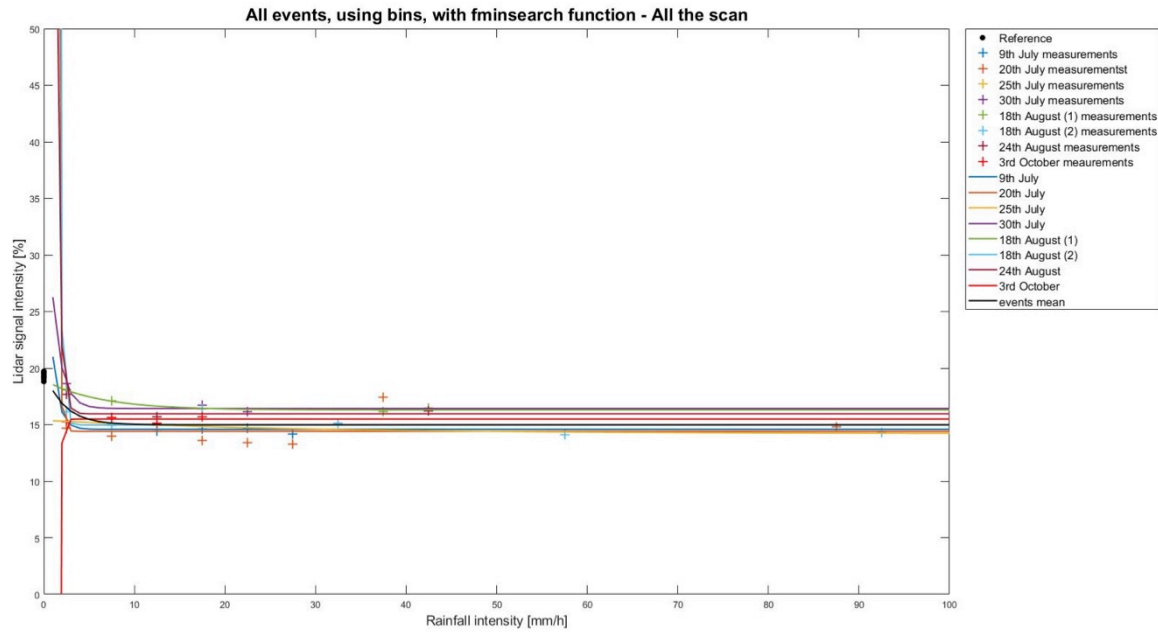


Fig. XXIV: Results, using bins, for all events having a rainfall intensity getting higher than 10 mm/h for all the scan, using the fminsearch function on Matlab.

Table XIV: Results for the exponential function, using bins, with fminsearch , for all the scan.

Date	A	B	C	RMSE
9 July	27.0006	1.4377	14.5916	0.2627
20 July	1.6320E+04	4.4440	14.4108	1.3437
25 July	1.1793	0.0362	14.2101	4.3751E-07
30 July	26.6728	0.9974	16.4267	0.2137
18 August (1)	2.6298	0.1630	16.2946	0.0996
18 August (2)	2.5133E+04	3.9956	14.9788	0.7448
24 August	829.8370	2.4659	15.9523	0.1915
3 October	-2.1122E+04	4.5977	15.4950	0.2275

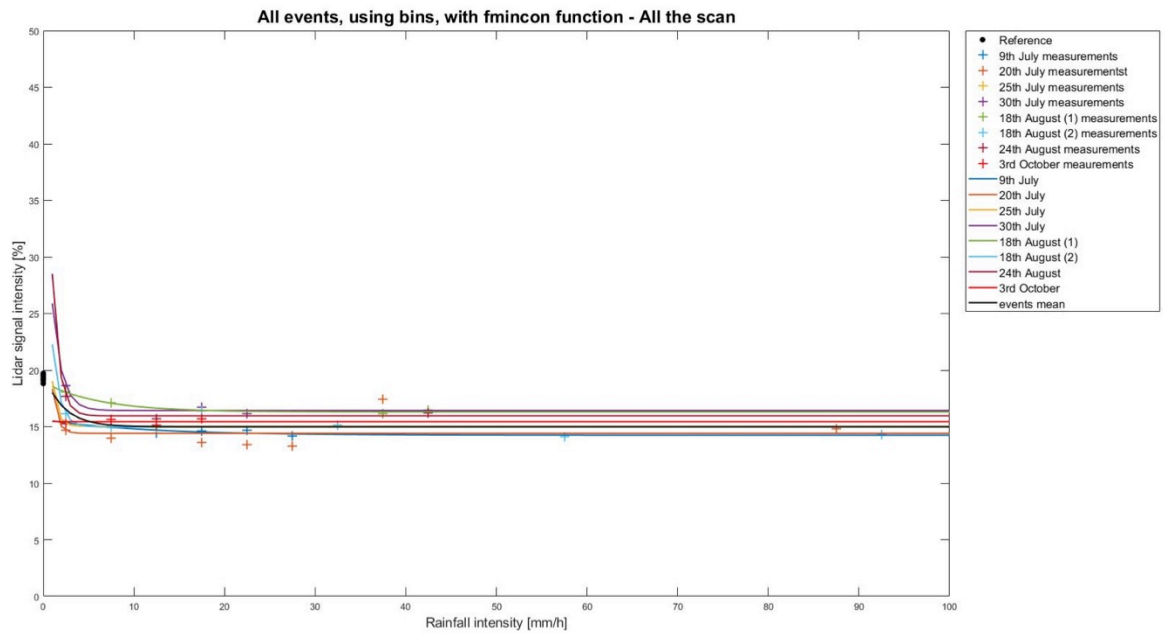


Fig. XXV: Results, using bins, for all events having a rainfall intensity getting higher than 10 mm/h for the all the scan, using the fmincon function on Matlab.

Table XV: Results for the exponential function, using bins, with fmincon, for all the scan.

Date	A	B	C	RMSE
9 July	1.3786	0.0895	14.2410	0.1721
20 July	24.9841	1.8515	14.4108	1.3437
25 July	24.9852	1.8371	15.0342	0.0608
30 July	24.9992	0.9715	16.4267	0.2137
18 August (1)	2.6298	0.1630	16.2946	0.0996
18 August (2)	24.9954	1.2302	14.9783	0.7448
24 August	46.7969	1.3157	15.9523	0.1915
3 October	24.8998	6.9277	15.4412	0.2459

B.III. Individual events graphic results

This part is the different graphs for the events individually. The four graphs up are with all measurements. The four graphs down are using bins.

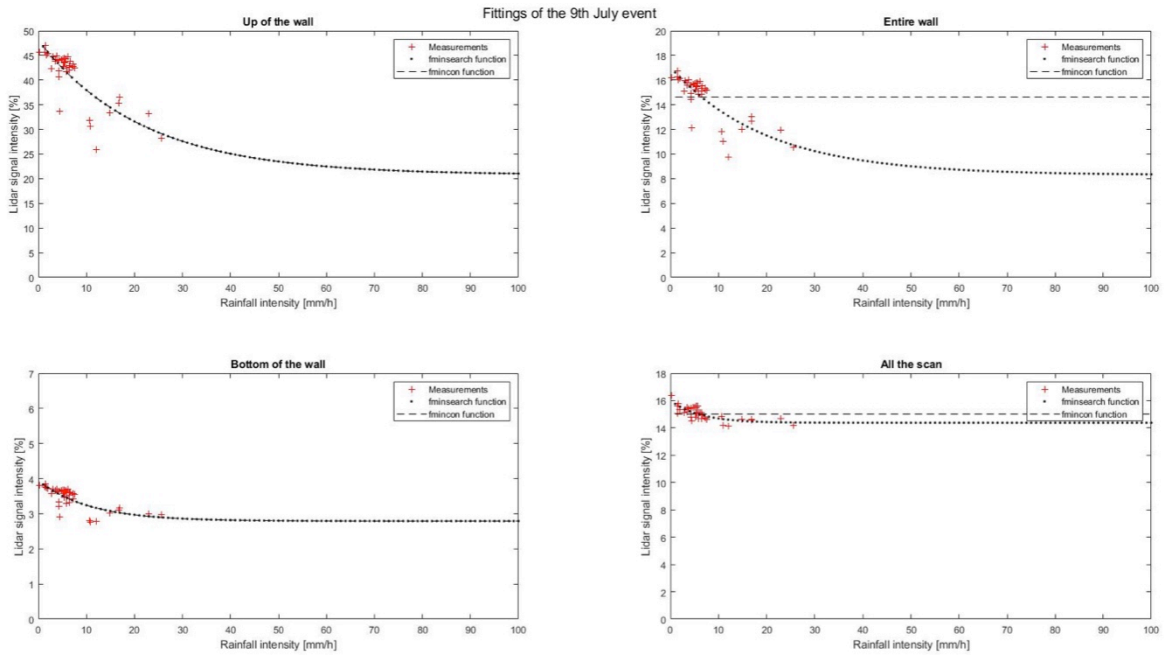


Fig. XXVI: Graphs for all the parts, for the 9th July event.

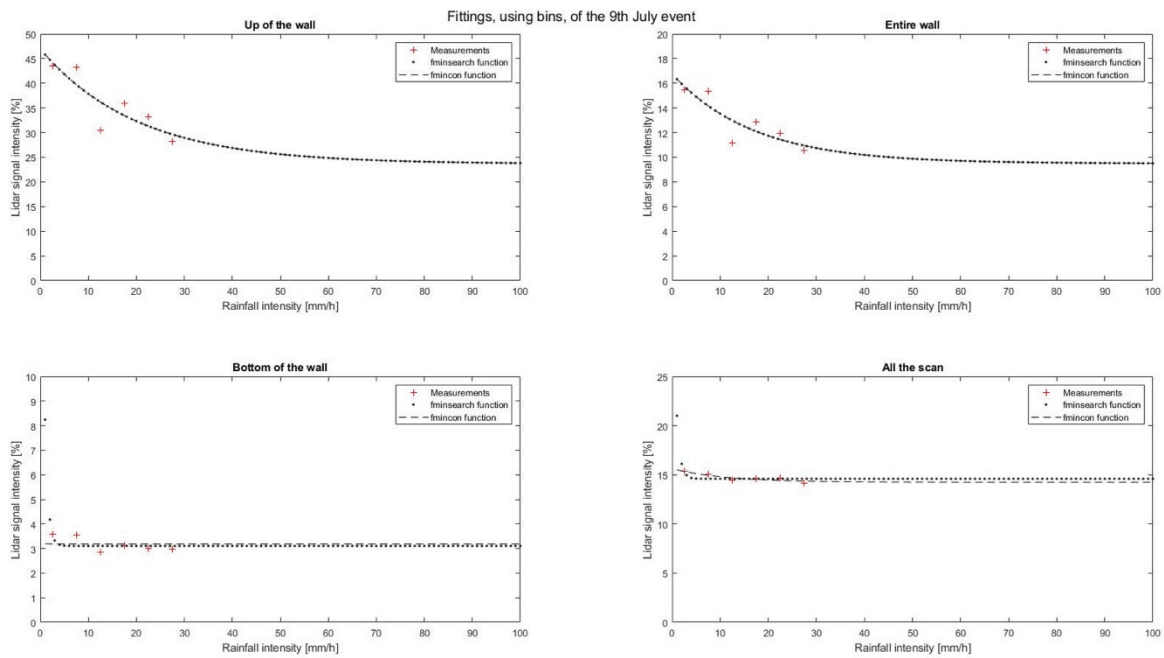


Fig. XXVII: Graphs for all the parts, using bins, for the 9th July event.

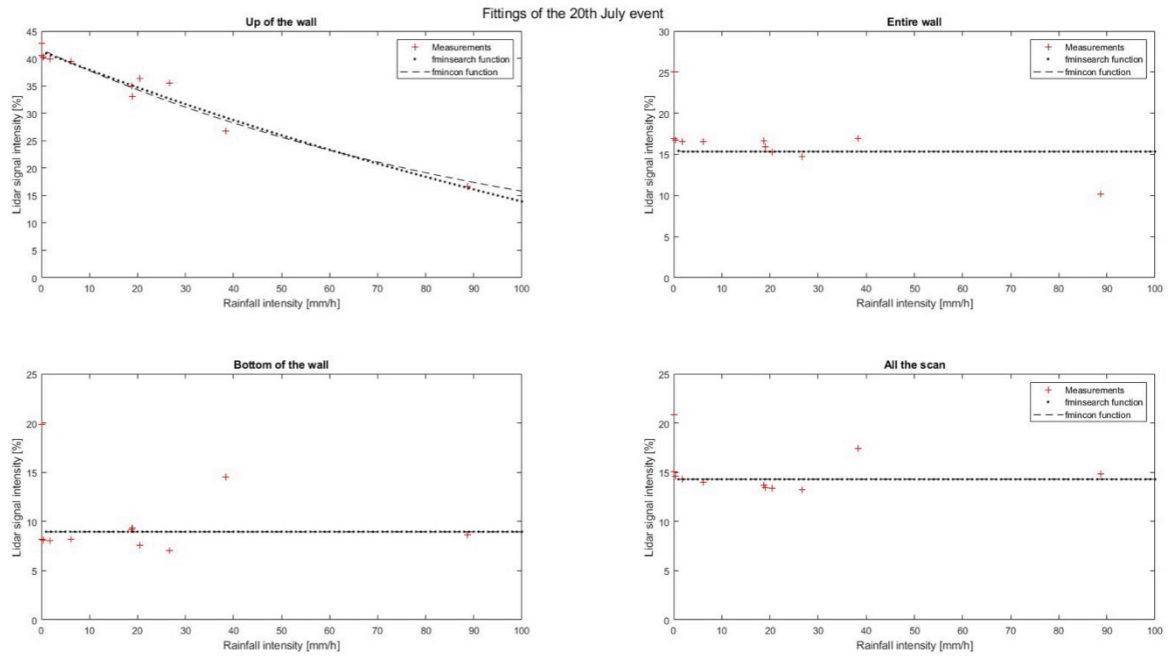


Fig. XXVI: Graphs for all the parts, for the 20th July event.

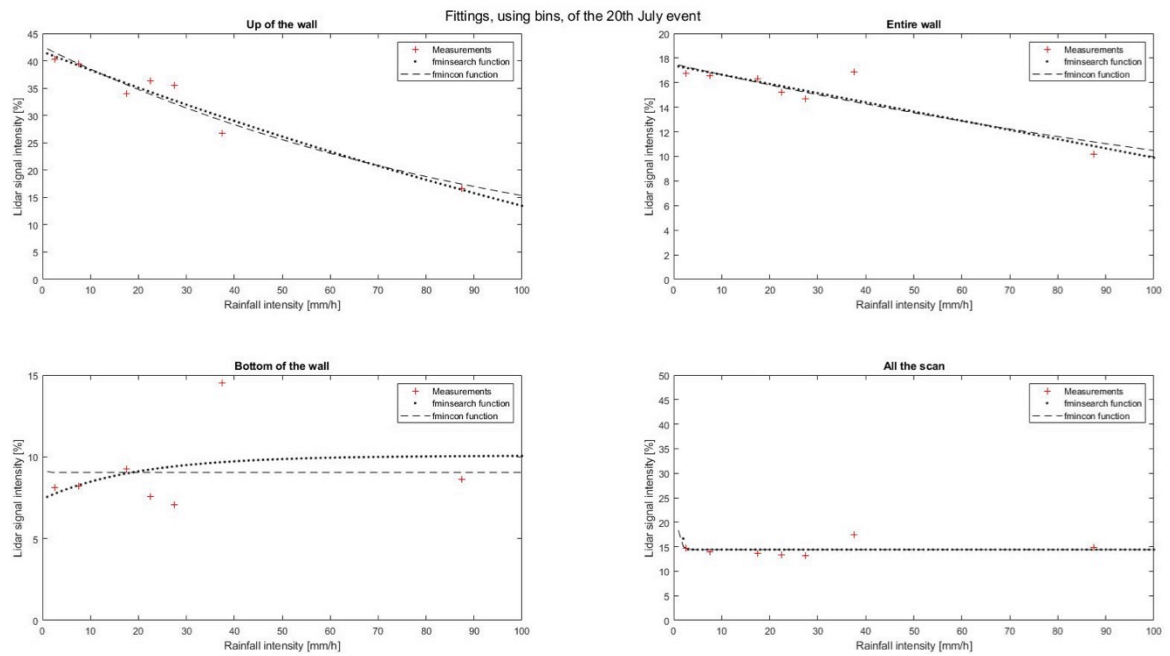


Fig. XXVIII: Graphs for all the parts, using bins, for the 20th July event.

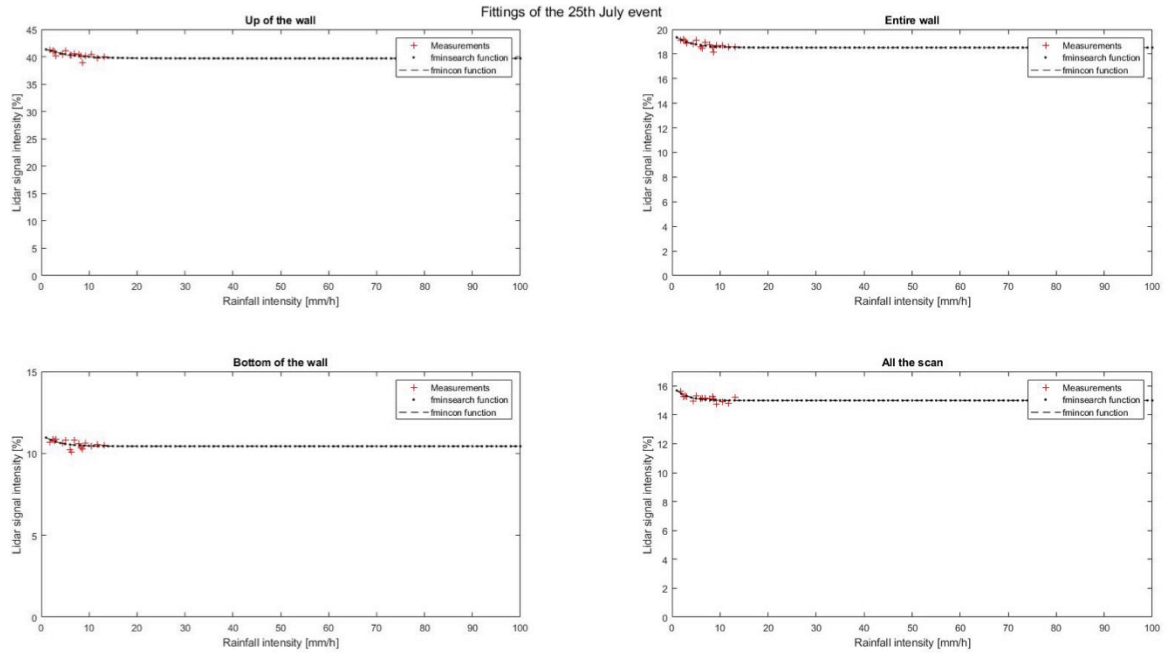


Fig. XXIX: Graphs for all the parts, for the 25th July event.

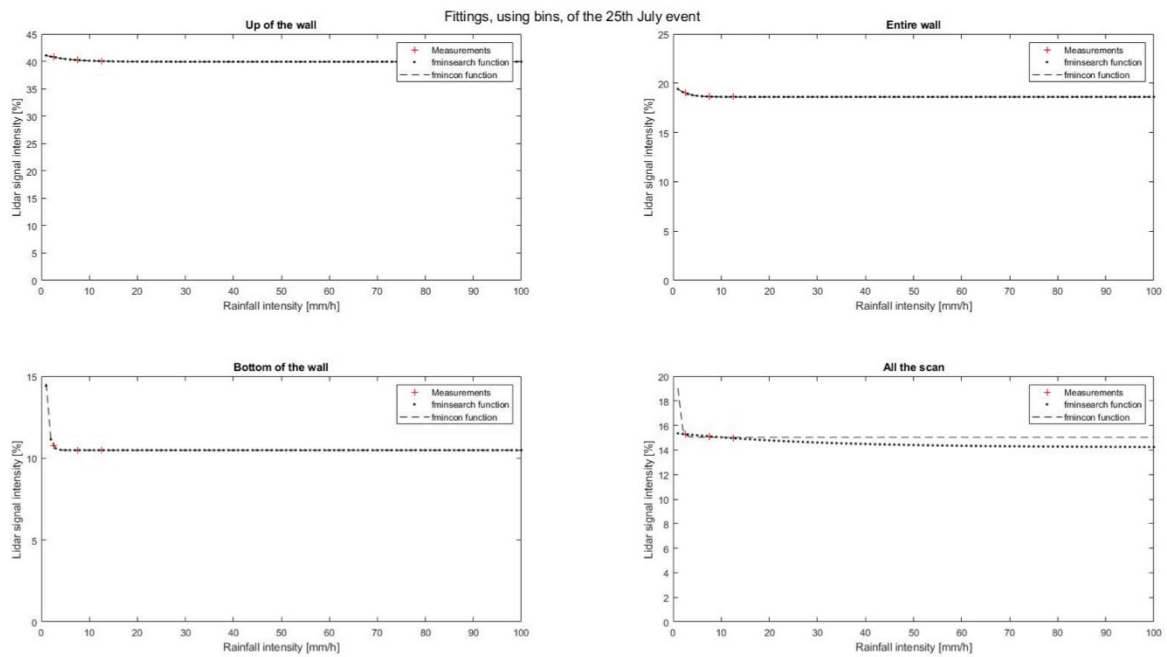


Fig. XXX: Graphs for all the parts, using bins, for the 25th July event.

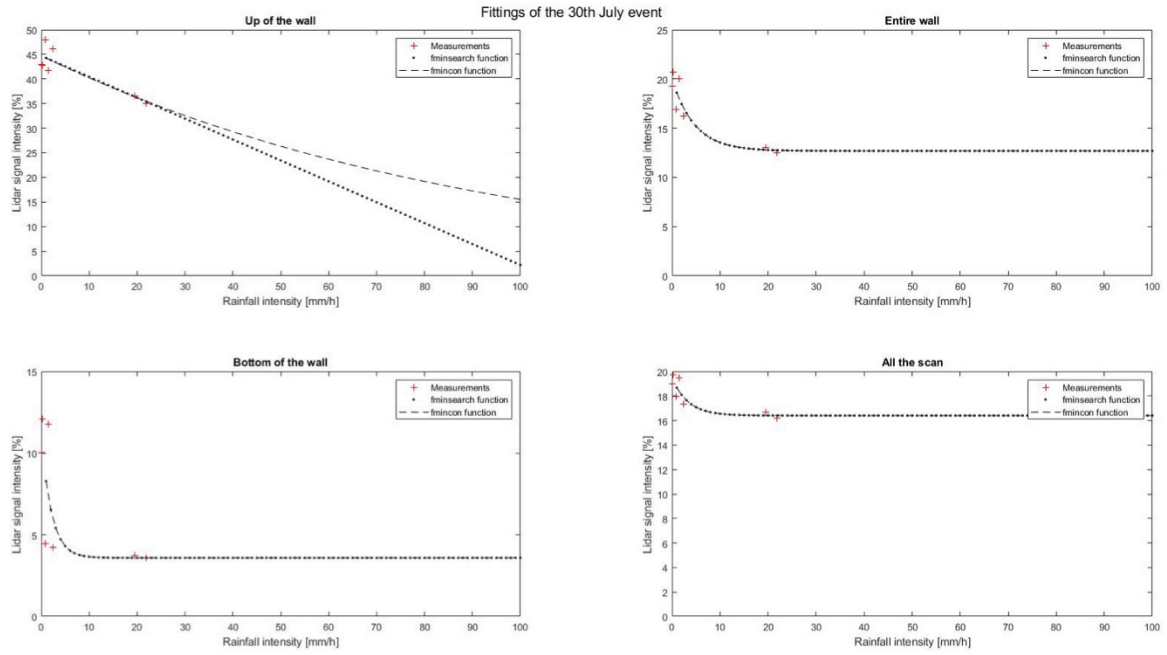


Fig. XXXI: Graphs for all the parts, for the 30th July event.

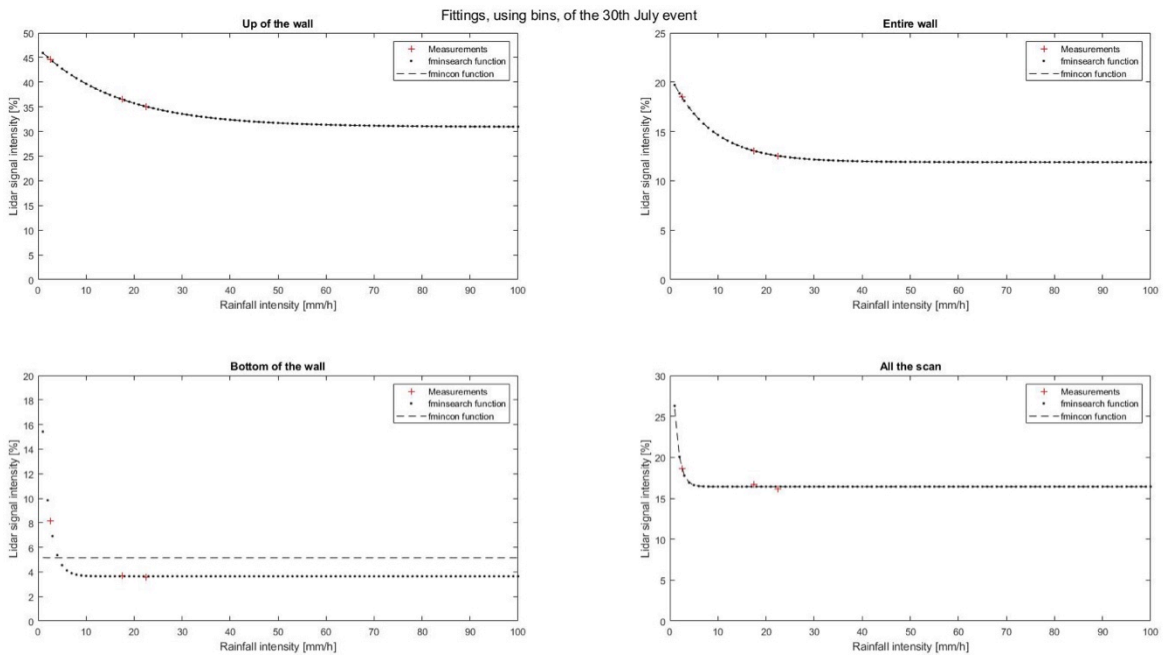


Fig. XXXII: Graphs for all the parts, using bins, for the 30th July event.

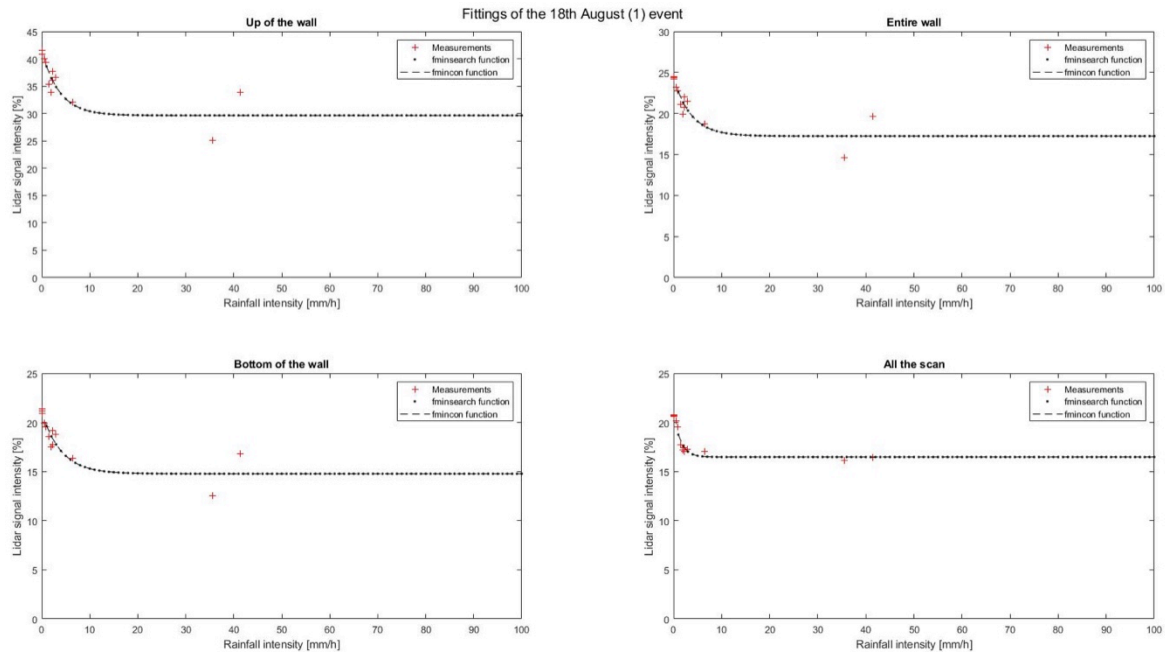


Fig. XXXIII: Graphs for all the parts, for the 18th August (1) event.

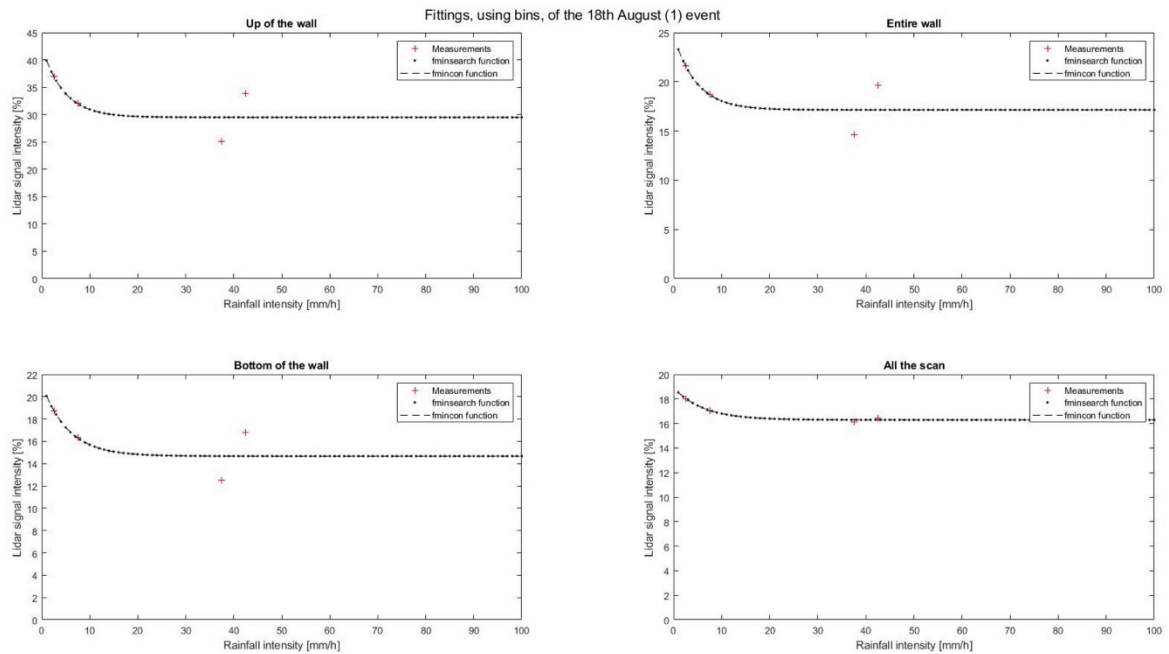


Fig. XXXIV: Graphs for all the parts, using bins, for the 18th August (1) event.

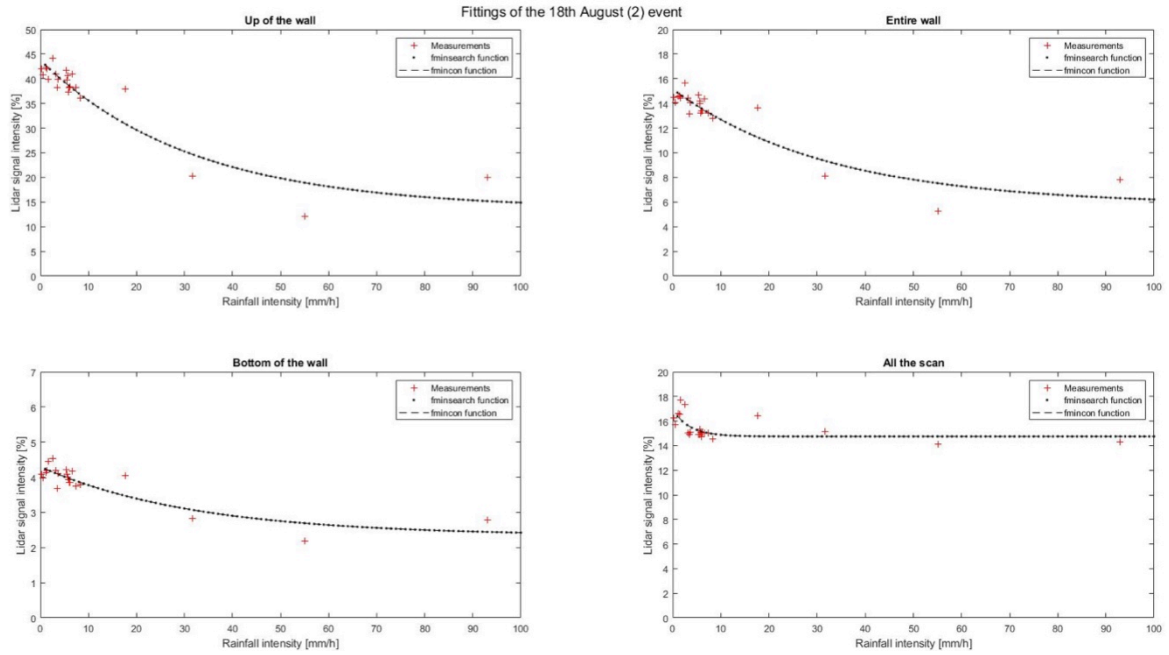


Fig. XXXV: Graphs for all the parts, for the 18th August (2) event.

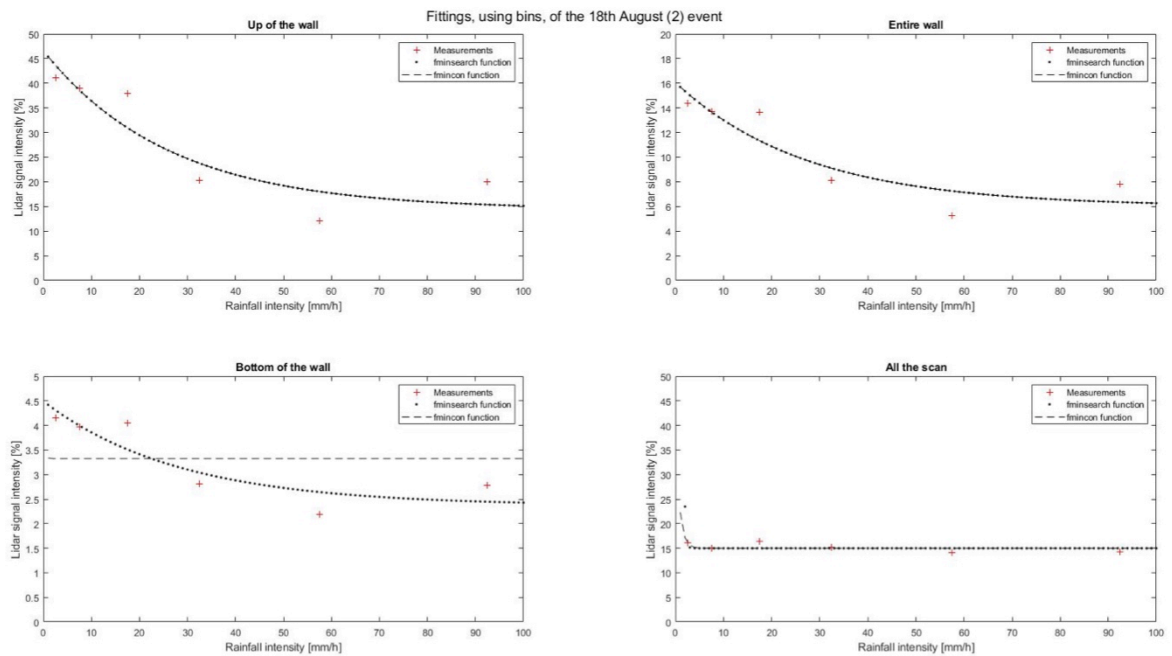


Fig. XXXVI: Graphs for all the parts, using bins, for the 18th August (2) event.

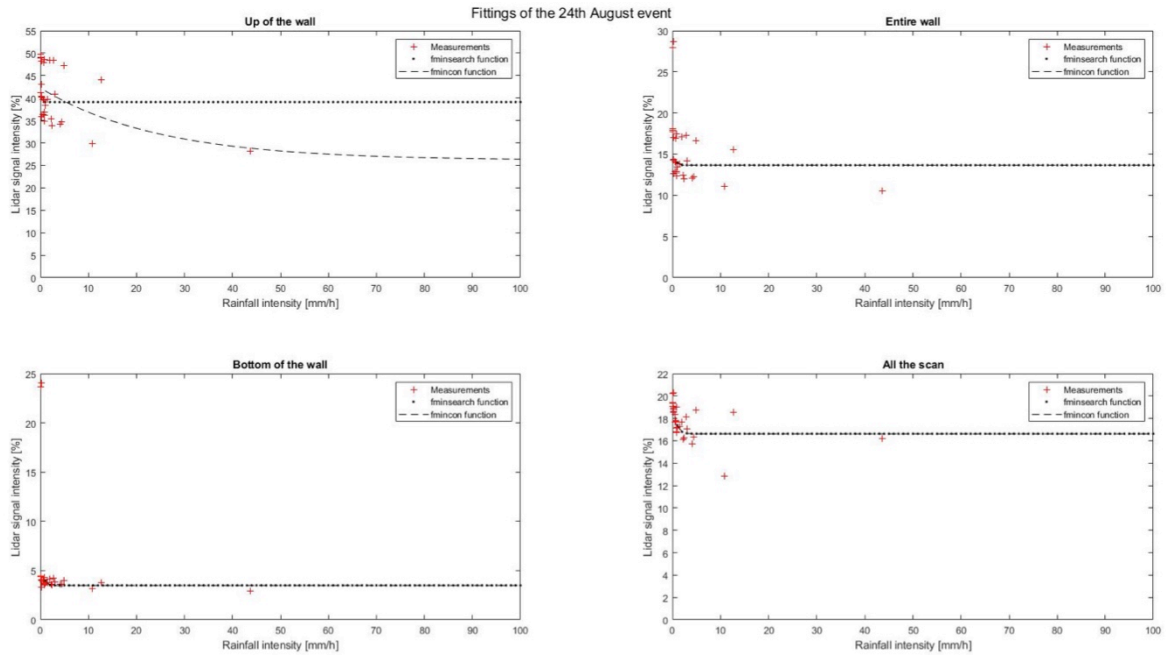


Fig. XXXVII: Graphs for all the parts, for the 24th August event.

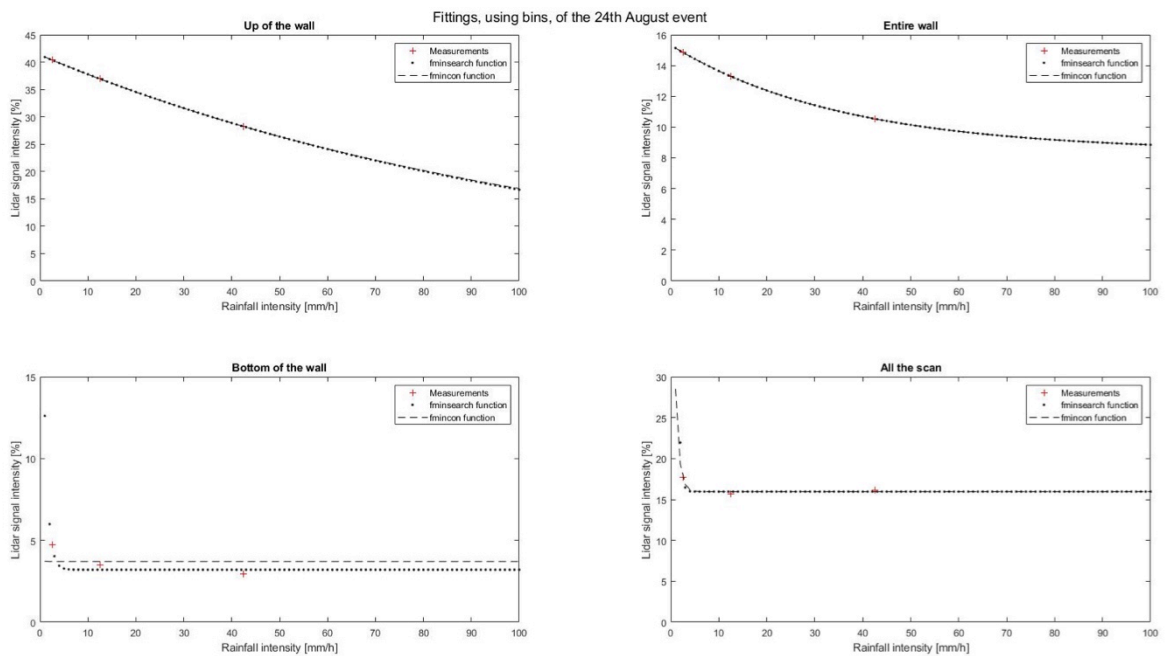


Fig. XXXVIII: Graphs for all the parts, using bins, for the 24th August event.

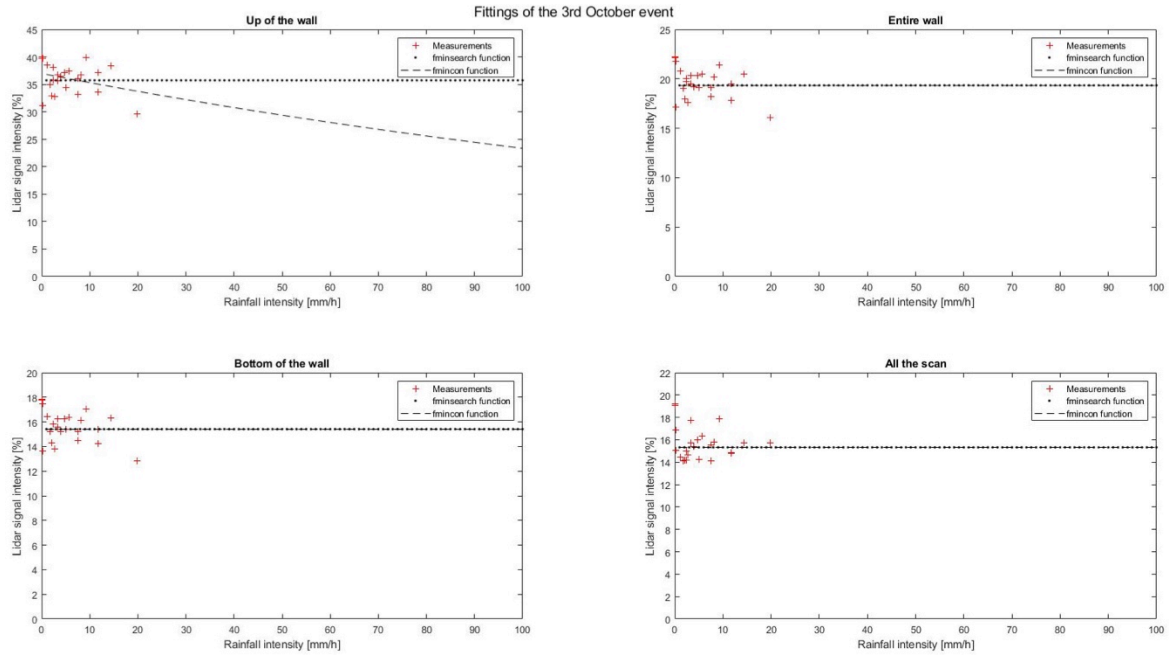


Fig. XXXIX: Graphs for all the parts, for the 3rd October event.

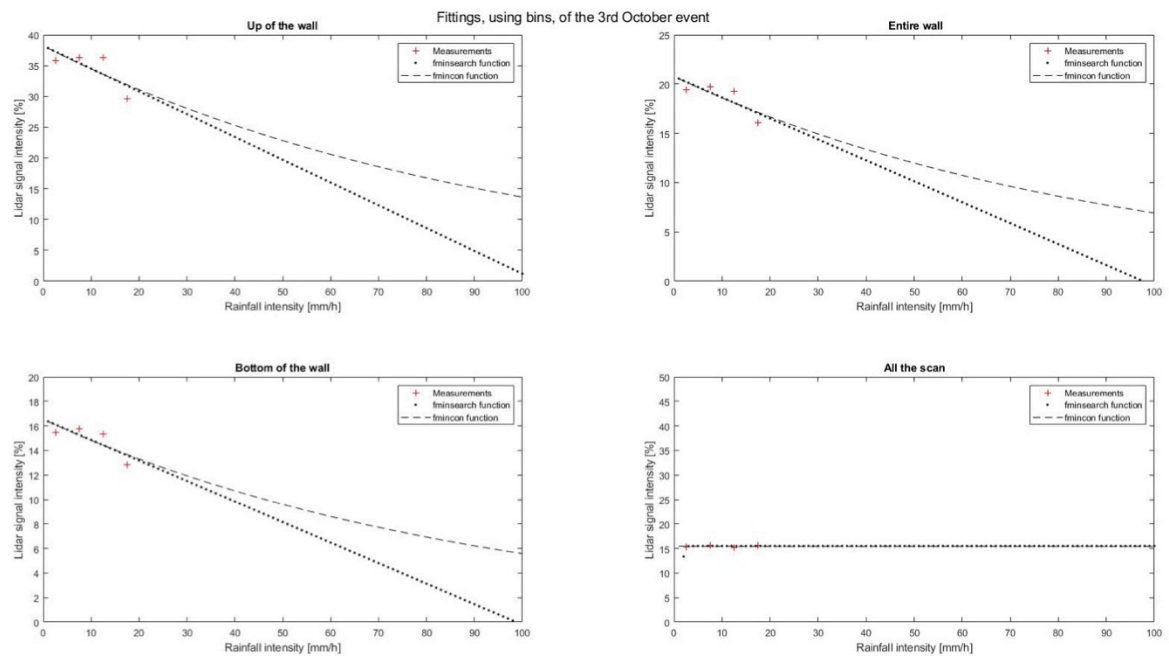


Fig. XL: Graphs for all the parts, using bins, for the 3rd October event.

Appendix C - Scans results

This appendix presents the different results obtained for the scans. The various numbers represent the mean intensity of each scan, for the different parts.

Table 5: Results for reference scans.

Date	Hour of measurement	Up part of the wall	Bottom part of the wall	Entire wall	All the scan
7 April	17:30	49.8741	4.2751	17.8884	18.8090
28 May	16:31	60.9207	6.0786	21.1000	19.2688
28 May	16:39	54.1603	5.7172	19.0971	19.0383
17 July	23:01	56.8948	5.5695	19.9242	19.4510
17 July	23:09	58.5343	5.4246	20.2162	19.6808
17 July	23:16	58.1942	5.2915	19.9794	19.7205
17 July	23:22	55.0571	5.2577	19.0511	19.6688
17 July	23:29	51.5122	5.0759	17.8907	19.6375
26 July	20:14	48.2220	4.2780	19.4585	19.1362
26 July	20:24	45.7007	4.2810	18.6313	19.1613
26 July	20:34	46.2726	4.2219	18.7248	19.2054
26 July	20:44	46.9345	4.1679	18.8504	19.3991
26 July	20:54	48.2892	4.1485	19.3040	19.5381
26 July	21:04	49.3811	4.1444	19.6822	19.5769
26 July	21:14	49.5196	4.1504	19.7419	19.6069
26 July	21:24	49.3342	4.1234	19.6562	19.5130
26 July	21:34	49.4982	4.1409	19.7388	19.5517
26 July	21:44	49.3939	4.1278	19.6959	19.5904
26 July	21:54	49.6775	4.1587	19.8025	19.6729
26 July	22:04	49.6462	4.1448	19.7932	19.6557

Table 6: Results for the 19th May 2017.

Hour of measurement	Up part of the wall	Bottom part of the wall	Entire wall	All the scan	Rainfall [mm/h]
10:24	24.4926	2.9538	8.7202	13.5313	2.6
10:40	29.0609	3.4838	10.1184	13.3059	1.8
10:55	23.3282	2.8212	8.2019	12.9104	2.0
11:10	15.4657	1.8589	5.5870	12.4575	2.8
11:25	26.0218	3.0901	8.9831	12.7533	1.6
11:40	19.8213	2.0723	6.6501	12.8674	2.2
11:45	20.4862	2.0251	6.8300	12.8629	3.4
11:55	35.4507	3.5075	11.4323	13.4151	2.8
12:10	16.3632	1.7199	5.5975	12.3089	3.6
12:25	23.2965	2.4483	7.8427	12.0481	3.6
12:40	28.2889	3.3191	9.4518	12.1793	8.0

Table 7: Results for the 4th June 2017.

Hour of measurement	Up part of the wall	Bottom part of the wall	Entire wall	All the scan	Rainfall [mm/h]
00:58	46.7350	4.0972	15.8537	17.7896	1.2
01:04	47.0820	4.0671	15.8991	17.4709	2.8
01:13	39.1589	3.6810	13.4219	17.1659	2.8
01:29	41.4508	3.7107	14.0107	17.1158	1.2
01:45	42.8980	3.7939	14.6051	17.6384	0.8
02:01	36.8071	3.5631	12.6759	17.5752	0.8

Table 8: Results for the 6th June 2017 AM.

Hour of measurement	Up part of the wall	Bottom part of the wall	Entire wall	All the scan	Rainfall [mm/h]
09:45	42.7560	5.1607	14.9798	17.9433	0.8
10:00	45.0124	4.2373	14.9438	17.9734	2.4
10:15	47.1140	4.3738	15.6310	18.2752	0.4
10:30	49.4947	3.9229	16.1324	18.2409	0.0
10:38	44.6599	3.7723	14.6094	17.7718	2.4
10:45	42.0416	3.8684	13.7741	16.2123	4.0
11:00	43.6324	3.8870	14.2614	17.1396	0.8
11:15	37.5624	3.8654	12.6762	15.7000	6.4
11:30	38.5891	4.3928	13.3133	15.8044	2.0
11:45	41.4932	4.3276	13.9967	17.5035	0.4
11:47	41.0654	4.2780	13.8650	17.6104	0.0
11:49	42.9730	4.3579	14.4130	17.8386	0.3
11:51	44.1080	4.4397	14.8264	17.9950	0.9
11:53	45.6083	4.4197	15.1894	18.0532	0.3
11:55	45.9177	4.4255	15.3337	17.9836	0.3
11:57	47.9252	4.6473	16.0447	18.1405	0.3
12:00	48.0620	4.5426	16.0746	18.2552	0.0
12:15	51.4235	4.3275	17.0125	18.6834	0.0
12:30	37.4540	3.4199	12.7995	17.7332	0.0
09:45	42.7560	5.1607	14.9798	17.9433	0.8

Table 9: Results for the 6th June 2017 PM.

Hour of measurement	Up part of the wall	Bottom part of the wall	Entire wall	All the scan	Rainfall [mm/h]
14:00	32.4228	3.1418	11.3660	14.3527	7.2
14:15	29.8276	3.0058	10.5257	13.9661	1.2
14:30	30.4622	3.0985	10.7022	14.2256	2.4
14:36	28.2081	2.7795	9.9583	13.4737	9.6
14:45	25.1346	2.5144	8.9041	13.3827	3.6
15:00	25.5010	2.3884	8.8071	13.3075	6.8
15:15	32.5633	3.3687	11.8311	15.2428	0.0

Table 10: Results for the 9th July scan.

Hour of measurement	Up part of the wall	Bottom part of the wall	Entire wall	All the scan	Rainfall [mm/h]
22:04	25.9765	2.7914	9.7319	14.1412	14.4
22:06	28.2609	2.9829	10.5641	14.1744	28.8
22:11	31.8136	2.8169	11.8045	14.8430	7.2
22:14	42.3231	3.5641	15.0975	15.0979	2.4
22:17	45.6822	3.7600	16.2339	15.0601	1.2
22:27	46.9895	3.8609	16.7547	15.6084	1.5
22:34	45.3131	3.7318	16.1698	15.3581	2.4
22:37	44.1416	3.6574	15.7813	15.1902	3.3
22:40	44.3276	3.6676	15.7755	15.6010	5.7
22:43	42.7174	3.5665	15.2086	14.8169	5.4
22:45	42.4957	3.5477	15.1378	14.6368	8.16
22:47	35.3685	3.0947	12.6825	14.6324	16.08
22:49	33.3285	3.0268	11.9899	14.6473	15.12
22:52	33.1733	3.0046	11.9518	14.6939	22.2
22:54	36.4756	3.1795	13.0372	14.5433	16.56
22:57	30.6744	2.7586	11.0421	14.1808	9.9
22:59	33.6939	2.9065	12.1339	14.5177	4.56
23:04	40.6509	3.2062	14.4356	14.7865	3.9
23:07	42.0759	3.3163	14.8855	14.9767	6.6
23:10	41.7727	3.2871	14.8595	15.1028	5.7
23:13	41.8140	3.3501	14.9051	15.0285	4.5
23:16	43.7679	3.4583	15.5114	15.0540	5.4
23:19	42.7902	3.4159	15.2011	14.7169	7.2
23:23	42.4247	3.4860	15.1165	14.6729	5.7
23:26	42.9315	3.5891	15.3260	14.6844	6.6
23:28	43.1647	3.5829	15.3704	14.7224	7.2
23:30	43.9114	3.6257	15.5544	14.9562	6.72
23:32	43.5814	3.6144	15.4660	15.1068	5.52
23:35	44.9029	3.7107	15.9967	15.4107	3.6
23:39	42.7021	3.5305	15.1058	15.1043	6.6
23:42	44.6853	3.7107	15.8811	15.1111	5.7
23:46	44.7829	3.7077	15.9296	15.3327	3
23:50	43.9077	3.6519	15.5700	15.4768	3.3
23:54	44.0127	3.6424	15.6146	15.4727	4.5
23:56	44.2619	3.6774	15.7156	15.5047	5.04
23:58	43.5342	3.6282	15.4606	15.6077	5.28
00:01	44.5026	3.6890	15.7704	15.4884	5.4
00:03	44.1538	3.6559	15.6639	15.4961	4.8
00:06	45.0422	3.7420	15.9984	15.7961	1.5
00:11	45.6067	3.8015	16.1876	16.3572	0.3

Table 11: Results for the 20th July 2017.

Hour of measurement	Up part of the wall	Bottom part of the wall	Entire wall	All the scan	Rainfall [mm/h]
21:24	42.7691	19.8792	25.0252	20.8627	0
21:27	26.8012	14.5188	16.8780	17.4496	38.4
21:29	16.6105	8.6316	10.1652	14.8156	88.7
21:32	33.0542	9.3097	15.9325	13.4326	19
21:34	34.9225	9.1855	16.6610	13.7075	18.8
21:38	35.5456	7.0518	14.7106	13.2582	26.7
21:40	36.3139	7.5587	15.2493	13.4087	20.5
21:42	39.5134	8.2067	16.5675	13.9628	6.2
21:44	39.9239	8.0533	16.5721	14.2617	1.8
21:46	40.2469	8.1014	16.6923	14.6122	0.4
21:50	40.5031	8.2120	16.9169	15.0910	0.1

Table 12: Results for the 25th July 2017.

Hour of measurement	Up part of the wall	Bottom part of the wall	Entire wall	All the scan	Rainfall [mm/h]
20:18	40.1270	10.8488	18.8509	15.2567	3
20:20	41.0990	10.7961	19.1183	15.3226	5.1
20:23	40.3149	10.1049	18.4372	15.1700	6.3
20:25	40.2934	10.2432	18.5416	15.0827	6
20:28	40.3815	10.6137	18.7843	14.9685	4.5
20:30	40.0895	10.3452	18.5346	15.2390	8.4
20:33	38.9590	10.2729	18.1619	15.0831	8.7
20:36	40.4135	10.6011	18.7431	15.1097	7.8
20:39	40.3665	10.4619	18.6871	14.8777	10.5
20:42	39.9927	10.4759	18.5886	15.2062	13.2
20:44	39.7381	10.5621	18.5765	14.7955	11.7
20:46	40.0983	10.6166	18.6973	14.7207	9.3
20:48	40.5352	10.8053	18.9417	15.1419	6.9
20:52	41.1508	10.8767	19.1984	15.2419	2.4
20:54	40.9343	10.7638	19.0562	15.3394	2.7
20:57	41.2364	10.6675	19.0968	15.6296	1.8

Table 13: Results for the 30th July 2017.

Hour of measurement	Up part of the wall	Bottom part of the wall	Entire wall	All the scan	Rainfall [mm/h]
14:29	36.5077	3.7184	13.0444	16.6884	19.5
14:31	35.0636	3.5682	12.5370	16.1649	22.1
14:34	46.0849	4.2528	16.2498	17.3191	2.4
14:38	47.9073	4.4624	16.9323	17.9650	0.9
14:51	42.8906	10.0340	19.2903	19.0204	0
15:02	42.8378	12.0868	20.6728	19.7455	0.3
15:04	41.7200	11.7687	20.0231	19.4913	1.5

Table 14: Results for the 8th August 2017.

Hour of measurement	Up part of the wall	Bottom part of the wall	Entire wall	All the scan	Rainfall [mm/h]
13:28	40.8670	3.5647	14.3262	16.5647	2.9
13:31	40.6708	3.5459	14.2642	15.7262	4.3
13:45	28.7079	2.9040	10.5704	14.3568	1.8
13:52	30.6151	2.9872	11.0996	14.3240	0.9
13:57	40.9082	3.5451	14.2167	15.0833	3.2
13:59	40.3247	3.5508	14.0856	15.2577	5.3
14:04	41.2145	3.6694	14.3565	14.5670	5.4
14:08	41.1573	3.6737	14.3170	14.6688	2.4
14:14	27.4213	2.8613	10.1515	14.4876	1.9
14:21	19.8168	2.1739	7.6561	14.4441	1.5
14:44	42.7595	3.8687	14.8378	16.3159	1.5
14:47	41.6885	3.8084	14.5317	16.1331	2.7
14:50	42.7067	3.8520	14.8151	15.9503	3.9
14:53	43.0023	3.8982	14.9743	14.9350	3.3
14:56	42.4942	3.8550	14.7712	14.3482	5.7
14:59	42.7355	3.9198	14.8340	14.4972	4.8
15:02	42.6990	3.9515	14.8604	14.5775	5.6
15:05	42.3948	3.9430	14.7484	14.4633	6
15:09	42.6883	4.0219	14.8956	14.7198	4.2
15:12	42.7103	4.0487	14.8784	14.8256	4.2
15:23	28.1662	3.0496	10.3964	15.3064	0.3
15:32	43.4890	4.1603	15.2462	16.8139	0
15:34	43.2336	4.1394	15.1555	16.9787	0.3
15:36	41.5707	3.9879	14.5962	16.8698	0.3
15:39	42.5772	4.0752	14.9345	17.0879	2.4
15:42	42.6859	4.0947	14.9818	16.7477	5.7
15:44	42.7905	4.0995	15.0008	16.4135	3.6
15:47	41.7640	4.0169	14.6518	16.0760	3.7
15:49	41.8443	4.0075	14.6576	15.9292	5.9
15:51	40.4071	3.8655	14.1026	15.7552	7.5
15:53	40.7769	3.8822	14.2155	15.7505	8.4
15:55	39.7601	3.8112	13.8351	15.7463	7
15:58	41.6376	3.9684	14.4934	16.0306	3.3
16:01	40.9499	3.9353	14.2963	15.7863	5.4
16:04	41.1114	3.9601	14.3747	15.6433	2.8
16:08	41.9353	4.0302	14.6224	15.9757	2.7
16:11	40.9700	3.9663	14.3087	15.8202	4.8
16:15	41.2493	4.0030	14.3826	15.7866	5.7
16:17	38.9135	3.8762	13.6193	15.7505	4.6
16:20	41.3782	3.9974	14.4291	15.9055	1.5
16:28	42.4179	4.1093	14.8627	16.7245	0.9
16:36	44.0397	4.0970	15.3311	18.1032	3
16:42	43.6053	4.0533	15.2306	17.3096	0.6
16:50	44.9158	4.1461	15.6227	18.3477	0.3
16:56	42.9819	4.0146	15.0272	16.6272	4.2
17:03	42.4854	4.0041	14.8328	15.8809	6.2
17:09	43.9487	4.1166	15.2629	16.2651	3.9
17:14	44.7174	4.1510	15.4928	16.7491	0.6

Table 15: Results for the 11th August 2017.

Hour of measurement	Up part of the wall	Bottom part of the wall	Entire wall	All the scan	Rainfall [mm/h]
10:52	51.7569	13.0884	22.8482	17.9624	0.6
10:55	48.7896	12.4153	21.5983	18.0174	0.6
10:58	46.0016	12.1711	20.7077	18.0672	0.9
11:03	43.1043	11.9913	19.8718	17.9694	1.2
11:13	42.0647	11.4842	19.2969	17.5700	0.3
11:18	43.0130	11.5515	19.5738	17.5699	0.3
11:26	42.5711	11.2422	19.2373	17.3170	0.3

Table 16: Results for the 18th August 2017 (1).

Hour of measurement	Up part of the wall	Bottom part of the wall	Entire wall	All the scan	Rainfall [mm/h]
17:51	40.8581	21.3899	24.4967	20.7094	0
17:54	41.5330	21.1141	24.3909	20.7549	0
17:57	41.4599	20.9173	24.2284	20.6017	0
18:04	40.0125	19.9173	23.1730	20.1449	0.6
18:06	39.2880	19.5822	22.7718	19.5256	0.8
18:08	35.9820	17.7183	20.7081	17.4487	2.3
18:10	33.8000	16.8187	19.6563	16.4368	41.4
18:12	25.1513	12.5180	14.6146	16.1584	35.6
18:14	32.0178	16.3250	18.7025	17.0727	6.5
18:16	33.7930	17.5054	19.9643	17.1587	2
18:20	35.3234	18.5492	21.0952	17.6938	1.5
18:26	36.6211	18.7897	21.4913	17.2668	2.9
18:30	37.6946	19.1925	21.9965	17.0608	2.3

Table 17: Results for the 18th August 2017 (2).

Hour of measurement	Up part of the wall	Bottom part of the wall	Entire wall	All the scan	Rainfall [mm/h]
21:37	39.9543	4.4397	14.4090	17.7150	1.7
21:41	44.1539	4.5455	15.6617	17.3200	2.6
21:43	37.8519	4.0524	13.6268	16.4085	17.7
21:45	20.0211	2.7803	7.8416	14.2992	93
21:47	12.1326	2.1852	5.2437	14.0868	55.1
21:50	20.2263	2.8196	8.0952	15.1403	31.7
21:52	40.6537	4.0094	14.1783	15.3578	5.7
21:54	37.2909	3.9349	13.2257	15.0778	5.9
21:57	39.8353	4.1107	14.0941	15.0864	3.6
22:00	40.9761	4.1829	14.4634	15.0117	3.2
22:02	41.7033	4.2238	14.6648	14.9178	5.3
22:04	40.9031	4.1821	14.3833	15.0238	6.6
22:06	39.7989	4.0929	14.0168	14.9253	5.6
22:10	36.0931	3.7905	12.7712	14.5422	8.3
22:12	38.2802	3.8562	13.4017	14.7019	6
22:14	38.4059	3.8572	13.3783	15.0499	6.2
22:16	38.1735	3.7374	13.2215	15.0355	7.4
22:18	38.1473	3.6749	13.1420	14.9356	3.5
22:23	40.8741	3.9730	14.0706	15.7196	0.5
22:29	42.0030	4.0888	14.4765	16.2425	0.3
22:34	42.2876	4.1338	14.5876	16.5960	1.1
22:37	41.9865	4.1840	14.5962	16.5641	1.4

Table 18: Results for the 24th August 2017.

Hour of measurement	Up part of the wall	Bottom part of the wall	Entire wall	All the scan	Rainfall [mm/h]
13:47	49.7118	4.4709	18.1204	19.1061	0
13:53	49.0777	4.4479	17.9389	19.4354	0
13:57	48.8418	4.3737	17.7064	19.3661	0
13:59	48.5938	4.2929	17.5053	19.0402	0.8
14:02	48.3546	4.2202	17.2740	18.1273	2.8
14:04	48.3371	4.1853	17.1406	17.6658	2
14:07	47.9158	4.0919	16.9536	17.7340	0.7
14:19	48.1474	4.1137	17.0213	18.9433	0.3
14:29	47.3048	4.0210	16.6770	18.7478	4.9
14:31	44.0203	3.8101	15.5470	18.5603	12.7
14:33	28.2316	2.9311	10.5394	16.1868	43.7
14:36	29.8539	3.1423	11.0457	12.8754	10.8
14:45	36.8925	3.5487	12.9424	17.1184	0.8
14:50	34.8537	3.5299	12.3539	16.7061	0.8
14:54	36.1125	3.5834	12.7299	16.7950	0.9
14:59	38.4252	3.7318	13.4613	17.2142	1
15:06	39.6370	3.8058	13.8599	17.2777	1.5
15:09	40.7988	3.8721	14.1928	17.0761	3
15:12	34.7535	3.5993	12.2870	16.3529	4.4
15:16	33.8144	3.5666	11.9965	16.2503	2.4
15:20	34.1866	3.6069	12.0864	15.7551	4.1
15:32	35.3428	3.6544	12.4306	16.1103	2.3
15:48	36.3831	3.8389	12.9110	17.6701	0.6
16:06	35.8606	3.2792	12.6073	18.5754	0.3
16:19	40.2237	4.0428	14.2356	18.7850	0.3
16:24	39.7369	4.0263	14.0832	18.3498	0.6
16:29	39.5597	3.9715	13.9751	17.7967	0.7
16:42	40.2911	4.0282	14.3398	18.6190	0.2
16:55	41.1342	23.6523	27.9773	20.1900	0
17:14	43.0498	24.0511	28.6947	20.3216	0.3

Table 19: Results for the 31st August 2017.

Hour of measurement	Up part of the wall	Bottom part of the wall	Entire wall	All the scan	Rainfall [mm/h]
08:01	47.0461	4.9607	17.2539	19.3964	0
08:11	45.7537	4.7377	16.6430	19.1106	0
08:15	45.2275	4.6645	16.3782	18.8370	0
08:27	42.5473	4.2888	15.2155	18.2469	0.2
08:31	42.6341	4.3084	15.2352	17.7565	0.5
09:08	44.6371	4.6002	15.7980	15.5159	1.9
09:37	26.7797	3.2496	10.2008	14.7587	3.2
09:46	44.4892	4.5546	15.7235	16.0771	0.9
09:56	45.4657	4.7312	16.1263	17.4233	0.2
10:04	43.5360	4.6198	15.5385	17.9686	0
10:06:30	33.1947	3.8695	12.3121	16.9512	1.4
11:53	43.1742	4.5804	15.3173	17.1579	2.9
11:56	44.2835	4.6480	15.6434	17.0375	3.6
11:59	44.9511	4.7148	15.8998	16.5332	5.2
12:01:30	45.3146	4.7413	16.0179	16.3618	4.1
12:03:30	45.4563	4.7611	16.0697	16.4217	3.1
12:06	45.6963	4.7829	16.1536	16.4246	2.7
12:10	44.9759	4.7386	15.9228	16.4488	1.6
12:15	44.0418	4.6805	15.6763	16.8282	0.5

Table 20: Results for the 3rd October 2017.

Hour of measurement	Up part of the wall	Bottom part of the wall	Entire wall	All the scan	Rainfall [mm/h]
09:41	39.8888	17.0723	21.4040	17.8617	9.3
09:44	38.2980	16.2826	20.4575	15.7235	14.4
09:46:30	35.9852	15.2029	19.1060	15.5451	7.5
09:49	36.4260	15.2437	19.2162	15.3615	3.9
09:52:30	37.1816	15.4165	19.5100	14.7694	11.7
09:55	38.0977	15.8253	19.9857	15.0103	2.4
10:19	29.6285	12.8502	16.0640	15.7008	19.8
10:21:30	33.5345	14.2355	17.8525	14.8798	11.7
12:08	39.9502	17.8172	22.2506	19.2491	0
12:10	39.7502	17.7597	22.1581	19.0497	0
12:13	36.7336	16.2268	20.2937	17.7080	3.3
12:15:30	37.3468	16.3539	20.4871	16.3600	5.7
12:18	37.1799	16.2215	20.3332	16.0018	4.8
12:21	36.7577	16.1397	20.1798	15.8003	8.1
12:24	35.6127	15.5747	19.4969	15.7491	3.3
12:27:30	32.7291	13.8200	17.5652	14.6542	2.7
12:30	33.1876	14.5052	18.1848	14.1136	7.5
12:32:30	34.9787	15.1920	19.0712	14.1320	1.8
12:36	32.9588	14.3091	17.9570	14.1979	2.1
12:38:30	34.3688	15.3945	19.1171	14.2796	5.1
12:43	35.8216	15.8304	19.7524	14.1805	2.4
12:46	38.5695	16.4599	20.7815	14.4835	1.2
12:56:30	31.0762	13.6508	17.1402	15.0349	0.3
13:20:30	39.7102	17.4692	21.7988	16.8445	0.3

Table 21: Results for the 5th November 2017.


Hour of measurement	Up part of the wall	Bottom part of the wall	Entire wall	All the scan	Rainfall [mm/h]
07:25	40.4062	18.5463	23.5044	16.5071	4.5
07:35	41.4428	18.9754	24.1027	15.8842	1.8
07:51	40.5128	18.7117	23.6931	15.7210	2.4
08:11	38.0176	17.6666	22.3336	15.9983	3
08:23	38.9672	18.2905	23.0247	16.9011	1.2
08:42	36.5366	17.0999	21.5835	16.6855	2.4
08:45	40.8412	18.9783	23.9787	16.9383	3.3
08:48	41.4353	19.3585	24.3973	16.7372	3.9
08:51	40.9930	19.0973	24.0895	16.3744	4.5
08:54	41.0000	19.0969	24.0777	16.1722	5.7
08:56	41.2042	19.2164	24.2076	16.2192	5.4
08:59	41.3662	19.1507	24.1931	16.3349	5.1
09:02:30	41.6170	19.3328	24.3945	16.4309	4.5
09:07:30	41.9221	19.5301	24.6127	16.6168	3
09:11	41.7527	19.5592	24.5974	16.6368	3.9
09:14	41.7233	19.5506	24.5888	16.1147	3.6
09:18	41.1013	19.3478	24.3204	16.1550	2.4
09:25	41.8771	19.5557	24.6412	16.8679	1.5
09:31	42.2072	19.8073	24.9135	16.7469	2.1
09:35	41.9999	19.4468	24.5877	16.4408	2.7
09:38:30	41.4212	19.2354	24.2836	16.4934	2.4
09:44:30	41.6102	19.4915	24.5489	16.2939	3
09:46:30	41.5983	19.4447	24.4999	16.1460	3.3
09:52	41.2765	19.3651	24.3608	16.3117	2.7
09:56	41.3929	19.3720	24.3916	16.2534	3.6
10:02	41.4341	19.3926	24.4091	16.2130	4.8
10:05	40.7939	18.9271	23.8824	16.1050	4.5
10:13	41.3202	19.4272	24.3827	15.9184	3.6
10:20	41.1100	19.3039	24.3041	16.6508	3
10:27	41.1566	19.3071	24.3207	16.9737	3.6
10:29	40.5786	19.0304	23.9637	16.6936	3.9
10:41	40.0175	18.3917	23.3349	16.3524	2.7
10:49	40.9276	18.8865	23.9287	16.0900	3.3
10:56	39.9420	18.3512	23.2955	15.5270	6.6
11:00	38.8823	17.8958	22.6837	15.7139	5.4
11:04	39.2496	18.1168	22.9444	15.3508	8.4
11:07	39.2059	18.2018	23.0000	15.3578	9.9
11:12	40.2597	18.3852	23.3892	15.4471	5.7
11:15	39.1925	17.6857	22.5832	15.2148	4.6
11:21	40.9277	18.2470	23.4205	15.1204	2.4
11:25	41.1818	18.4706	23.6356	15.4209	2.7
11:28:30	41.3039	18.4454	23.6562	15.3591	3.6
11:32:30	40.6764	18.1964	23.3073	15.2087	3.3

Appendix D - Velodyne LiDAR Puck VLP-16 specifications

Specifications of the lidar, from VLP-16 Data sheet (spotted at: <https://velodynelidar.com/vlp-16.html>).

Velodyne LiDAR™ Puck™

REAL-TIME 3D LIDAR SENSOR



VLP-16


Velodyne LiDAR PUCK™

Velodyne's new Puck, VLP-16 sensor is the smallest, and most advanced product in Velodyne's 3D LIDAR product range. Vastly more cost-effective than similarly priced sensors, and developed with mass production in mind, it retains the key features of Velodyne's breakthroughs in LIDAR: Real-time, 360°, 3D distance and calibrated reflectivity measurements.

Real-Time 3D LIDAR

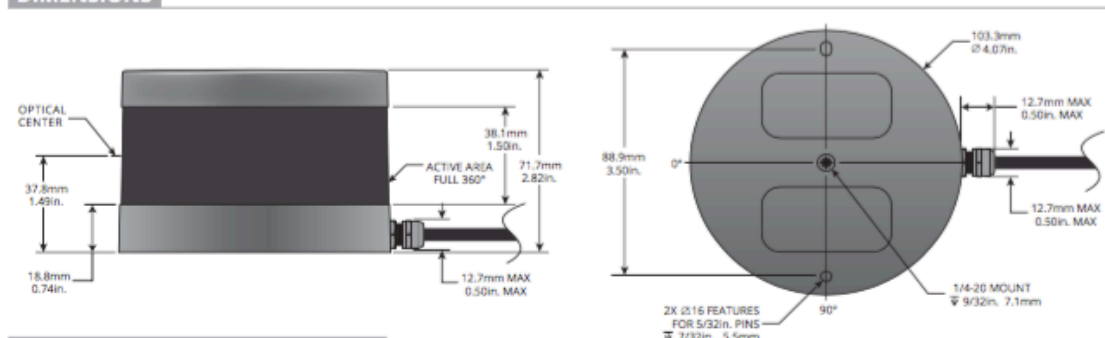
The VLP-16 has a range of 100 m, and the sensor's low power consumption (~8 W), light weight (830 g), compact footprint (~Ø103 mm x 72 mm), and dual return capability make it ideal not only for autonomous vehicles but also robotics and mobile terrestrial 3D mapping applications.

Velodyne's LIDAR Puck supports 16 channels, ~300,000 points/second, 360° horizontal field of view and a 30° vertical field of view, with ±15° up and down. The Velodyne LIDAR Puck does not have visible rotating parts, making it highly resilient in challenging environments (Rated IP67) while operating over a wide temperature range (-10°C to +60°C).

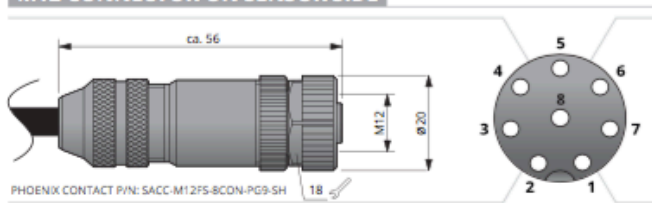


VLP-16

DIMENSIONS



M12 CONNECTOR ON SENSOR SIDE



Pin	Wire Color	Function
8	Black	Ground
7	Red	+12 V
6	Yellow	GPS Pulse Per Second (PPS)
5	White	GPS Serial Data
4	Light Orange	Ethernet TX+
3	Orange	Ethernet TX-
2	Light Blue	Ethernet RX+
1	Blue	Ethernet RX-

www.velodynelidar.com

Fig. XLI: LiDAR Puck VLP-16, data sheet, p.1

VLP-16

Real-Time 3D LiDAR Sensor

The VLP-16 provides high definition 3-dimensional information about the surrounding environment.

**Specifications:**

Sensor:	<ul style="list-style-type: none"> • Time of Flight Distance Measurement with Calibrated Reflectivities • 16 Channels • Measurement Range: Up to 100 m • Accuracy: ± 3 cm (Typical) • Single and Dual Returns (Strongest, Last) • Field of View (Vertical): $+15.0^\circ$ to -15.0° (30°) • Angular Resolution (Vertical): 2.0° • Field of View (Horizontal): 360° • Angular Resolution (Horizontal/Azimuth): $0.1^\circ - 0.4^\circ$ • Rotation Rate: 5 Hz – 20 Hz • Integrated Web Server for Easy Monitoring and Configuration
Laser:	<ul style="list-style-type: none"> • Laser Product Classification: Class 1 Eye-safe per IEC 60825-1:2007 & 2014 • Wavelength: 903 nm • Beam Size @ Screen: 9.5 mm x 12.7 mm • Beam Divergence: 0.18° (3.0 mrad)
Mechanical/ Electrical/ Operational	<ul style="list-style-type: none"> • Power Consumption: 8 W (Typical) • Operating Voltage: 9 V – 18 V (with Interface Box and Regulated Power Supply) • Weight: 830 g (without Cabling and Interface Box) • Dimensions: 103 mm Diameter x 72 mm Height • Shock: 500 m/s² Amplitude, 11 ms Duration • Vibration: 5 Hz to 2,000 Hz, 3 G_{rms} • Environmental Protection: IP67 • Operating Temperature: -10°C to $+60^\circ\text{C}$ • Storage Temperature: -40°C to $+105^\circ\text{C}$
Output:	<ul style="list-style-type: none"> • 3D LIDAR Data Points Generated: <ul style="list-style-type: none"> - Single Return Mode: ~300,000 points per second - Dual Return Mode: ~600,000 points per second • 100 Mbps Ethernet Connection • UDP Packets Contain: <ul style="list-style-type: none"> - Time of Flight Distance Measurement - Calibrated Reflectivity Measurement - Rotation Angles - Synchronized Time Stamps (μs resolution) • GPS: \$GPRMC NMEA Sentence from GPS Receiver (GPS not included)

63-9229 Rev-E

Product Ordering Information:

Product Name	SKU Ordering Number	Sensor		Interface Box			
		Connector	Cable Length	Included	Connector to Sensor	Cable Length	I/O Connectors
Puck	80-VLP-16	None	3.0 m	Yes	None	-	RJ45, GPS and Power
Puck	80-VLP-16 M12-0.3M	M12 Female	0.3 m	Yes	M12 Male	1.6 m	RJ45, GPS and Power
Puck	80-VLP-16 M12	M12 Female	0.3 m	No	-	-	-

**CLASS 1 LASER PRODUCT**

Copyright ©2017 Velodyne LIDAR, Inc. Specifications are subject to change without notice. Other trademarks or registered trademarks are property of their respective owners.

Velodyne LIDAR, Inc. 345 Digital Drive, Morgan Hill, CA 95037 / lidar@velodyne.com / 408.465.2800

www.velodynelidar.com

Fig. XLII: LiDAR Puck VLP-16, data sheet, p.2

Specifications from the user's manual.

PRINCIPLES OF OPERATION

VLP-16 USER'S MANUAL

Calibrated Reflectivities

The VLP-16 measures the reflectivity of an object with 256-bit resolution independent of laser power and distance over a range from 1m to 100m. Commercially available reflectivity standards and retro-reflectors are used for the absolute calibration of the reflectivity, which is stored in a calibration table within the FPGA of the VLP-16.

- Diffuse reflectors report values from 0-100 for reflectivities from 0% to 100%.
- Retro-reflectors report values from 101 to 255 with 255 being the reported reflectivity for an ideal retro-reflector and 101-254 being the reported reflectivity for partially obstructed or imperfect retro-reflectors.

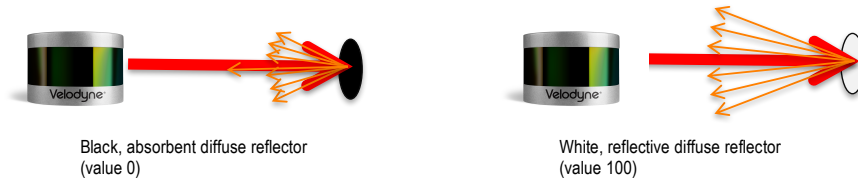
Diffuse Reflector**Retro-Reflector:**

Figure 2. Reflector Types

PRINCIPLES OF OPERATION

VLP-16 USER'S MANUAL

Return Modes

Due to the laser's beam divergence, a single laser firing often hits multiple objects producing multiple returns. The VLP-16 analyzes multiple returns and reports either the strongest return, the last return, or both returns.

In the illustration below, the majority of the beam hits the near wall while the remainder of the beam hits the far wall. The VLP-16 will record both returns only if the distance between the two objects is greater than 1m.

In the event that the strongest return is the last return, the second-strongest return is reported.

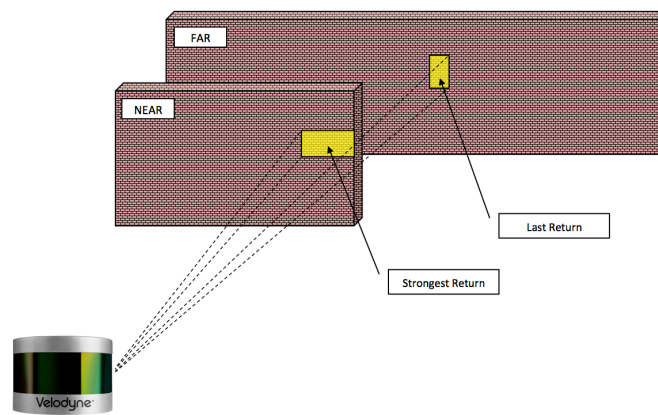


Figure 3. Return Modes

The dual return function is often used in forestry applications where the user needs to determine the height of the trees. The figure below illustrates what happens when the laser spot hits the outer canopy, penetrates the leaves and branches, and eventually hits the ground.

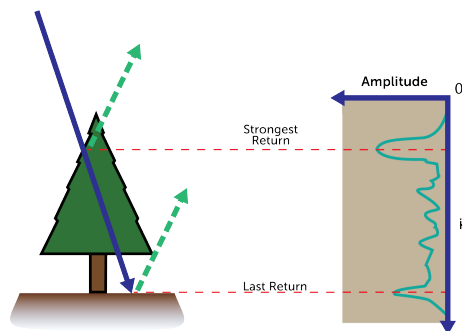


Figure 4a. Dual Returns Example 1